

**DEVELOPMENT OF COST-OPTIMIZED INSULATION  
SYSTEM FOR USE IN LARGE SOLID ROCKET MOTORS**

**Volume III: Task III - Material Performance Determination**

**CASE FILE  
COPY**

by:

**Dr. B. A. Simmons, Manager, Space Booster Department  
and**

**D. L. Nachbar, Project Manager, LMISD Program**

**AEROJET-GENERAL CORPORATION**

**Prepared for:**

**NATIONAL AERONAUTICS AND SPACE ADMINISTRATION**

**NASA Lewis Research Center  
Contract NAS3-11224**

**J. J. Pelouch, Jr., Project Manager**



**AEROJET-GENERAL CORPORATION**

**SACRAMENTO, CALIFORNIA**

NOTICE

This report was prepared as an account of Government-sponsored work. Neither the United States, nor the National Aeronautics and Space Administration (NASA), nor any person acting on behalf of NASA:

- A.) Makes any warranty or representation, expressed or implied, with respect to the accuracy, completeness, or usefulness of the information contained in this report, or that the use of any information, apparatus, method, or process disclosed in this report may not infringe privately-owned rights; or
- B.) Assumes any liabilities with respect to the use of, or for damages resulting from the use of, any information, apparatus, method or process disclosed in this report.

As used above, "person acting on behalf of NASA" includes any employee or contractor of NASA, or employee of such contractor, to the extent that such employee or contractor of NASA or employee of such contractor prepares, disseminates, or provides access to any information pursuant to his employment or contract with NASA, or his employment with such contractor.

FINAL REPORT

Development of Cost-Optimized Insulation  
System for Use in Large Solid Rocket Motors  
Volume III: Task III - Material Performance Determination

by:

Dr. B. A. Simmons, Manager, Space Booster Department  
and  
D. L. Nachbar, Project Manager, LMISD Program

Aerojet-General Corporation  
Sacramento Facility, Solid Rocket Division  
Sacramento, California

Prepared for:

National Aeronautics and Space Administration

August 1969

Contract NAS3-11224

NASA-Lewis Research Center  
Cleveland, Ohio  
J. J. Pelouch, Jr., Project Manager  
Chemical Propulsion Office

FOREWORD

The insulation development work described herein, which was conducted by the Solid Rocket Division of Aerojet-General Corporation, was performed under NASA Contract NAS3-11224. The work was accomplished under the management of the NASA Project Manager, Mr. J. J. Pelouch, Jr., Chemical Propulsion Division, NASA-Lewis Research Center.

Special acknowledgement is accorded to Mr. R. L. Knapp for preparation and analysis of the insulation material thermal behavior model.

TABLE OF CONTENTS

	<u>Page</u>
I. Summary	1
II. Introduction	3
A. Purpose of Report	3
B. Scope of Effort	3
III. Phase I - Verification Motor Testing	3
A. Test Motor Configuration	4
B. Test Results	5
IV. Phase II - Thermal Behavior of Internal Insulations	11

FIGURE LIST

	<u>Figure</u>
Test Motor Configuration	1
Task III Aft Closure Insulation Specimen Locations	2
Aft Closure Thermocouple Locations	3
Record Sheet for Insulation Specimen Profile Measurements	4
Closure Specimen Locations	5
Test Motor Performance	6
Summary of Insulation Specimen Performance Data, S/N III-1	7
Summary of Insulation Specimen Performance Data, S/N III-2	8
Summary of Insulation Specimen Performance Data, S/N III-3	9
Summary of Insulation Specimen Performance Data, S/N III-4	10
Summary of Insulation Specimen Performance Data, S/N III-5	11
Motor S/N III-1, Thickness Loss Rate-vs-Initial Mach Number for IBS-109, IBC-101, and V-44 Control	12
Motor S/N III-2, Thickness Loss Rate-vs-Initial Mach Number for Avcoat II, IBS-107, and V-44 Control	13
Motor S/N III-3, Thickness Loss Rate-vs-Initial Mach Number for IBT-106, IBC-111 and 111G, and V-44 Control	14
Motor S/N III-4, Thickness Loss Rate-vs-Initial Mach Number for 40SD-80, IBT-106, IBT-100, USR-3800, and V-44 Control	15
Motor S/N III-5, Thickness Loss Rate-vs-Initial Mach Number for TI-H704B, IBT-100, and V-44 Control	16
Comparison of TLR-vs-Initial Mach Number Data for IBS-109, IBC-101, and V-44 Controls in Motors S/N I-1, I-2, and III-1	17
Comparison of TLR-vs-Initial Mach Number Data for IBS-107, Avcoat II, and V-44 Controls in Motors I-1, I-2, and III-2	18
Comparison of TLR-vs-Initial Mach Number Data for IBT-106, IBC-111, and V-44 Controls in Motors I-1, I-2, and III-3	19
Comparison of TLR-vs-Initial Mach Number Data for 40SD-80, USR-3800, IBT-106, IBT-100, and V-44 Controls in Motors I-1, I-2, III-3, and III-4	20
Comparison of TLR-vs-Initial Mach Number Data for IBT-100, TI-H704B, and V-44 Controls in Motors I-1, I-3A, and III-5	21

APPENDIXES

Ballistic Performance Curves for Task III LMISD Test Motors  
S/N III-1 through S/N III-5  
Insulation Material Specimen Pre- and Posttest Profiles,  
Motor S/N III-1 through S/N III-5  
Thermal Behavior of Internal Insulation

Appendix

I  
II  
III

ABSTRACT

A program to develop a cost-optimized insulation system for large solid rocket motors was conducted by Aerojet-General Corporation under Contract NAS3-11224. Four tasks were derived to accomplish the program objective: Task I, Survey and Screening; Task II, Process Demonstration; Task III, Material Performance Determination; and Task IV, Preparation of 260-in.-dia full-length motor insulation system Design and Process Plan. Task III is the subject of this volume of the final report. The candidate materials selected from the Task I effort were evaluated in five solid-propellant test motors, using V-44 rubber as the control material. The 20-in.-dia test motors operated 632 to 654 psia over a web burning duration of 17.3 to 17.6 sec. Two candidate material specimens, plus a V-44 control specimen, were tested in each motor. Initial Mach numbers and material thickness loss were obtained from pre- and posttest profile measurements. Plots of material thickness loss rates as a function of Mach numbers provided a performance comparison of each material relative to V-44. Performance results also were compared to those obtained previously in the Task I motor tests. Results indicated that IBT-100, IBT-106, USR-3800, IBC-111, and IBS-107 performed better than V-44. The performance of TI-H704B was equivalent to that of V-44, while IBC-101, IBS-109, 40SD-80, and Avcoat II exhibited erosion resistance poorer than that of V-44. These results agreed with the data obtained in Task I.

Thermal behavior model preparation showed that analytical treatment of internal insulation thermal response not only provides realistic estimates of insulation material performance, but also affords a means of interpreting experimental erosion data and scaling these results to large motors.

NASA report numbers and corresponding volume numbers are as follows:

CR-72581	Volume I
CR-72582	Volume II
CR-72583	Volume III
CR-72584	Volume IV

I. SUMMARY

The objective of the Large Motor Insulation System Development (LMISD) Program is to evaluate low-cost insulation materials which are applicable to large solid-propellant rocket motors. Four tasks were derived to accomplish the planned objective. Task I, which is described in Volume I of this report, involved a survey of available materials applicable to large motors; selection of twenty candidate materials, including Gen-Gard V-44 and V-61 as controls; measurement of candidate material physical, chemical, mechanical, thermal, and adhesive properties; evaluation of material erosion resistance in three solid-propellant motor tests; evaluation of property measurement and motor test data; and selection of twelve materials, including V-44 control, for further evaluation in Tasks II and III. In Task II, candidate materials selected in Task I were installed into a 54-in.-dia motor chamber. Task III includes material performance determinations in five solid-propellant motor tests. Task IV is the preparation of a 260-in.-dia full length motor cost-optimized insulation system design and process plan, using materials selected on the basis of data obtained from Tasks II and III.

The following materials were recommended for performance determination in Task III:

<u>Pressure-Cured</u>	<u>Trowelable</u>	<u>Castable</u>	<u>Sprayable</u>
V-44 (control)	IBT-100	IBC-101	IBS-107
USR-3800	IBT-106	IBC-111	IBS-109
	TI-H704B	40SD-80	Avcoat II

The following is a summary of the insulation material specimens tested in each motor:

<u>S/N III-1</u>	<u>S/N III-2</u>	<u>S/N III-3</u>	<u>S/N III-4</u>	<u>S/N III-5</u>
V-44 control	V-44 control	V-44 control	V-44 control	V-44 control
IBC-101	IBS-107	IBT-106	USR-3800	IBT-100
IBS-109	Avcoat II	IBC-111	40SD-80	TI-H704B

Phase I of Task III included the processing and test of 20-in.-dia solid-propellant insulation test motors, identical to those tested in Task I. Two candidate material specimens, plus a V-44 control, were installed into the aft closure. Pre- and posttest insulation specimen profiles were measured and recorded using a Portage Layout Machine. These profile measurements were used to determine initial Mach numbers at the specimen surfaces and the material thickness loss.

Five Task III insulation test motors, identified as S/N III-1 through III-5 were test fired during February through May 1969.

## I. Summary (cont)

	<u>S/N III-1</u>	<u>S/N III-3</u>	<u>S/N III-3</u>	<u>S/N III-4</u>	<u>S/N III-5</u>
Web average pressure, psia	635	632	648	645	654
Maximum pressure, psia	644	643	665	663	673
Web duration, sec	17.6	17.5	17.5	17.5	17.3

Following each test, the motor was visually inspected, the char layer was removed, and posttest profiles were obtained. Using pre- and posttest profiles, each material thickness loss was measured at specified locations normal to the specimen surfaces. Gas flow Mach numbers at the specimen surfaces were calculated. Thickness loss rates were calculated, and a visual comparison of each candidate material performance relative to V-44 was obtained by plotting the thickness loss rate as a function of Mach number, then drawing the most representative line through the data points for each material. Material performance relative to V-44 are summarized as follows:

- |                   |               |
|-------------------|---------------|
| 1. USR-3800       | 7. IBS-109    |
| 2. IBT-100        | 8. IBC-101    |
| 3. IBS-107        | 9. TI-H704B   |
| 4. IBT-111        | 10. 40SD-80   |
| 5. IBT-106        | 11. Avcoat II |
| 6. V-44 (control) |               |

The similarity between the thermal decomposition behavior of elastomeric type materials and ablative plastics used for booster nozzle throats suggests that a transient charring-ablation computer program developed primarily for the latter could be applied to internal insulation materials. Thus, a thermal model was developed in Phase II to include all energy transport processes that occur in the virgin, decomposition, and fully charred zones; a basis for prediction of char rates, erosion rates and transient temperature distributions; and a treatment of the surface regression by combining all modes of removal into an "effective removal rate" which is obtained from subscale motor firings. Use of this data, together with measured values of thermal properties and internal decomposition rates, provides a means by which the designer can scale insulation material performance to any motor where the local environment can be established.

To apply this analysis technique and better understand the internal insulation response problem, considerable effort is required in the evaluation of propellant exhaust gas properties, the internal flow field, and the magnitude of the convective heat transfer. The recommended procedure for evaluating each of these factors was outlined.

## I. Summary (cont)

The adequacy of the thermal model to predict erosion, char, and thermal gradients by describing the complicated energy transfer, decomposition, and pyrolysis gas transpiration processes which occur within the insulation structure was indicated by comparison with measured data. It was shown that predicted material degradation depths were well within the variational limits of actual posttest measurements over a wide range of heat fluxes. Likewise, thermocouple data obtained within selected samples indicated reasonable agreement.

Thus, it was established that analytical treatment of internal insulation thermal response not only provided realistic estimates of material performance, but also afforded a means of interpreting experimental erosion data and scaling these results to large motors.

## II. INTRODUCTION

### A. PURPOSE OF REPORT

This document is the third volume in a series of final reports dealing with the major tasks of the Large Motor Insulation System Development (LMISD) Program, Contract NAS3-11224. This series of reports constitute the LMISD Program final report. This report summarizes in detail the Task III effort for the LMISD Program.

### B. SCOPE OF EFFORT

This report volume summarizes in detail the Task III effort for the LMISD Program. The following work was accomplished:

1. Five insulation test motors were processes and assembled, including installation of insulation specimens in the motor aft closure.
2. Five LMISD test motors were statically fired to evaluate candidate insulation material performance.
3. A material thermal behavior model was prepared.

## III. PHASE I - VERIFICATION MOTOR TESTING

Five motor tests were conducted to evaluate the performance of the ten candidate insulation materials selected from the Task I effort. The following materials were tested:

III. Phase I - Verification Motor Testing (cont)

Pressure-Cured Group

V-44 Control, NBR/silica/asbestos

USR-3800, NBR-phenolic/boric acid

Trowelable Group

IBT-100, PBAN-epoxy/Sb<sub>2</sub>O<sub>3</sub>/Asbestos

IBT-106, PBAN-epoxy/Sb<sub>2</sub>O<sub>3</sub>/Asbestos

TI-H704B, PBAA/carbon black/Asbestos

Castable Group

IBC-101, PBAN-epoxy/Sb<sub>2</sub>O<sub>3</sub>/Asbestos

IBC-111, PBAN-epoxy/Refrasil

40SD-80, Polyurethane

Sprayable Group

IBS-107, CTPB/Sb<sub>2</sub>O<sub>3</sub>/Silica

IBS-109, PBAN-epoxy/Sb<sub>2</sub>O<sub>3</sub>/Asbestos

Avcoat II, Epoxy-polyamide

A. TEST MOTOR CONFIGURATION

The LMISD test motor configuration for Task III was the same as that used in Task I. However, only three insulation material specimens were evaluated in each motor instead of eight specimens. The test motor configuration is shown in Figure 1.

The Task III motor test plan required five motor firings, with two insulation material specimens plus a V-44 control specimen in each motor. The planned material specimen locations are shown in Figure 2. The Task III material specimens included thermocouples for temperature measurements during the test. Each chromel-alumel thermocouple was ranged from 0 to 2500°F, and located so that exposure occurred near web burnout. Thermocouples were installed at an area ratio of approximately 2.2, as shown in Figure 3. For these experiments, the pre- and posttest specimen profiles were measured with a Portage Layout Machine, as previously described in Volume I of this final report, and recorded on a data sheet like the one shown in Figure 4. The profiles of each specimen in each motor were measured in three locations. The centerline of each of the three specimens in each closure located at 0, 120, and 240 degrees, with the V-44 control specimen always located at 0 degrees, as shown in Figure 2. Each specimen profile was measured at 0, 120, and 240 degrees, and at 45 degrees on each side of the specimen surface.

## III.A. Test Motor Configuration (cont)

The following table shows the materials that were evaluated in each motor:

<u>Location, degrees</u>	<u>S/N III-1</u>	<u>S/N III-2</u>	<u>S/N III-3</u>	<u>S/N III-4</u>	<u>S/N III-5</u>
0	V-44 control	V-44 control	V-44 control	V-44 control	V-44 control
75	N/A	N/A	N/A	IBT-106	N/A
120	IBS-109	IBS-107	IBT-106	USR-3800	IBT-100
165	N/A	N/A	N/A	IBT-100	N/A
240	IBC-101	Avcoat II	IBC-111G	40SD-80	TI-H704B
285	N/A	N/A	IBC-111	N/A	N/A

For clarity, sketches of the specimen locations in each motor are shown in Figure 5. In Motor S/N III-3, two formulations of IBC-111 were tested. The formulation identified as IBC-111G used 0.25-in.-long commercial Refrasil fibers which were processed through a Mikropulverizer prior to mixing. IBC-111 contained Refrasil fibers which were processed in a Waring Blender with DER curing agent prior to batch mixing. Both formulations were tested to determine if the processing method affected material erosion performance. In Motor S/N III-4, the USR-3800 specimen was fabricated from 0.1-in.-thick plies of raw stock. Two 16-in.-long by 2.0-in.-wide by 1.0-in.-thick bars were layed-up and cured, using vacuum bag and autoclave cure method. IBT-100 and IBT-106 were used as potting materials around the USR-3800, so that additional performance data were obtained for these materials.

## B. TEST RESULTS

1. Motor Performance

The five Task III LMISD motors were test fired successfully and nominal performance was obtained. Ballistic pressure-vs-time curves are shown in Appendix I. A ballistic performance summary of all LMISD motors fired in the program is shown in Figure 6.

2. Material Performance

Pre- and posttest specimen profiles for each material at three radial locations in each motor are presented in Appendix II.

Using the pre- and posttest profiles shown in Appendix II, each material thickness loss was measured at 23 specified locations normal to the specimen surface, as shown in Figure 4. The initial area ratio ( $A/A^*$ ) and

## III.B. Test Results (cont)

initial Mach number at each of the 23 locations in each closure were calculated from the recorded profiles. Thickness loss rates were calculated by dividing the measured thickness loss at each location by the web burning duration for each motor. Initial Mach numbers at the specimen surface, thickness losses, and calculated thickness loss rates are summarized in Figures 7 through 11.

In an effort to compare visually the relative erosion resistances of the candidate materials, the measured thickness loss rates at three locations measured for each material are plotted as a function of the initial Mach number at the specimen surface for each motor in Figures 12 through 16. These graphs are not intended as a material design guide, but only to show the relative performance of each specimen, and were prepared by plotting the TLR-vs-Mach number data summarized in Figures 7 through 11, then drawing the most representative line through the data points at the three locations for each material. Performance of some of the materials in Task III motors varied from the performance previously observed in Task I motors, particularly in the performance of V-44 control material. On the other hand, most of the material performances were similar. To highlight some of the differences that will be discussed, graphical comparisons of thickness loss rate-vs-initial Mach number data for materials tested in Task I and III motors are shown in Figure 17 through 21.

The erosion rate of the V-44 control varied between Task I and Task III motors, as shown in the following table:

Initial Mach No.	Calculated Thickness Loss Rates, in./sec								
	S/N I-1	S/N I-2	S/N I-3A	S/N III-1	S/N III-2	S/N III-3	S/N III-4	S/N III-5	
					0° 45° & 315°				
.05	.009	.008	.009	.011	.007	.007	.011	.008	.009
.10	.015	.011	.013	.022	.021	.019	.023	.021	.020
.15	.021	.018	.014	.031	.031	.024	.031	.030	.026
.20	.027	.019	.016	*	.036	.028	.037	.036	.031
.25	.032	.022	.018	*	.042	.031	.039	.040	.034

\* The 0.5-in.-thick V-44 specimen was eroded away at locations aft of the 0.15 Mach number region, thus exposing potting material.

In Task III motors, the V-44 erosion rate generally was higher than in previous Task I motors. This was attributed to the thinner plies of V-44 used to build up the Task III control specimen. In Task I motors, the V-44 specimen was fabricated with 0.5-in.-thick cured sheets bonded together with

## III.B. Test Results (cont)

epoxy adhesive. As a result, the initial bondline was 0.5-in. away from the surface exposed to erosion. 0.1-in.-thick plies were used to fabricate the 0.5-in.-thick specimen in S/N III-1 and III-2. Apparently, V-44 erosion was accelerated as the bondline layers were weakened by the approaching flame front. This same bondline-accelerated V-44 erosion pattern was observed in the performance of sidewall insulation in Motor 260-SL-1. For this reason, three 0.1-in.-thick plies were used in 260-SL-2, and a single 0.2-in.-thick ply was used in 260-SL-3.

As shown in the foregoing table, the S/N III-2 V-44 specimen had two distinct erosion patterns. The first pattern, measured at 0 degree, was much like the performance observed in S/N III-1. The second pattern, measured at 45 and 315 degrees, was close to the V-44 performance observed in Motor S/N I-1.

V-44 specimens for Motor S/N III-3, -4, and -5, were fabricated with three, 0.2-in.-thick plies of cured sheets which were residual from the 260-SL-3 program. The V-44 erosion performance in these three motors was fairly consistent. There appears to be three distinct V-44 erosion patterns. The first pattern was observed in Motor S/N I-1 and at 45 and 315 degrees in Motor S/N III-2. The second pattern was consistent in Motors S/N III-1, III-3, III-4, and III-5, and at zero degrees in Motor S/N III-2. A third pattern, which was different from the two foregoing patterns, was measured in Motor S/N I-2 and I-3A. There is no apparent reason for the three observed erosion patterns. As discussed in the Requirement/Capability Analysis section, Volume IV of this final report, the one-sigma thickness loss rate variation observed for V-44 rubber in Polaris, Minuteman, etc., is 15 percent. The V-44 performance data obtained in the LMISD test motors exceeded this value, indicating that either there was a significant variation in the cure hardness of the specimens or the small nozzle size adversely affected the thickness loss rate variation.

Performances of the candidate insulation materials are discussed in the following paragraphs.

a. IBC-101 and IBS-109 (Motor S/N III-1)

Comparisons of these material performances are shown in Figure 17 and in the following table:

## III.B. Test Results (cont)

Initial Mach No.	IBC-101 TLR, in./sec		IBS-109 TLR, in./sec	
	S/N I-1	S/N III-1	S/N I-1	S/N III-1
0.05	0.011	0.014	0.011	0.013
0.10	0.019	0.028	0.018	0.027
0.15	0.031	0.038	0.027	0.036
0.20	0.041	0.044	0.030	0.042
0.25	0.045	0.045	0.029	0.044

For both materials, the measured performance in the Task III motor was better than that in Task I, which also was the case for the V-44 control. However, the performance of each material relative to the V-44 control was reasonably consistent. It is concluded that the erosion rate of IBC-101 and IBS-109 exceeds that of V-44 by approximately 10 to 20 percent.

## b. Avcoat II and IBS-107 (Motor S/N III-2)

Comparisons of these material performances are shown in Figure 18 and in the following table:

Initial Mach No.	Avcoat II TLR, in./sec		IBS-107 TLR, in./sec	
	S/N I-2	S/N III-2	S/N I-1	S/N III-2
0.05	0.015	0.011	0.006	0.008
0.10	0.031	0.040	0.009	0.013
0.15	0.046	0.048	0.013	0.016
0.20	0.055	0.055	0.018	0.018
0.25	-	0.056	0.023	0.019

The erosion rate of Avcoat II consistently was 200 to 300 percent greater than V-44. For this reason, Avcoat II was eliminated as a candidate material, and a Task II process evaluation was not conducted. This material is more suitable for external insulation applications, such as base-heating insulation, where gas flow rates are low (<0.01 Mach number).

IBS-107 performance exceeded that of V-44 by 25 to 50 percent. This material would be a prime candidate insulation material if the processing problems involved in spray application were overcome.

## III.B. Test Results (cont)

## c. IBC-111 and IBT-106 (Motor S/N III-3)

Comparisons of these material performances are shown in Figure 19 and in the following table:

Initial Mach No.	IBC-111 TLR, in./sec		IBT-106 TLR, in./sec		
	S/N I-2	S/N III-3	S/N I-1	S/N III-3	S/N III-4
0.05	0.007	0.007	0.014	0.010	0.009
0.10	0.008	0.011	0.017	0.015	0.016
0.15	0.010	0.015	0.018	0.020	0.022
0.20	0.014	0.019	0.018	0.025	0.028
0.25	0.025	0.024	0.019	0.028	0.033

IBT-106 also was evaluated in Motor S/N III-4, and comparison of material performance in Motors S/N III-3 and III-4 are included in Figure 20. IBT-106 erosion resistance was approximately 25 percent better than that for V-44.

There was no measurable performance difference between IBC-111 material processed with ground and unground commercial Refrasil. The performance of IBC-111 also was approximately 25 percent better than V-44 control performance.

## d. 40SD-80 and USR-3800 (Motor S/N III-4)

Comparisons of these material performances are shown in Figure 20 and in the following table:

Initial Mach No.	40SD-80 TLR, in./sec		USR-3800 TLR, in./sec	
	S/N I-2	S/N III-4	S/N I-3A	S/N III-4
0.05	0.013	0.015	0.004	0.004
0.10	0.023	0.029	0.004	0.006
0.15	0.033	0.031	0.005	0.003
0.20	0.035	0.032	0.005	0.003
0.25	-	0.033	0.006	0.002

High material erosion was experienced by 40SD-80 in relatively low gas velocity regions ( $<0.15$  Mach No.). As a result, the area ratios

## III.B. Test Results (cont)

were increased to such an extent that further thickness loss was minimal. This accounts for the break in the TLR-vs-Mach number curves at a Mach number of approximately 0.10. This condition was true in varying degrees with all materials tested, but was most pronounced with 40SD-80. The high erosion rate, particularly at low Mach numbers, makes 40SD-80 a less desirable material for large motor insulation system applications.

Pressure-cured USR-3800, like V-61, exhibited exceptional erosion resistance, and, also like V-61, contains a high percentage of boric acid filler. Materials with high boric acid filler concentrations experience weight-gain and subsequent swelling due to moisture absorption. In the LMISD program, it was necessary to quench the motor after each test, thus exposing USR-3800 and V-61 to high moisture environments. The actual erosion rates then were masked to a certain degree by material swelling. Data from stop-start motor tests, where combustion termination was accomplished by rapid depressurization rather than by water quench, show that the performance of USR-3800 is approximately 100 percent better than V-44.

## e. TI-H704B and IBT-100 (Motor S/N III-5)

Comparisons of these material performances are shown in Figure 21 and in the following table:

Initial Mach No.	TI-H704B TLR, in./sec		IBT-100 TLR, in./sec		
	S/N I-3A	S/N III-5	S/N I-1	S/N III-4	S/N III-5
0.05	0.009(est)	0.010	0.006	0.006	0.009
0.10	0.021	0.023	0.012	0.009	0.016
0.15	0.040	0.030	0.017	0.012	0.021
0.20	0.052	0.036	0.018	0.014	0.025
0.25	-	0.042	0.018	0.016	0.028

When the results of the first motor test including TI-H704B were analyzed, it was suspected that the properties of the TI-H704B sample received for Task I evaluation were not indicative of this material. The measured tensile strength and Shore A hardness were 123 psi and 31, respectively. This tensile strength value was lower than the 175 psi reported by the supplier. This conclusion was verified in Task III, as shown in the foregoing table. The thickness loss observed in Motor S/N III-5 more nearly approached the performance reported by the supplier.

## III.B. Test Results (cont)

Performance of IBT-100 was from 50 to 100 percent better than that for V-44. This same performance relationship was observed in Motor 260-SL-3 and in the stop-start motor insulation development program. The performance characteristics of IBT-100 make this material a prime candidate for large motor dome and nozzle insulation.

IV. PHASE II - THERMAL BEHAVIOR OF INTERNAL INSULATIONS

In general, the solid propellant motor designer is faced with the problem of defining the internal insulation type and amount for a wide variety of motors, operating conditions and/or environments. The criteria upon which this choice must be made depend primarily on the type of motor; i.e., end burner, stop-start capability, duration, propellant type, chamber pressure, etc. Each of these require different considerations; for example, it is recognized that upper stage motors are relatively sensitive to weight penalties thus insulation thickness and propellant loading become important items. In the design of case insulation for booster motors, it is recognized that residual weight is of lesser importance than cost or ease of fabrication. Thus, the need for a rigorous evaluation of insulation requirements, such as tapering or contouring to reflect the duration of exposure in local areas and minimizing insulation case operating temperatures, is not absolutely necessary, and as per the current practice, the insulation is designed with a large safety factor included. On the other hand, due to the large quantities of insulation used in booster motors, consideration of the cost per pound and total cost of material require that the "factor of safety" not be excessive. In addition, the insulation type and amount required for booster motors obviously must be evaluated and scaled from subscale firings. In each case, especially for the purpose of scaling subscale data, there is a need for describing analytically the thermal response of internal insulation when exposed to the local environment of large booster motors. This model must include prediction techniques which encompass all modes of heat transfer, i.e., conduction, convection and radiation, as well as the mass transfer of decomposition products away from exposed surfaces.

Appendix III summarizes the findings of an analytical study of elastomeric insulation performance conducted in support of the LMISD Program. The computer techniques which can be utilized for evaluating internal insulation designs are discussed and comparison of predicted and actual firing results presented. This information has been divided into four main categories:

- Heat fluxes or environment
- Thermal behavior
- Data reduction
- Thermal response calculations

## IV. Phase II - Thermal Behavior of Internal Insulations (cont)

The first pertains to the local environments to which internal insulation materials are exposed. Important criteria include gas-particle flow field, convection, radiation and the influence of oxide particle impaction. Secondly, the analytical treatment of internal response of the insulation to the environment is discussed. Method of predicting erosion, char growth and thermal profiles both during and subsequent to the exposure time are outlined. Third, the data reduction of laboratory experiments, such as thermal property measurements and thermo-gravimetric analyses, plus the utilization of erosion rates obtained from actual firings, are discussed. Techniques which provide realistic meaning to both material property measurements and the methods of acquisition for inclusion into the analytical model are outlined. Fourth, the thermal response of several candidate materials when exposed to the above environment are predicted and pertinent results discussed. This includes the internal heat-transfer mechanism as well as the interactions of chemical and/or mechanical material removal at the surface.

Based on the discussion of the thermal response predictions for booster motor internal insulations presented in Appendix III, the following comments are noted.

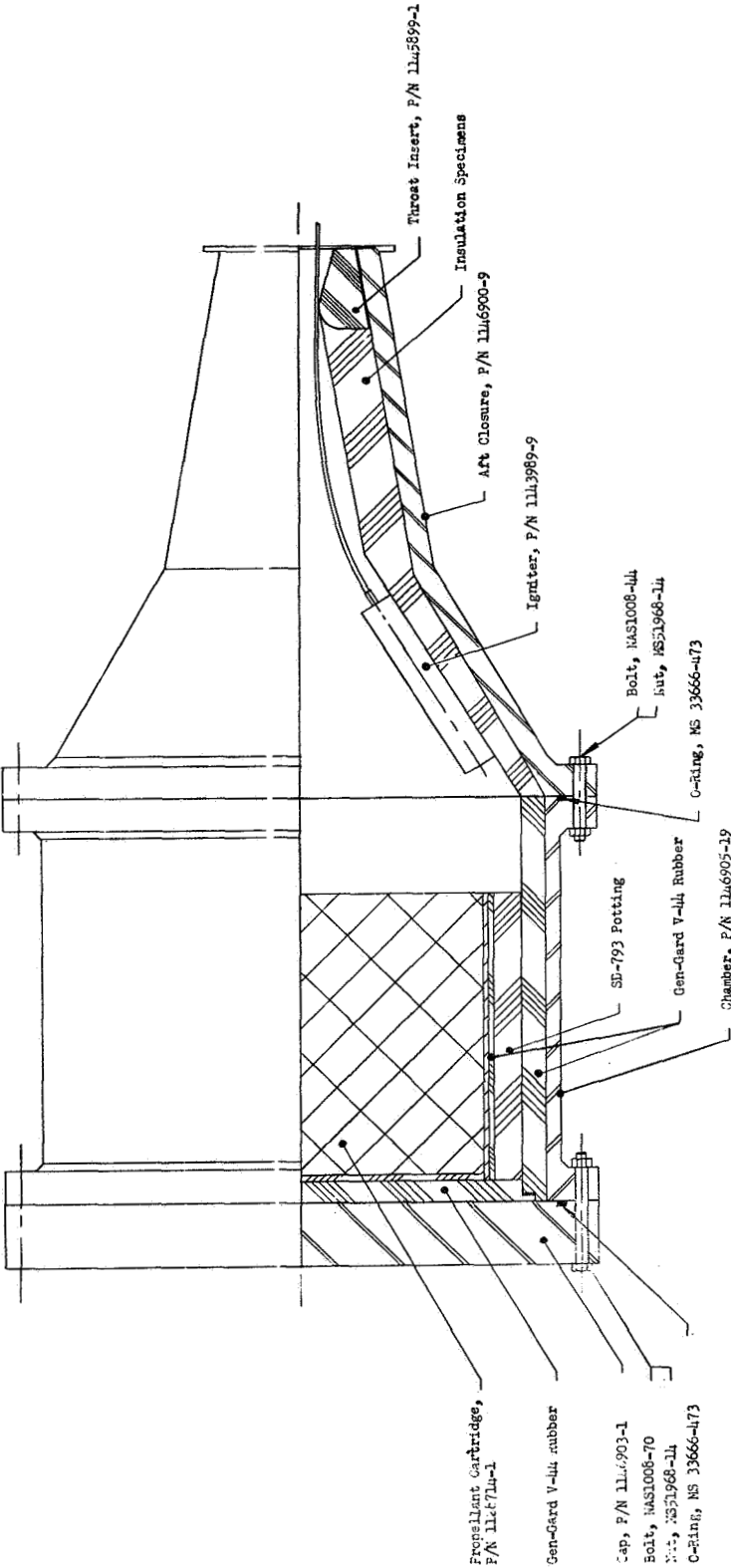
The similarity between the thermal decomposition behavior of elastomeric type materials and ablative plastics used for booster nozzles suggests that a transient charring-ablation computer program which has been developed primarily for the latter, could likewise be applied to internal insulation materials. Thus, a thermal model has been developed to include (1) all energy transport processes that occur in the virgin, decomposition and fully charred zones, (2) a basis for prediction of char rates, erosion rates and transient temperature distributions, and (3) a treatment of the surface regression by combining all modes of removal into an "effective removal rate" which is obtained from subscale motor firings. Use of this data, together with measured values of thermal properties and internal decomposition rates, provides a means by which the designer can scale insulation material performance to any motor where the local environment can be established. The procedure is to evaluate a scaling factor,  $B'$ , which relates the measured regression rates for a particular material with the magnitude of the local thermal environment. It is assumed this parameter remains invariant, not only for a wide range of heat fluxes within a given motor, but also over a similar range of values between different motors.

To apply this analysis technique and better understand the internal insulation response problem, considerable effort is required in the evaluation of propellant exhaust gas properties, the internal flow field, and the magnitude of the convective heat transfer. The recommended procedure for evaluating each of these factors is outlined. However, alternate or simplified techniques could be used for scaling purposes provided they are applied in a consistent manner.

IV. Phase II - Thermal Behavior of Internal Insulations (cont)

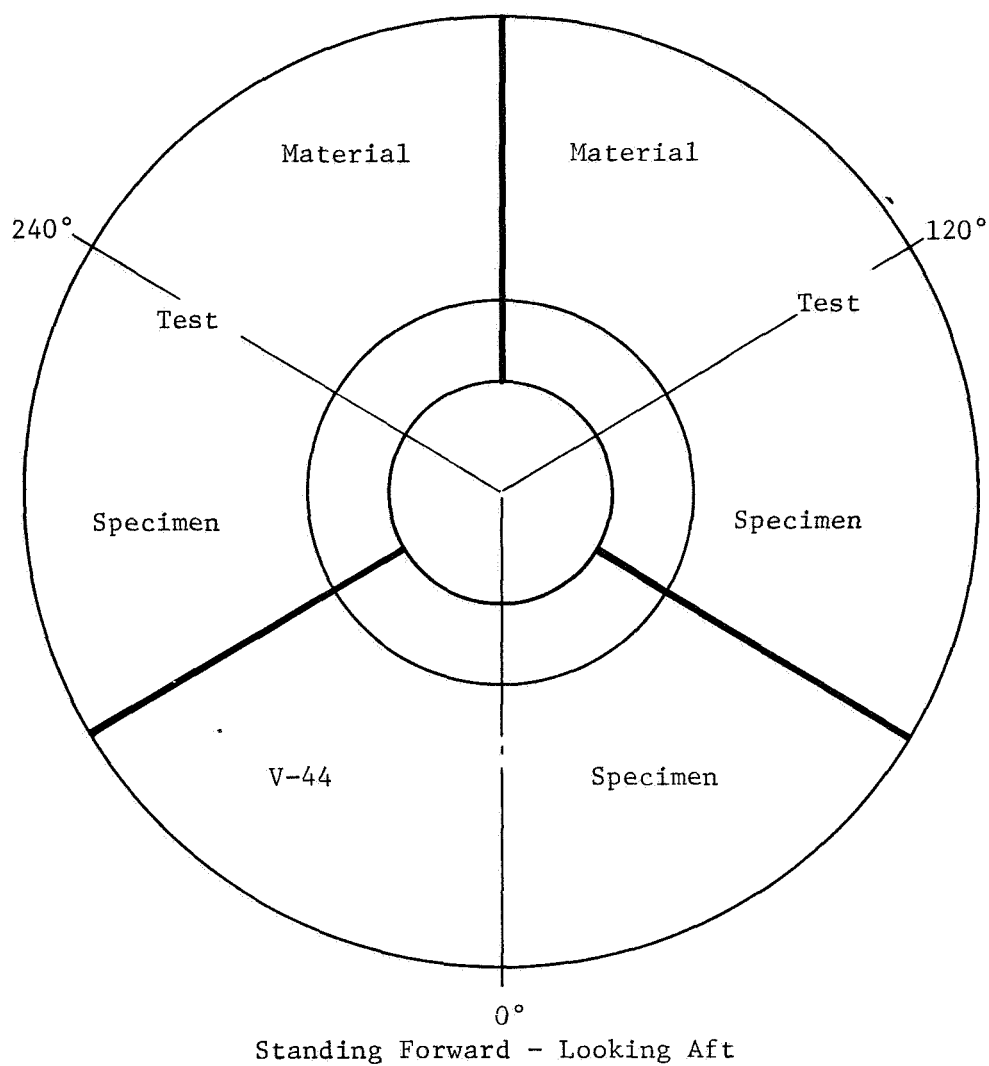
The adequacy of the thermal model to predict erosion, char and thermal gradients by describing the complicated energy transfer, decomposition and pyrolysis gas transpiration processes which occur within the insulation structure is indicated by comparison with measured data. It is shown that predicted material degradation depths are well within the variational limits of actual posttest measurements over a wide range of heat fluxes. Likewise, thermocouple data obtained within selected samples indicate reasonable agreement.

Thus, it has been established that analytical treatment of internal insulation thermal response not only provides realistic estimates of material performance, but also affords a means of interpreting experimental erosion data and scaling these results to large motors.



Test Motor Configuration

Figure 1

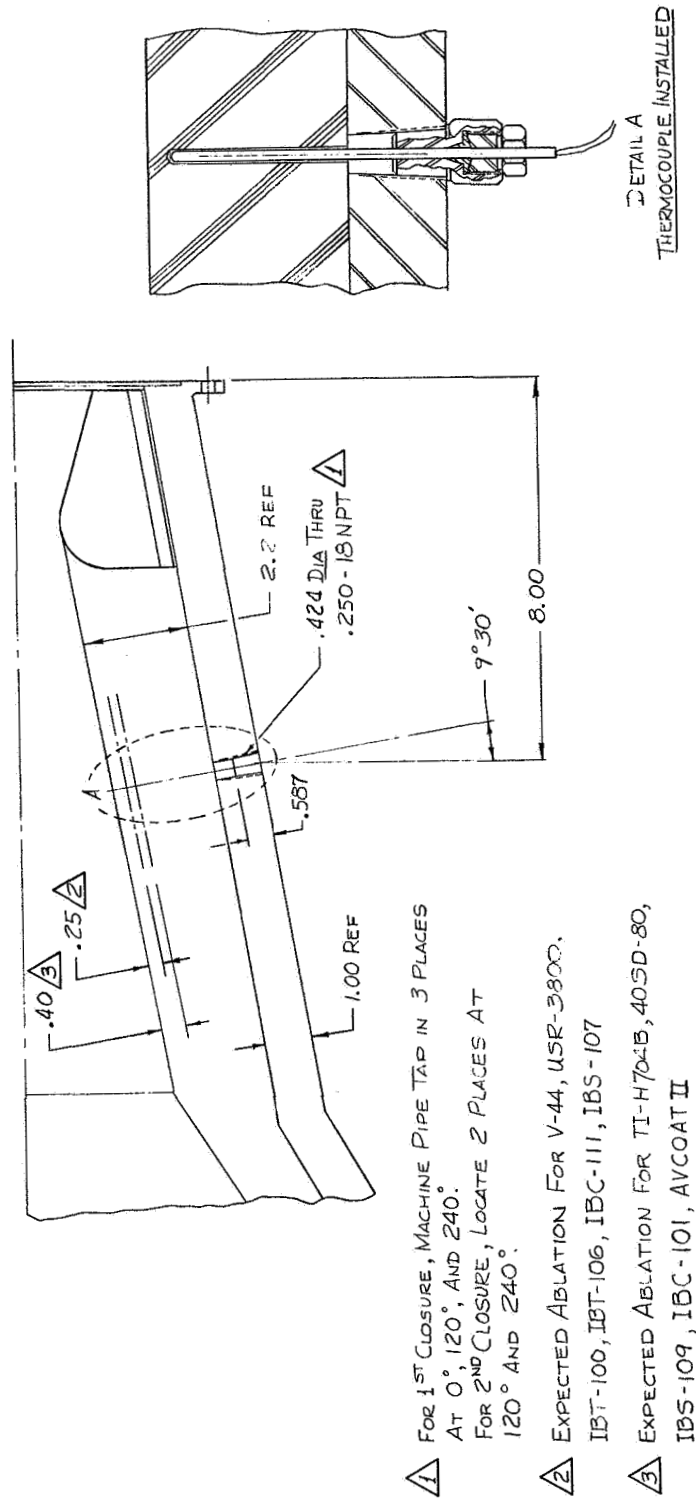


Material Specimens to be Installed:

USR-3800	IBC-111
IBT-100	40SD-80
IBT-106	IBS-107
TI-H704B	IBS-109
IBC-101	Avcoat II

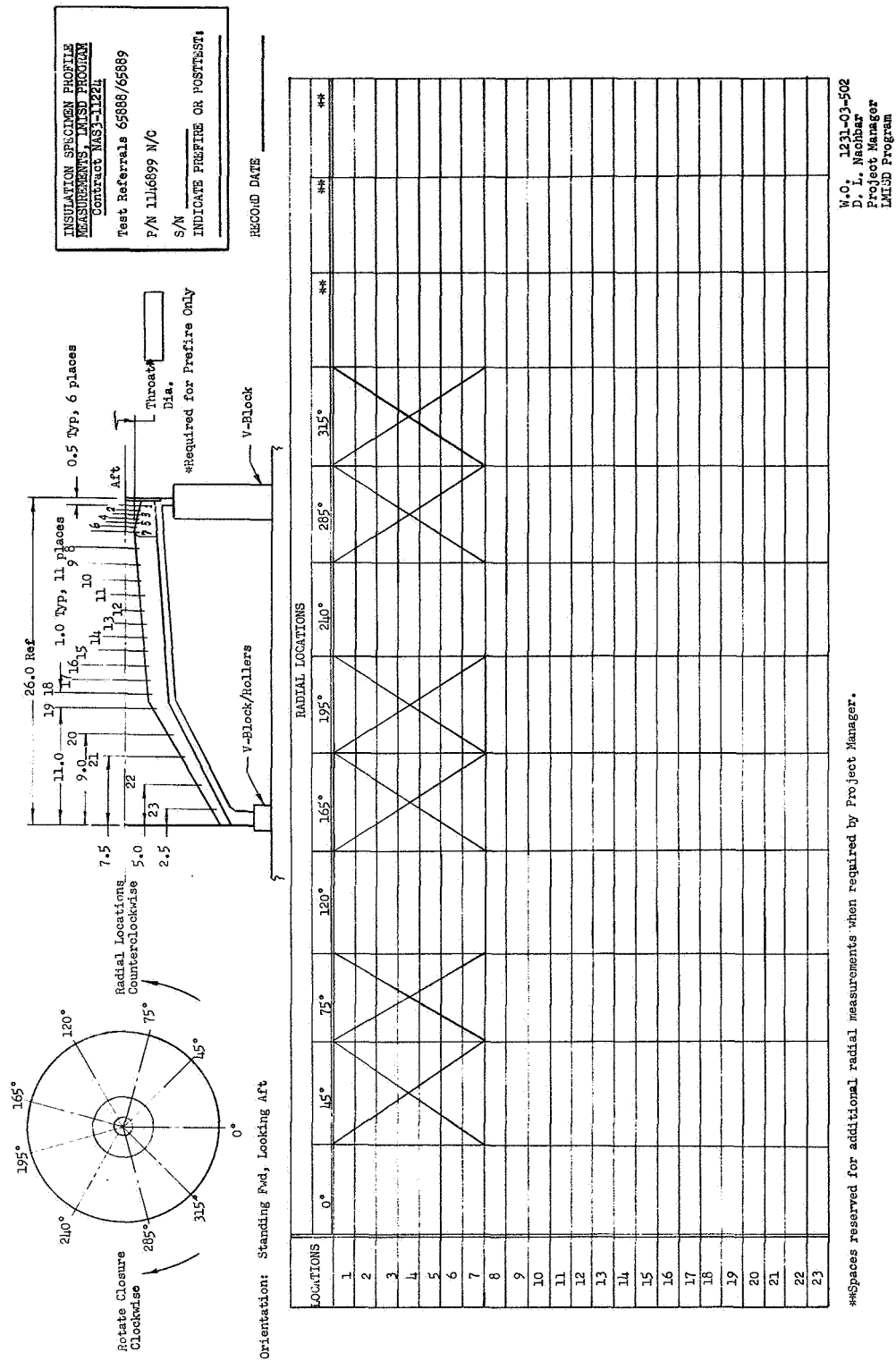
Task III Aft Closure Insulation Specimen Locations

Figure 2



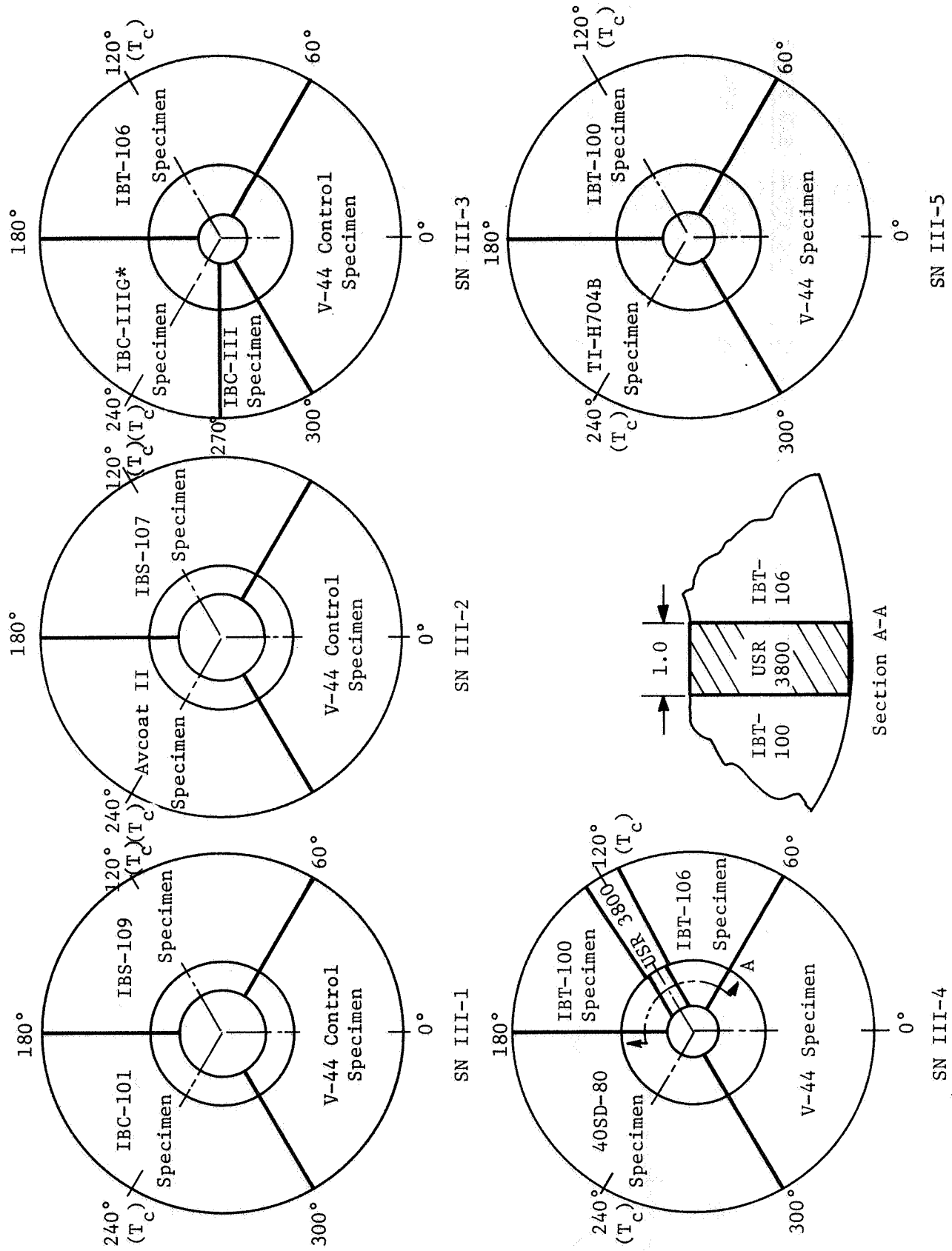
Aft Closure Thermocouple Locations

Figure 3



Record Sheet for Insulation Specimen Profile Measurements

Figure 4



Closure Specimen Locations

\*Contains ground Refrasil

Figure 5

	<u>S/N I-1</u>	<u>S/N I-2</u>	<u>S/N I-3A</u>	<u>S/N III-1</u>	<u>S/N III-2</u>	<u>S/N III-3</u>	<u>S/N III-4</u>	<u>S/N III-5</u>
Web Average Pressure, psia	640	641	643	635	632	648	645	654
Maximum Pressure, psia	680	668	662	644	643	665	663	673
Web Burning Duration, sec	17.6	17.7	17.6	17.6	17.5	17.5	17.5	17.3

Test Motor Performance

Figure 6

	Location																Max.
	8	9	10	11	12	13	14	15	16	17	18	19	20	21	22	23	
V-44 - 0°: Initial Mach No. Thickness Loss TLR Final Mach No.	.50	.33	.24	.19	.15	.12	.10	.085	.075	.065	.06	.04	-	-	-	-	.94
	-	.94	.81	.64	.49	.41	.31	.25	.21	.14	.14	.11	.09	.07	.09	.09	.94
	-	.053	.046	.035	.028	.023	.018	.014	.012	.008	.008	.006	.005	.004	.005	.005	.93
	-	.105	.105	.10	.10	.09	.08	.075	.065	.06	.055	.03	-	-	-	-	-
V-44: - 45°: Initial Mach No. Thickness Loss TLR Final Mach No.	.48	.30	.235	.18	.13	.11	.09	.08	.07	.06	.055	.04	-	-	-	-	.97
	-	.95	.76	.62	.48	.42	.34	.31	.29	.27	.25	.14	-	-	-	-	.955
	-	.054	.043	.035	.027	.024	.019	.018	.016	.015	.014	.008	-	-	-	-	-
	-	.10	.10	.095	.085	.08	.07	.065	.06	.055	.04	-	-	-	-	-	-
V-44 - 315°: Initial Mach No. Thickness Loss TLR Final Mach No.	.44	.305	.23	.18	.14	.12	.10	.085	.075	.065	.06	.04	-	-	-	-	.92
	-	.90	.82	.65	.56	.48	.39	.34	.30	.26	.30	-	-	-	-	-	.92
	-	.051	.047	.037	.032	.027	.022	.019	.017	0.15	.017	-	-	-	-	-	.92
	-	.095	.095	.09	.085	.08	.075	.07	.065	.055	.05	-	-	-	-	-	-
IBS-109 - 120°: Initial Mach No. Thickness Loss TLR Final Mach No.	.43	.255	.20	.16	.135	.11	.09	.08	.07	.06	.05	.04	-	-	-	-	.80
	-	.80	.76	.70	.60	.50	.46	.38	.35	.31	.24	.15	.12	.13	.11	.11	.80
	-	.045	.043	.040	.034	.028	.026	.022	.020	.018	.014	.009	.007	.007	.006	.006	.85
	-	.10	.09	.085	.08	.075	.07	.06	.055	.04	.04	-	-	-	-	-	.85
IBS-109 - 75°: Initial Mach No. Thickness Loss TLR Final Mach No.	.45	.29	.22	.17	.14	.115	.095	.08	.07	.06	.05	.04	-	-	-	-	.85
	-	.80	.81	.71	.61	.50	.44	.39	.38	.36	.30	-	-	-	-	-	.85
	-	.045	.046	.040	.035	.028	.025	.022	.022	.020	.017	-	-	-	-	-	.85
	-	.10	.09	.085	.08	.075	.07	.06	.055	.04	.04	-	-	-	-	-	.85
IBS-109 - 165°: Initial Mach No. Thickness Loss TLR Final Mach No.	.40	.255	.19	.15	.125	.105	.085	.075	.065	.06	.05	.04	-	-	-	-	.81
	-	.80	.76	.68	.57	.52	.45	.39	.38	.35	.28	.11	-	-	-	-	.81
	-	.045	.043	.039	.032	.030	.026	.022	.022	.020	.016	.006	-	-	-	-	.81
	-	.09	.085	.08	.075	.07	.065	.06	.05	.04	.03	-	-	-	-	-	.81
IBC-101 - 240°: Initial Mach No. Thickness Loss TLR Final Mach No.	.36	.22	.18	.145	.13	.10	.085	.07	.06	.055	.05	.04	-	-	-	-	.78
	-	.72	.76	.69	.55	.45	.39	.34	.31	.29	.29	.10	.10	.07	.07	.05	.78
	-	.041	.043	.039	.031	.026	.022	.019	.018	.016	.016	.006	.006	.004	.004	.003	.78
	-	.09	.085	.08	.075	.07	.065	.055	.05	.04	.03	-	-	-	-	-	.78
IBC-101 - 285°: Initial Mach No. Thickness Loss TLR Final Mach No.	.40	.315	.19	.16	.13	.11	.09	.08	.07	.06	.055	.04	-	-	-	-	.87
	-	.84	.70	.59	.52	.46	.41	.37	.36	.39	.37	.15	-	-	-	-	.87
	-	.048	.040	.034	.030	.026	.023	.021	.020	.022	.021	.009	-	-	-	-	.87
	-	.10	.095	.09	.08	.075	.07	.06	.05	.04	.03	-	-	-	-	-	.87
IBC-101 - 195°: Initial Mach No. Thickness Loss TLR Final Mach No.	.36	.235	.18	.14	.115	.10	.08	.07	.06	.05	.05	.05	-	-	-	-	.80
	-	.77	.71	.62	.52	.45	.41	.35	.34	.29	.29	-	-	-	-	-	.80
	-	.044	.040	.035	.030	.026	.023	.020	.019	.016	.016	-	-	-	-	-	.80
	-	.09	.085	.08	.075	.07	.06	.055	.04	.03	.03	-	-	-	-	-	.80

Summary of Insulation Specimen Performance Data, S/N III-1

Figure 7

	Location																	Max.
	8	9	10	11	12	13	14	15	16	17	18	19	20	21	22	23		
V-44 - 0°:																		
Initial Mach No.	.40	.27	.20	.165	.13	.115	.095	.085	.075	.065	.06	.03	-	-	-	-	-	
Thickness Loss	-	.75	.70	.56	.45	.39	.32	.25	.19	.14	.14	.11	.08	.06	.03	.78		
TTR	-	.043	.040	.032	.026	.022	.018	.014	.011	.008	.008	.006	.005	.005	.002	.045		
Final Mach No.	.15	.105	.095	.09	.085	.08	.075	.07	.065	.06	.05	-	-	-	-	-		
V-44 - 45°:																		
Initial Mach No.	.36	.255	.19	.16	.125	.11	.09	.08	.07	.06	.055	.03	-	-	-	.50		
Thickness Loss	-	.48	.49	.45	.44	.36	.31	.28	.19	.15	.15	.09	-	-	-	.029		
TTR	-	.027	.028	.026	.025	.021	.018	.016	.011	.009	.009	.005	-	-	-	-		
Final Mach No.	.19	.125	.11	.095	.085	.08	.075	.07	.06	.055	.045	-	-	-	-	-		
V-44 - 315°:																		
Initial Mach No.	.40	.30	.22	.17	.13	.115	.095	.08	.075	.065	.055	.03	-	-	-	.60		
Thickness Loss	-	.57	.52	.45	.39	.37	.34	.28	.25	.24	.22	.09	-	-	-	.034		
TTR	-	.033	.030	.026	.022	.021	.019	.016	.014	.014	.013	.005	-	-	-	-		
Final Mach No.	-	.125	.12	.105	.09	.08	.075	.005	.06	.05	.04	-	-	-	-	-		
IBS-107 - 120°:																		
Initial Mach No.	.42	.28	.20	.16	.13	.11	.09	.08	.07	.065	.05	.03	.09	.08	.04	.38		
Thickness Loss	-	.34	.34	.31	.27	.24	.22	.21	.20	.18	.15	.10	.09	.08	.08	.022		
TTR	-	.019	.019	.018	.015	.014	.013	.012	.011	.010	.009	.006	.005	.005	.002	-		
Final Mach No.	.33	.16	.13	.115	.10	.085	.08	.07	.06	.05	-	-	-	-	-	-		
IBS-107 - 75°:																		
Initial Mach No.	.42	.27	.21	.16	.13	.11	.09	.08	.07	.065	.045	.03	-	-	-	.35		
Thickness Loss	-	.30	.32	.23	.22	.21	.20	.18	.17	.16	.11	.10	-	-	-	.020		
TTR	-	.017	.018	.014	.013	.012	.011	.010	.010	.009	.006	.006	-	-	-	-		
Final Mach No.	.33	.17	.14	.12	.10	.09	.08	.07	.06	.055	-	-	-	-	-	-		
IBS-107 - 165°:																		
Initial Mach No.	.44	.28	.20	.17	.13	.11	.09	.08	.075	.065	.055	.03	-	-	-	.37		
Thickness Loss	-	.34	.32	.30	.25	.22	.21	.20	.18	.17	.18	.10	-	-	-	.021		
TTR	-	.019	.018	.017	.014	.013	.012	.011	.010	.010	.010	.006	-	-	-	-		
Final Mach No.	.28	.16	.14	.115	.105	.09	.08	.07	.065	.055	-	-	-	-	-	-		
Avcoat II - 240°:																		
Initial Mach No.	.50	.30	.21	.17	.135	.115	.095	.085	.075	.070	.055	.03	.13	.13	.13	.95		
Thickness Loss	-	.65	.95	.92	.85	.74	.65	.61	.51	.24	.15	.11	.13	.13	.13	.054		
TTR	-	.037	.054	.053	.049	.042	.037	.035	.029	.014	.009	.006	.007	.007	.007	.054		
Final Mach No.	.28	.085	.08	.07	.07	.065	.06	.055	.05	.055	-	-	-	-	-	-		
Avcoat II - 195°:																		
Initial Mach No.	.44	.27	.21	.165	.13	.11	.095	.085	.075	.065	.055	.03	-	-	-	.97		
Thickness Loss	-	.63	.97	.90	.84	.75	.67	.67	.70	.52	.28	.11	-	-	-	.055		
TTR	-	.036	.055	.051	.048	.043	.038	.038	.040	.030	.016	.006	-	-	-	-		
Final Mach No.	.30	.085	.08	.075	.07	.065	.055	.045	.03	.04	-	-	-	-	-	-		
Avcoat II - 285°:																		
Initial Mach No.	.46	.30	.22	.175	.14	.115	.095	.085	.075	.065	.055	.03	-	-	-	.100		
Thickness Loss	-	.70	.97	.90	.78	.70	.63	.60	.60	.39	.22	.10	-	-	-	.057		
TTR	-	.040	.055	.051	.045	.040	.036	.036	.034	.022	.013	.006	-	-	-	-		
Final Mach No.	.32	.09	.085	.075	.07	.065	.06	.05	.045	.05	--	-	-	-	-	-		

Summary of Insulation Specimen Performance Data, S/N III-2

Figure 8

	Locations																	Max.
	8	9	10	11	12	13	14	15	16	17	18	19	20	21	22	23		
V-44: 0° Initial Mach No. Thickness Loss TLR	.44 .25 .014	.27 .68 .039	.21 .70 .040	.17 .60 .034	.135 .51 .029	.11 .44 .025	.095 .36 .021	.085 .31 .018	.075 .27 .015	.065 .23 .014	.055 .22 .013	.03 .10 .006	- .07 .004	- .05 .003	- .03 .002	- .03 .002	.74 .042	
V-44: 45° Initial Mach No. Thickness Loss TLR	.38 -	.26 .68 .039	.21 .63 .036	.16 .60 .034	.13 .54 .031	.11 .44 .025	.09 .39 .022	.08 .33 .019	.07 .27 .015	.065 .24 .014	.055 .23 .014	.03 .15 .009	- - -	- - -	- - -	- - -	.68 .039	
V-44: 315° Initial Mach No. Thickness Loss TLR	.44 -	.30 .66 .038	.22 .64 .037	.175 .56 .032	.14 .48 .027	.115 .41 .023	.095 .35 .020	.085 .30 .017	.075 .26 .015	.07 .28 .016	.06 .24 .014	.03 .13 .007	- - -	- - -	- - -	- - -	.70 .040	
IBT-106: 75° Initial Mach No. Thickness Loss TLR	.38 - -	.26 .51 .029	.20 .43 .025	.16 .45 .026	.125 .32 .018	.11 .26 .015	.09 .22 .013	.08 .22 .013	.07 .21 .012	.06 .22 .013	.05 .17 .010	- .06 .003	- - -	- - -	- - -	- - -	.51 .029	
IBT-106: 120° Initial Mach No. Thickness Loss TLR	.40 .25 .014	.28 .53 .030	.21 .42 .024	.16 .40 .023	.125 .30 .017	.11 .20 .011	.09 .24 .014	.08 .25 .014	.07 .21 .012	.06 .20 .011	.05 .16 .009	- .05 .003	- .05 .003	- .05 .003	- .05 .003	- .05 .003	.53 .030	
IBT-106: 165° Initial Mach No. Thickness Loss TLR	.40 - -	.27 .50 .029	.21 .37 .021	.16 .35 .020	.13 .19 .011	.11 .20 .011	.09 .27 .015	.08 .22 .013	.07 .21 .012	.06 .20 .011	.055 .19 .011	- - -	- - -	- - -	- - -	- - -	.50 .029	
IBC-111G: 195° Initial Mach No. Thickness Loss TLR	.40 - -	.26 .38 .022	.20 .37 .021	.16 .24 .014	.125 .19 .011	.105 .20 .011	.09 .18 .010	.08 .16 .009	.07 .14 .008	.06 .14 .008	.055 .14 .008	.01 .14 .008	- - -	- - -	- - -	- - -	.40 .023	
IBC-111G: 240° Initial Mach No. Thickness Loss TLR	.40 .13 .007	.27 .30 .017	.21 .25 .014	.16 .29 .017	.13 .27 .015	.11 .19 .011	.09 .07 .010	.08 .16 .009	.075 .14 .008	.065 .14 .008	.055 .15 .009	.01 .10 .006	- .10 .006	- .10 .006	- .08 .005	- .08 .005	.32 .018	
IBC-111: 285° Initial Mach No. Thickness Loss TLR	.42 - -	.28 .42 .024	.21 .49 .028	.165 .37 .021	.13 .26 .015	.11 .20 .011	.09 .19 .011	.08 .17 .010	.075 .16 .009	.065 .14 .008	.055 .12 .007	- .10 .006	- - -	- - -	- - -	- - -	.49 .028	

Summary of Insulation Specimen Performance Data, S/N III-3

Figure 9

	Locations																	Max.
	8	9	10	11	12	13	14	15	16	17	18	19	20	21	22	23		
V-44: 0°																		
Initial Mach No.	.40	.28	.21	.165	.13	.11	.095	.085	.075	.065	.05	.03	-	-	-	-		
Thickness Loss	.46	.69	.68	.58	.47	.39	.35	.32	.25	.18	.12	.05	.05	.05	.04	.03	.69	
TTLR	.026	.039	.039	.033	.027	.022	.020	.018	.014	.010	.007	.003	.003	.003	.002	.002	.039	
V-44: 45°																		
Initial Mach No.	.40	.28	.22	.17	.135	.11	.095	.085	.075	.065	.055	.03	-	-	-	-	.74	
Thickness Loss	-	.74	.70	.60	.52	.42	.35	.32	.28	.24	.22	.08	-	-	-	-	.74	
TTLR	-	.042	.040	.034	.030	.025	.020	.018	.016	.014	.013	.005	-	-	-	-	.042	
V-44: 315°																		
Initial Mach No.	.38	.27	.20	.165	.13	.11	.09	.08	.07	.065	.05	.03	-	-	-	-	.62	
Thickness Loss	-	.60	.60	.56	.48	.40	.34	.29	.22	.24	.18	.08	-	-	-	-	.62	
TTLR	-	.034	.034	.032	.027	.023	.019	.017	.013	.014	.010	.005	-	-	-	-	.035	
IFT-106: 75°																		
Initial Mach No.	.38	.27	.21	.17	.13	.115	.095	.085	.075	.065	.055	.03	-	-	-	-	.59	
Thickness Loss	-	.59	.47	.39	.37	.32	.28	.22	.19	.18	.12	.07	-	-	-	-	.59	
TTLR	-	.034	.207	.022	.021	.018	.016	.013	.011	.010	.010	.007	-	-	-	-	.034	
USR-3800: 120°																		
Initial Mach No.	.44	.28	.21	.17	.135	.115	.095	.085	.075	.065	.055	.03	-	-	-	-	.11	
Thickness Loss	.05	.04	.05	.05	.05	.08	.11	.10	.09	.05	.05	.05	.05	.03	.03	.03	.11	
TTLR	.003	.002	.003	.003	.003	.005	.006	.006	.005	.003	.003	.003	.003	.002	.002	.002	.006	
IFT-100: 165°																		
Initial Mach No.	.38	.26	.2	.16	.13	.11	.09	.08	.07	.065	.055	-	-	-	-	-	.32	
Thickness Loss	-	.27	.26	.19	.19	.18	.13	.16	.07	.10	.12	-	-	-	-	-	.32	
TTLR	-	.017	.015	.011	.011	.010	.007	.009	.004	.006	.007	-	-	-	-	-	.018	
4OSD-80: 195°																		
Initial Mach No.	.32	.21	.18	.14	.12	.10	.085	.075	.065	.055	.05	.03	-	-	-	-	.58	
Thickness Loss	-	.51	.56	.51	.45	.45	.47	.46	.43	.33	.25	.16	-	-	-	-	.58	
TTLR	-	.029	.032	.029	.026	.026	.027	.026	.025	.019	.014	.009	-	-	-	-	.033	
4OSD-80: 240°																		
Initial Mach No.	.36	.23	.175	.14	.12	.095	.085	.075	.065	.055	.05	.03	-	-	-	-	.58	
Thickness Loss	.42	.56	.55	.58	.56	.50	.45	.38	.35	.33	.30	.10	.12	.10	.09	.06	.58	
TTLR	.025	.033	.031	.033	.032	.029	.026	.022	.020	.019	.017	.006	.007	.006	.005	.003	.033	
4OSD-80: 285°																		
Initial Mach No.	.37	.24	.18	.145	.12	.10	.085	.075	.065	.055	.05	.03	-	-	-	-	.63	
Thickness Loss	-	.58	.62	.52	.50	.44	.38	.38	.40	.36	.24	.10	-	-	-	-	.63	
TTLR	-	.033	.035	.030	.029	.025	.022	.022	.023	.021	.014	.006	-	-	-	-	.036	

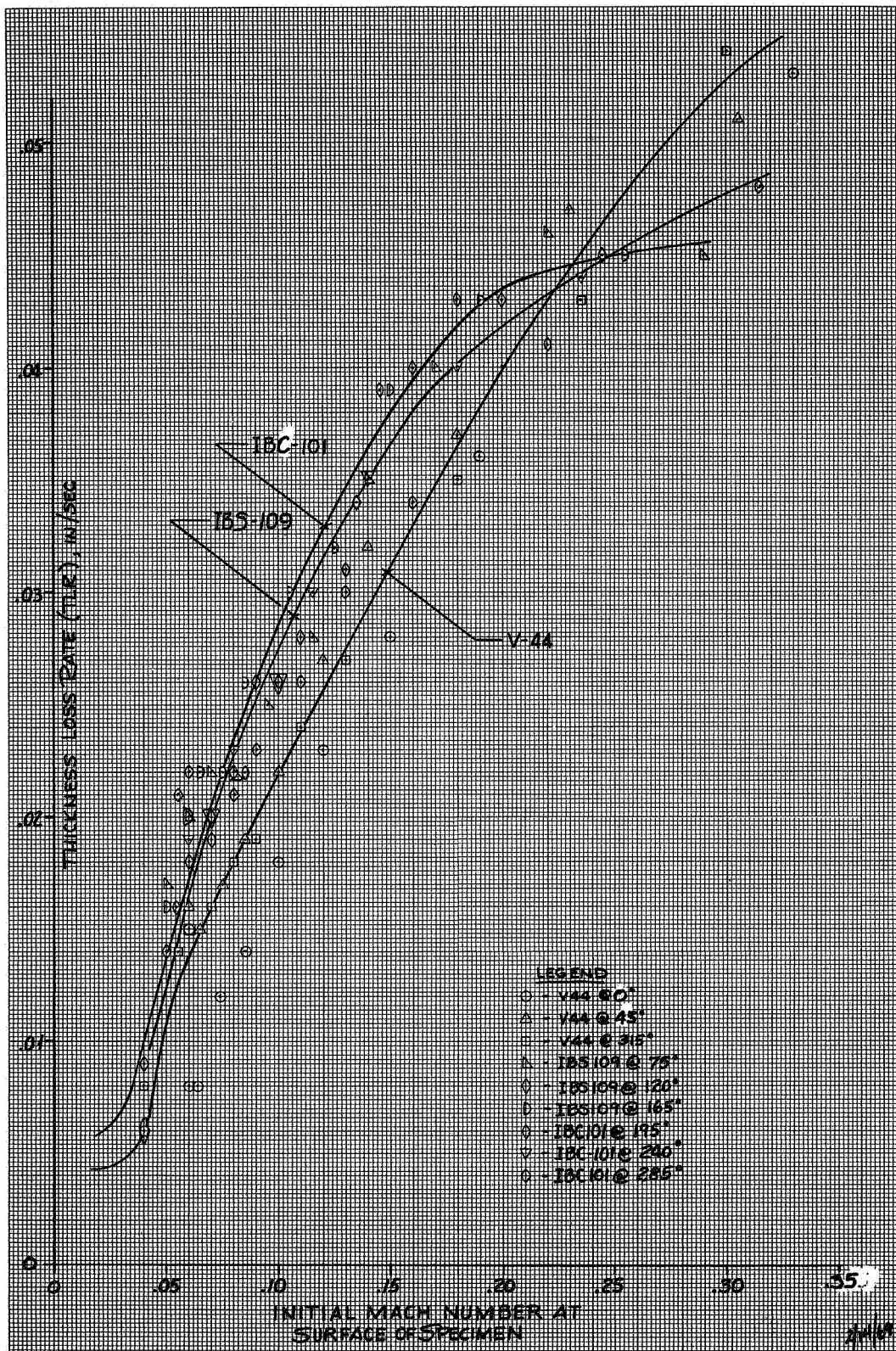
Summary of Insulation Specimen Performance Data, S/N III-4

Figure 10

	Location																	Max.
	8	9	10	11	12	13	14	15	16	17	18	19	20	21	22			
V-44: 0°																		
Initial Mach No.	.42	.28	.22	.17	.13	.115	.09	.085	.075	.065	.055	.03	-	-	-	-		
Thickness Loss	.21	.55	.63	.54	.46	.39	.34	.28	.22	.18	.17	.10	.08	.07	.06	.67		
TTLR	-	.032	.036	.031	.027	.023	.020	.016	.013	.010	.010	.006	.005	.004	.003	.039		
V-44: 45°																		
Initial Mach No.	.40	.26	.21	.16	.13	.115	.09	.085	.075	.065	.055	.03	-	-	-	-		
Thickness Loss	.15	.53	.51	.44	.39	.37	.32	.28	.22	.18	.16	.10	.05	-	-	.56		
TTLR	-	.031	.030	.025	.023	.021	.019	.016	.013	.010	.009	.006	.003	-	-	.032		
V-44: 315°																		
Initial Mach No.	.42	.28	.22	.17	.13	.115	.09	.085	.075	.065	.055	.03	-	-	-	-		
Thickness Loss	.20	.58	.58	.50	.47	.39	.32	.26	.22	.18	.14	.10	-	-	-	.67		
TTLR	-	.034	.034	.029	.027	.023	.019	.015	.013	.010	.008	.006	-	-	-	.039		
IBT-100: 75°																		
Initial Mach No.	.42	.27	.22	.17	.13	.115	.09	.085	.075	.065	.055	.03	-	-	-	-		
Thickness Loss	.16	.49	.43	.40	.34	.29	.26	.24	.24	.20	.14	.06	.05	-	-	.50		
TTLR	-	.028	.025	.023	.020	.017	.015	.014	.014	.012	.008	.003	.003	-	-	.029		
IBT-100: 120°																		
Initial Mach No.	.44	.28	.22	.17	.13	.11	.09	.085	.075	.065	.055	.03	-	-	-	-		
Thickness Loss	.18	.52	.44	.40	.35	.32	.32	.28	.25	.22	.20	.12	.06	.05	.04	.54		
TTLR	-	.030	.025	.023	.020	.019	.019	.016	.014	.013	.012	.007	.003	.003	.002	.031		
IBT-100: 165°																		
Initial Mach No.	.42	.28	.22	.17	.13	.11	.09	.085	.075	.065	.055	.03	-	-	-	-		
Thickness Loss	.15	.45	.41	.35	.32	.30	.25	.22	.23	.17	.16	.06	-	-	-	.48		
TTLR	-	.026	.024	.020	.019	.017	.014	.013	.013	.010	.009	.003	-	-	-	.028		
TI-H704B: 195°																		
Initial Mach No.	.40	.26	.21	.17	.13	.115	.09	.085	.075	.065	.06	.03	-	-	-	-		
Thickness Loss	.12	.72	.73	.64	.55	.48	.38	.33	.28	.24	.15	.05	-	-	-	.79		
TTLR	-	.042	.042	.037	.032	.028	.022	.019	.016	.014	.009	.003	-	-	-	.046		
TI-H704B: 240°																		
Initial Mach No.	.40	.26	.20	.16	.13	.115	.09	.085	.075	.065	.06	.03	-	-	-	-		
Thickness Loss	.23	.72	.61	.52	.46	.41	.37	.34	.28	.27	.20	.05	.05	.05	.05	.72		
TTLR	-	.042	.035	.030	.027	.024	.021	.020	.016	.016	.012	.003	.003	.003	.003	.042		
TI-H704B: 285°																		
Initial Mach No.	.42	.28	.21	.17	.13	.115	.095	.085	.075	.065	.06	.03	-	-	-	-		
Thickness Loss	.15	.68	.61	.56	.49	.47	.39	.31	.29	.28	.25	.06	-	-	-	.73		
TTLR	-	.039	.035	.032	.029	.027	.023	.018	.017	.016	.014	.003	-	-	-	.042		

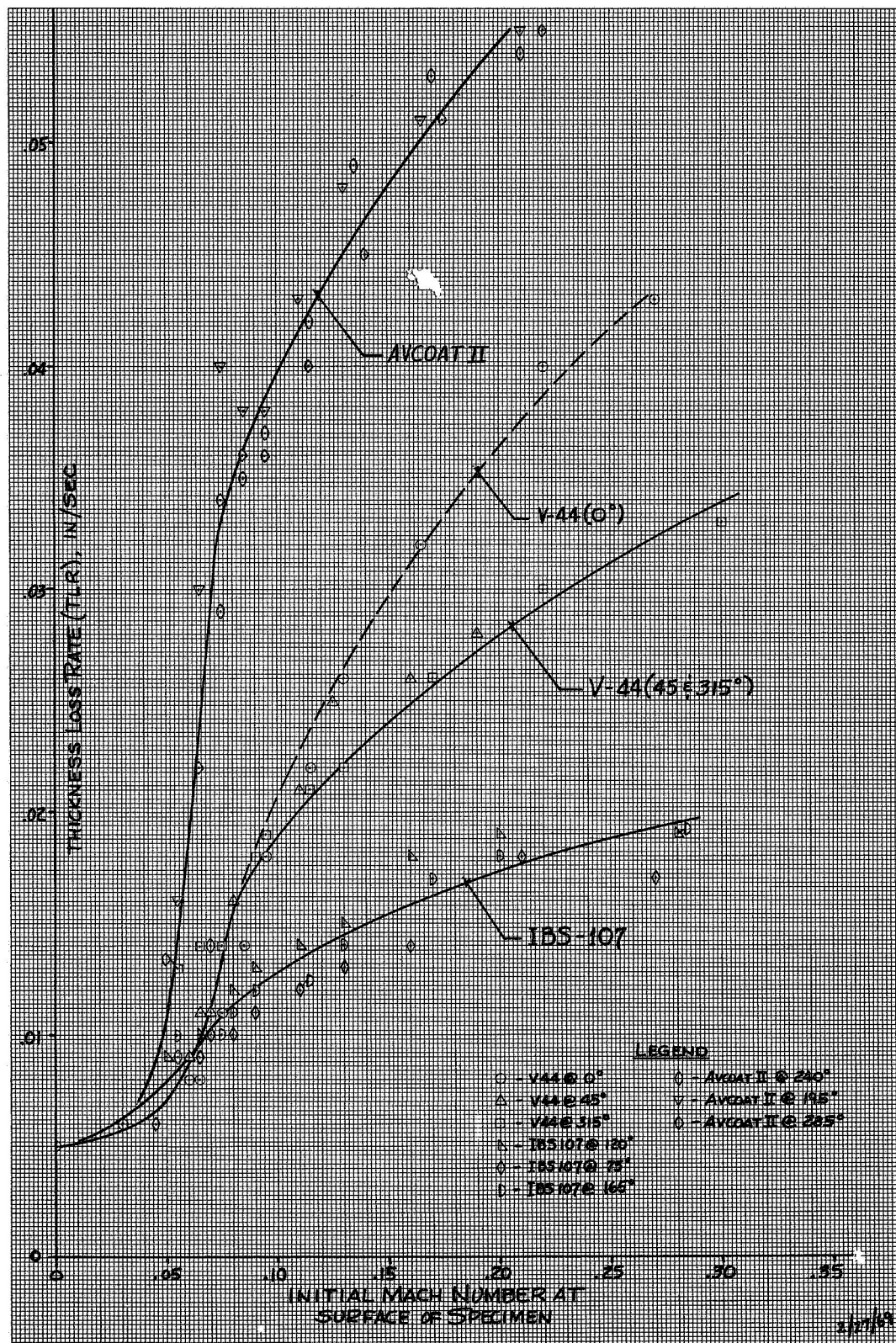
Summary of Insulation Specimen Performance Data, S/N III-5

Figure 11



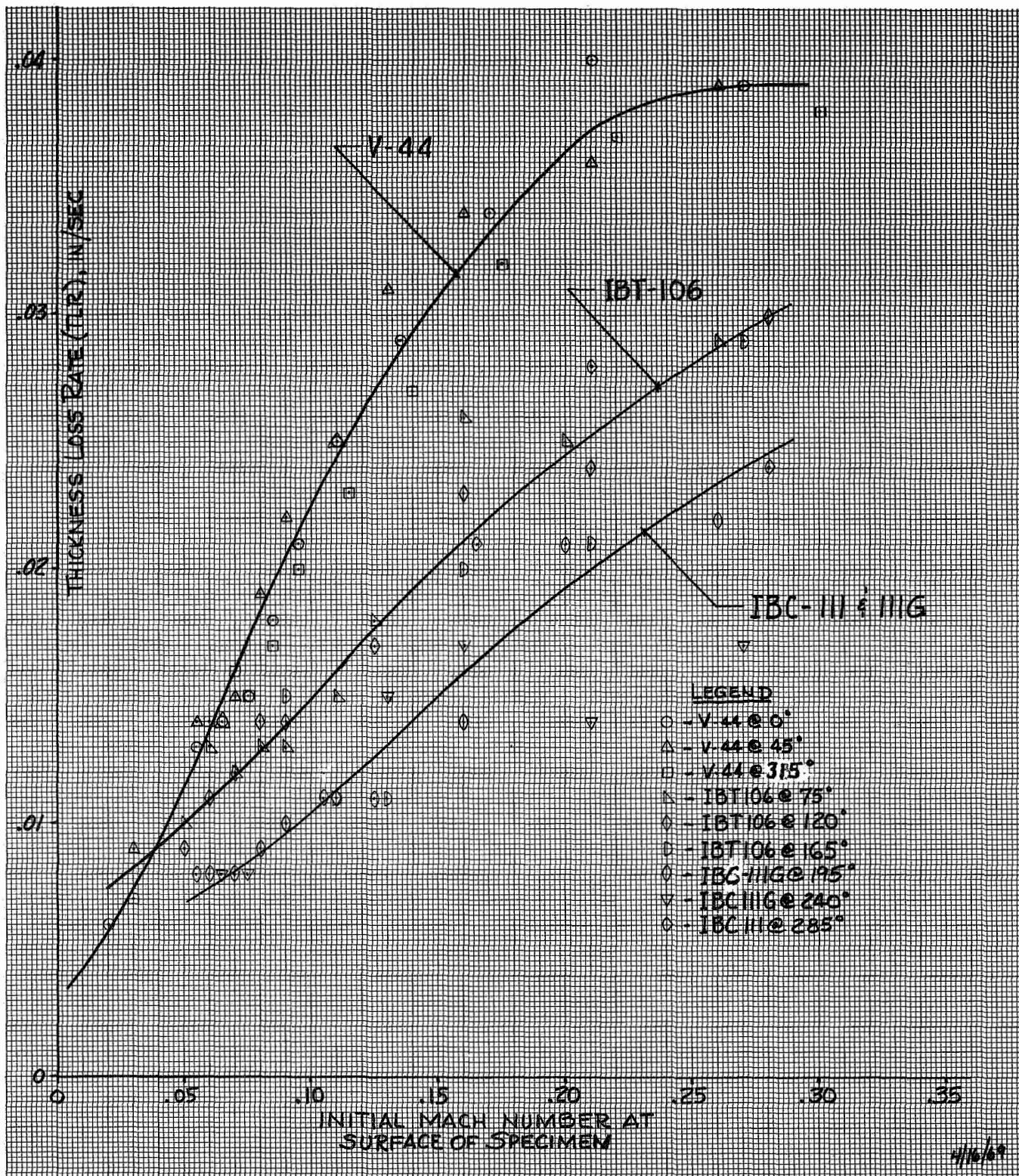
Motor S/N III-1, Thickness Loss Rate-vs-Initial Mach Number  
for IBS-109, IBC-101, and V-44 Control

Figure 12



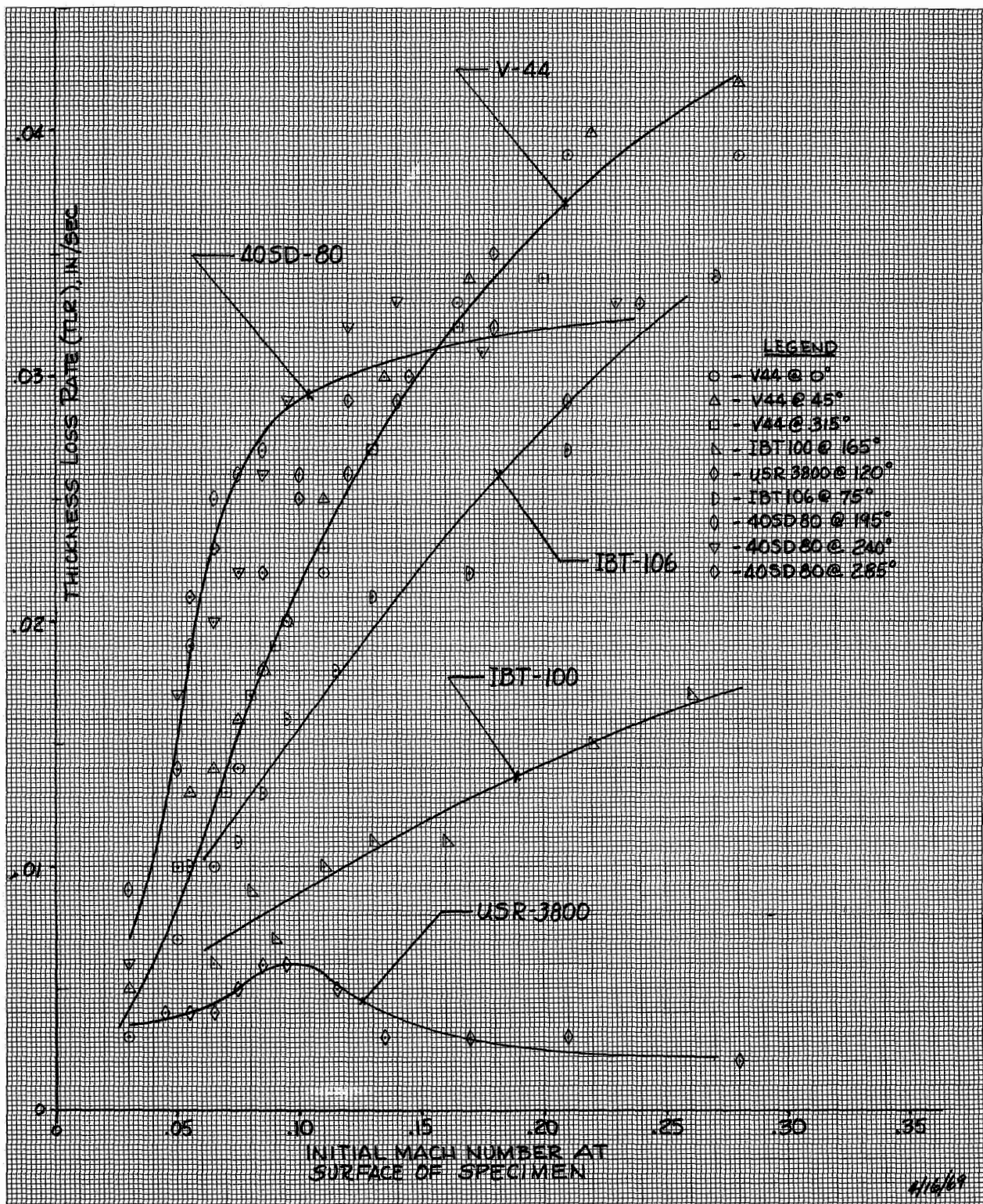
Motor S/N III-2, Thickness Loss Rate-vs-Initial Mach Number  
for Avcoat II, IBS-107, and V-44 Control

Figure 13



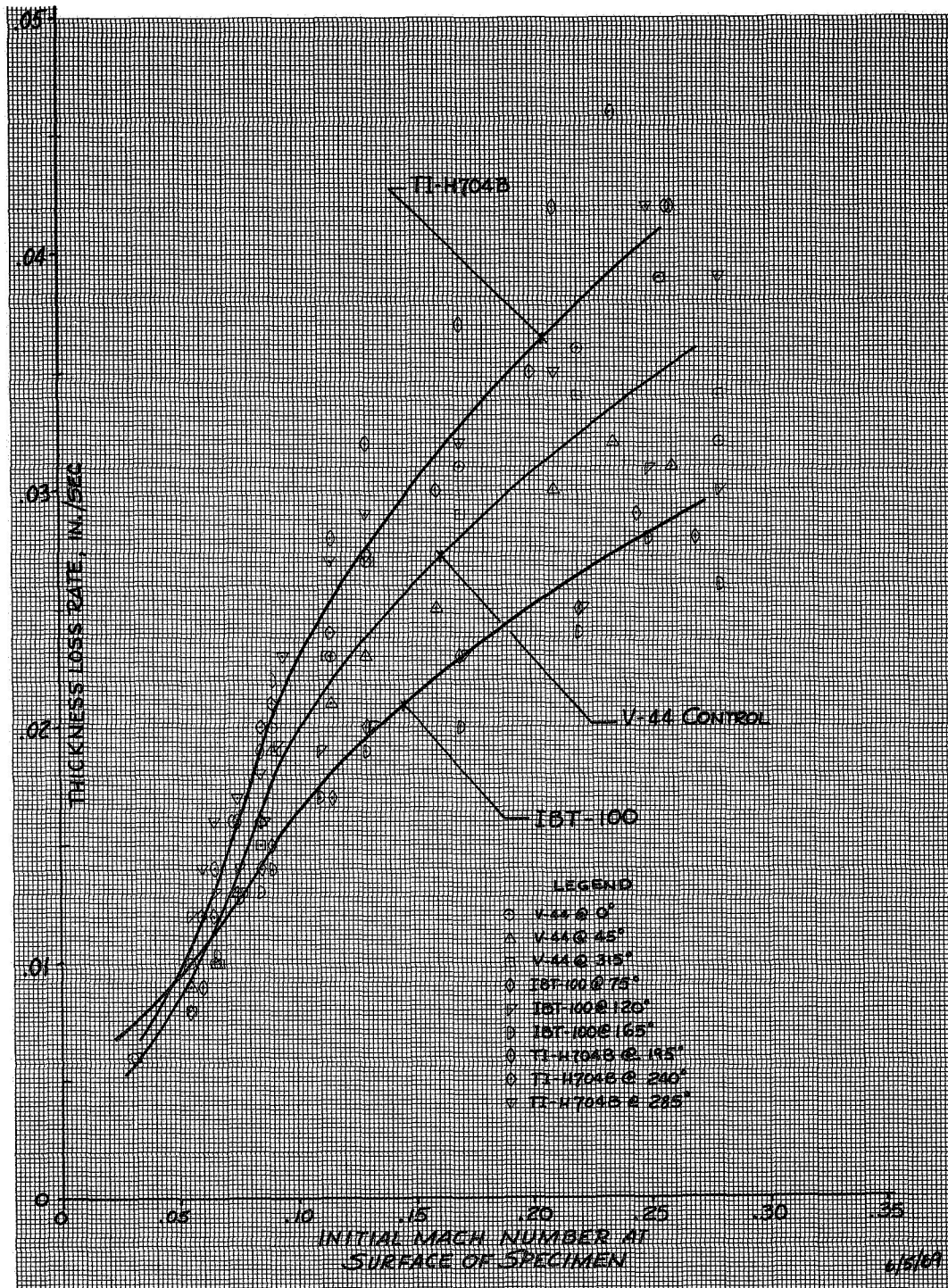
Motor S/N III-3, Thickness Loss Rate-vs-Initial Mach Number  
for IBT-106, IBC-111 and 111G, and V-44 Control

Figure 14



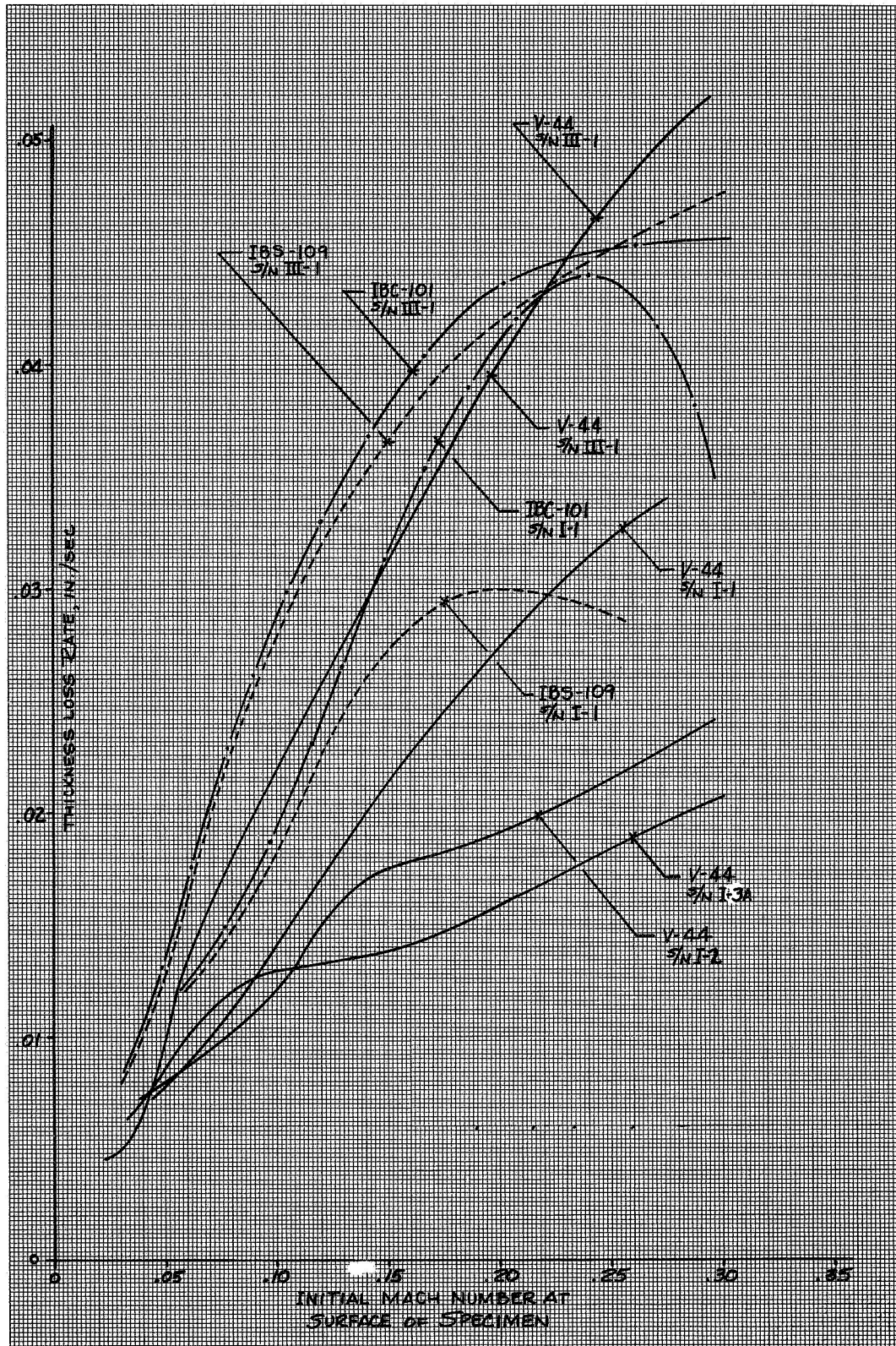
Motor S/N III-4, Thickness Loss Rate-vs-Initial Mach Number  
for 40SD-80, IBT-106, IBT-100, USR-3800, and V044 Control

Figure 15



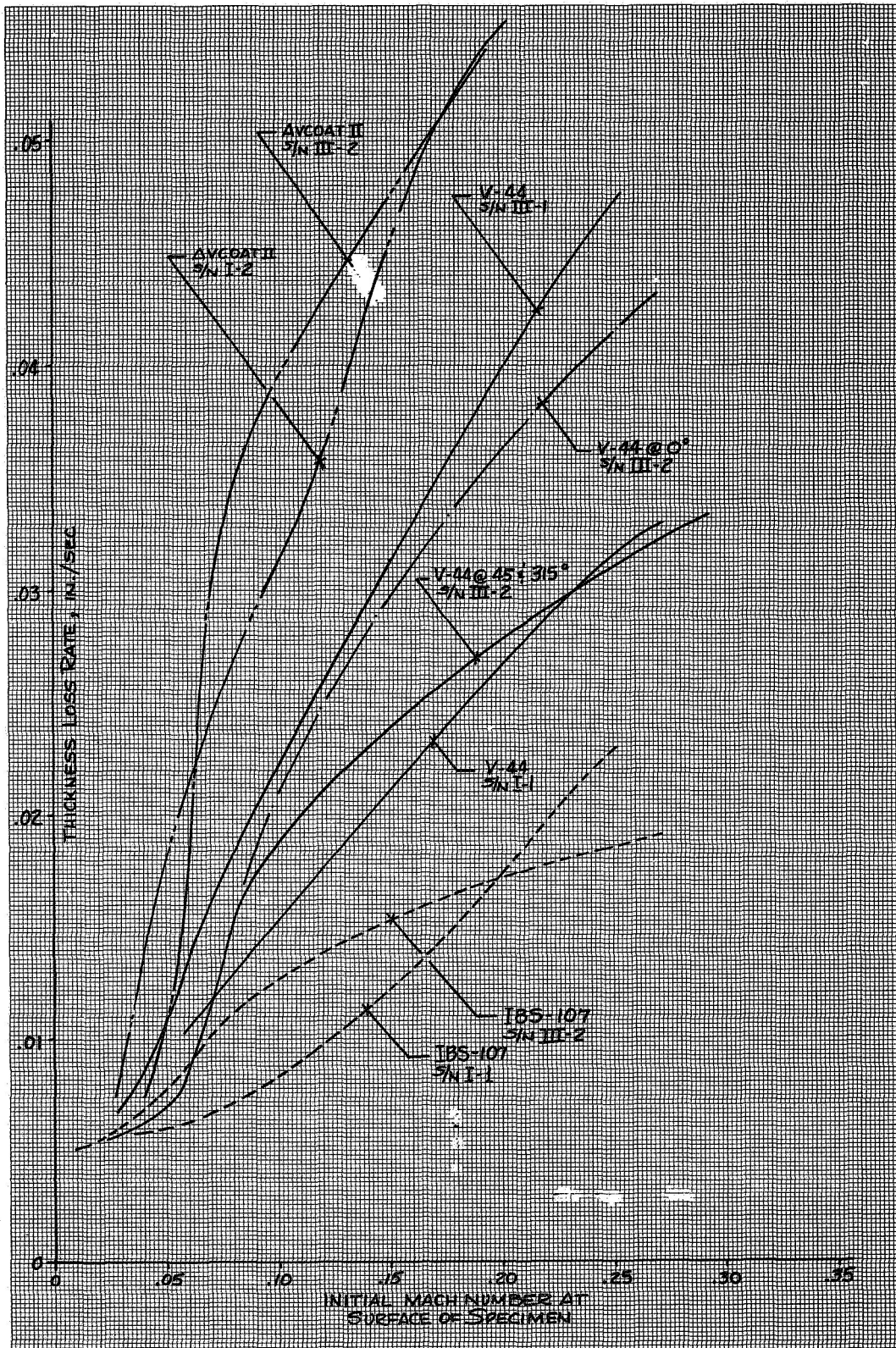
Motor S/N III-5, Thickness Loss Rate-vs-Initial Mach Number  
for TI-H704B, IBT-100, and V-44 Control

Figure 16



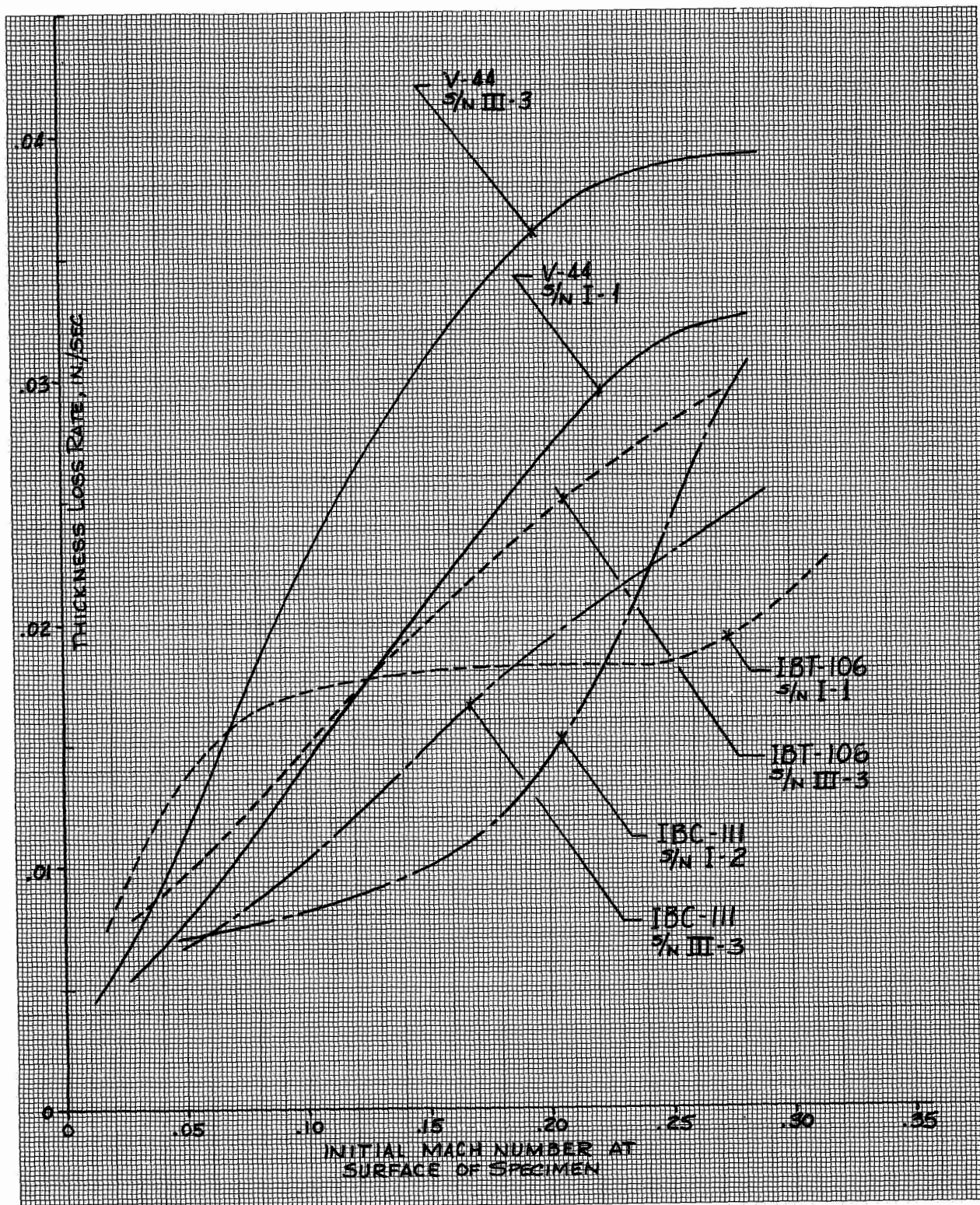
Comparison of TLR-vs-Initial Mach Number Data for IBS-109, IBC-101, and V-44 Controls in Motors S/N I-1, I-2, and III-1

Figure 17



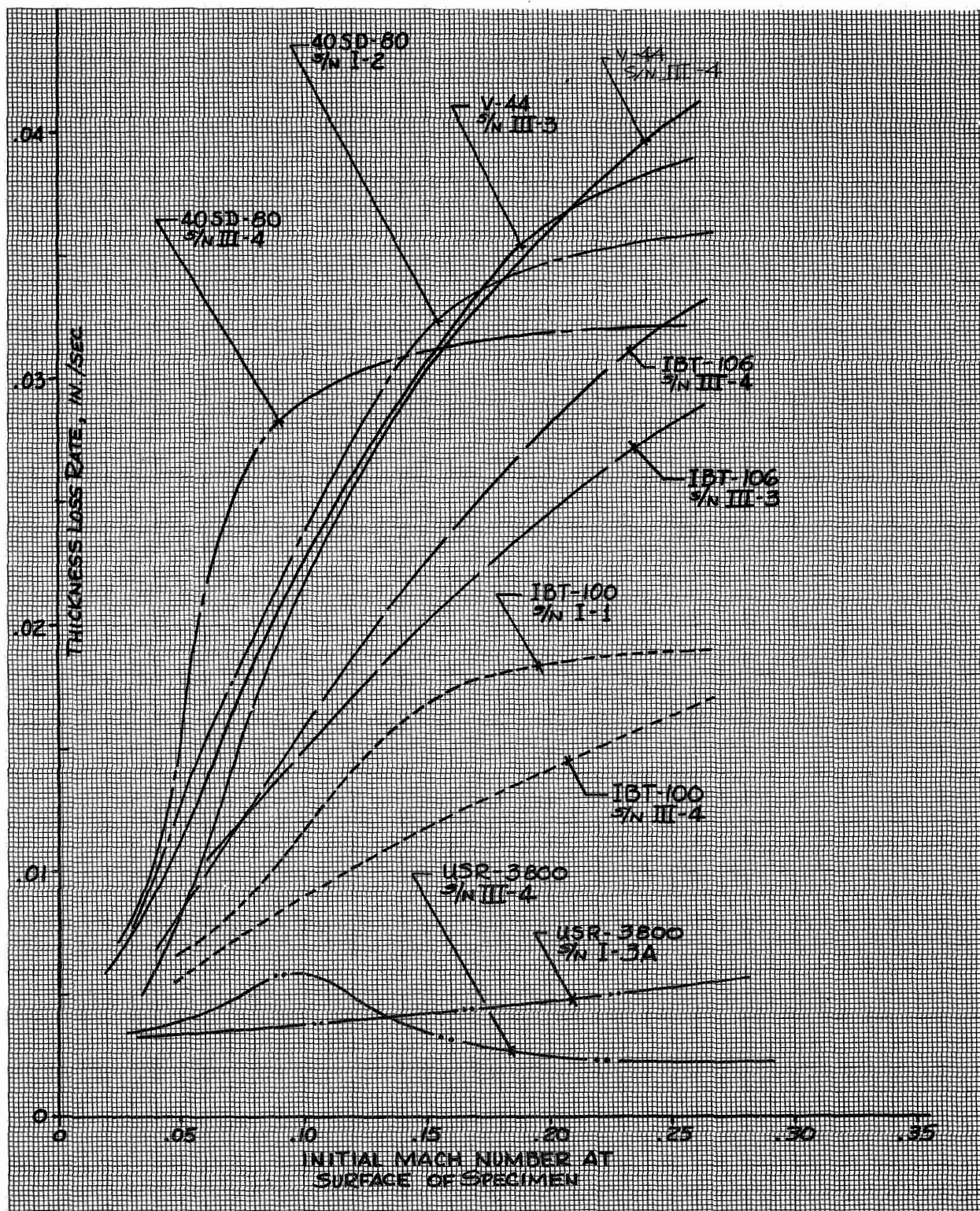
Comparison of TLR-vs-Initial Mach Number Data for IBS-107, Avcoat II, and V-44 Controls in Motors I-1, I-2, and III-2

Figure 18

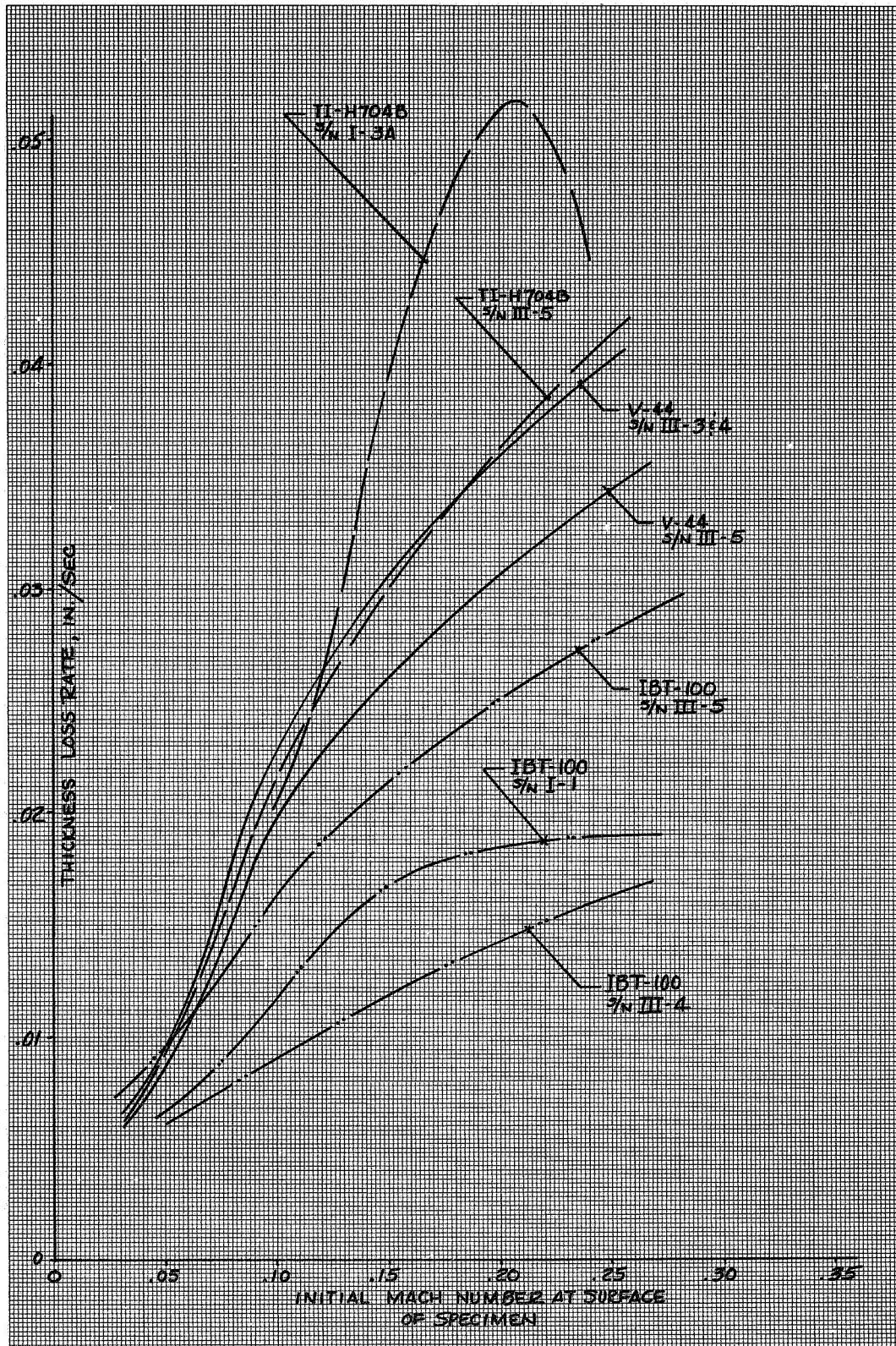


Comparison of TLR-vs-Initial Mach Number Data for IBT-106, IBC-111, and V-44 Controls in Motors I-1, I-2, and III-3

Figure 19

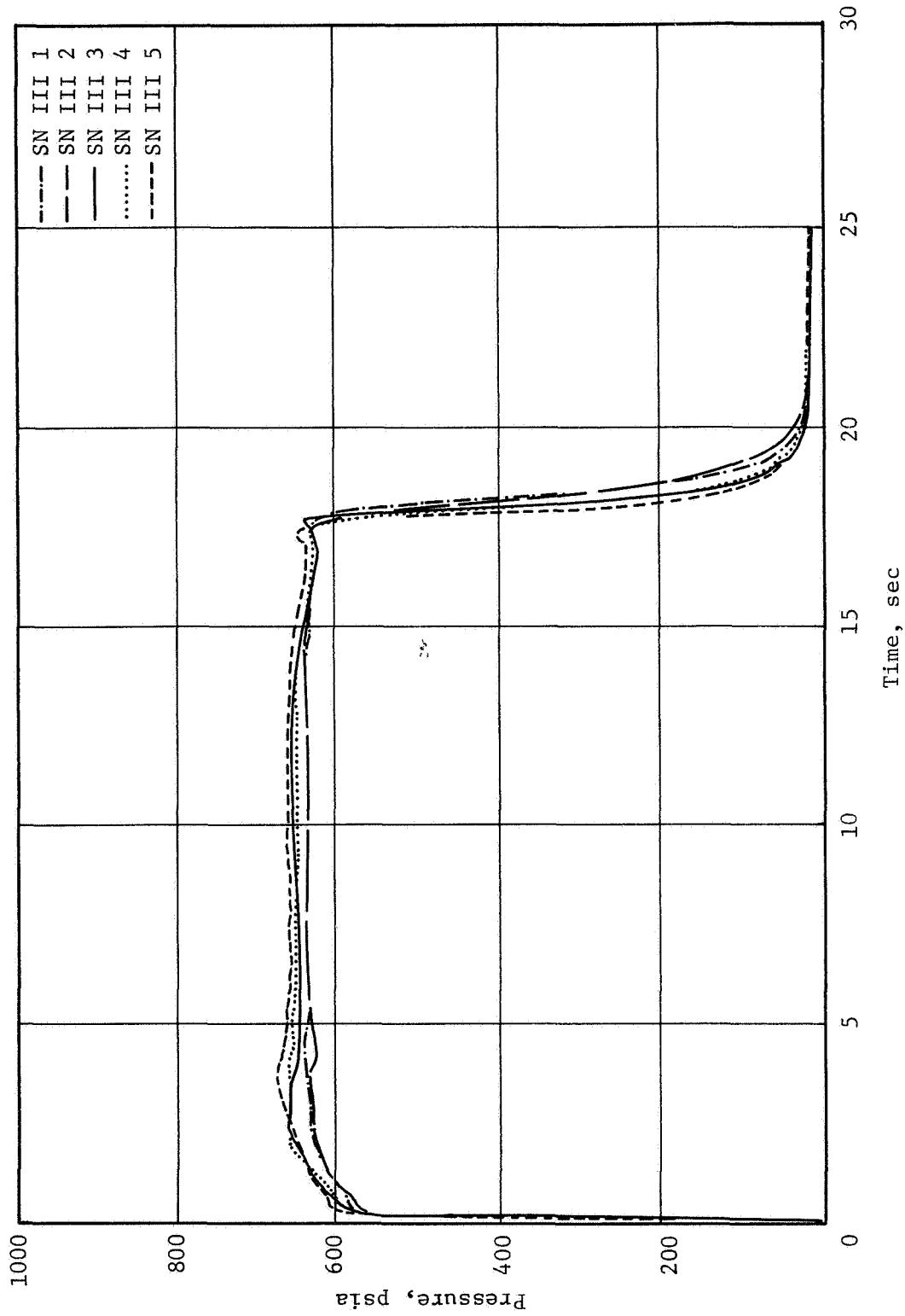


Comparison of TLR-vs-Initial Mach Number Data for 40SD-80, USR-3800, IBT-106, IBT-100, and V-44 Controls in Motors I-1, I-2, III-3, and III-4



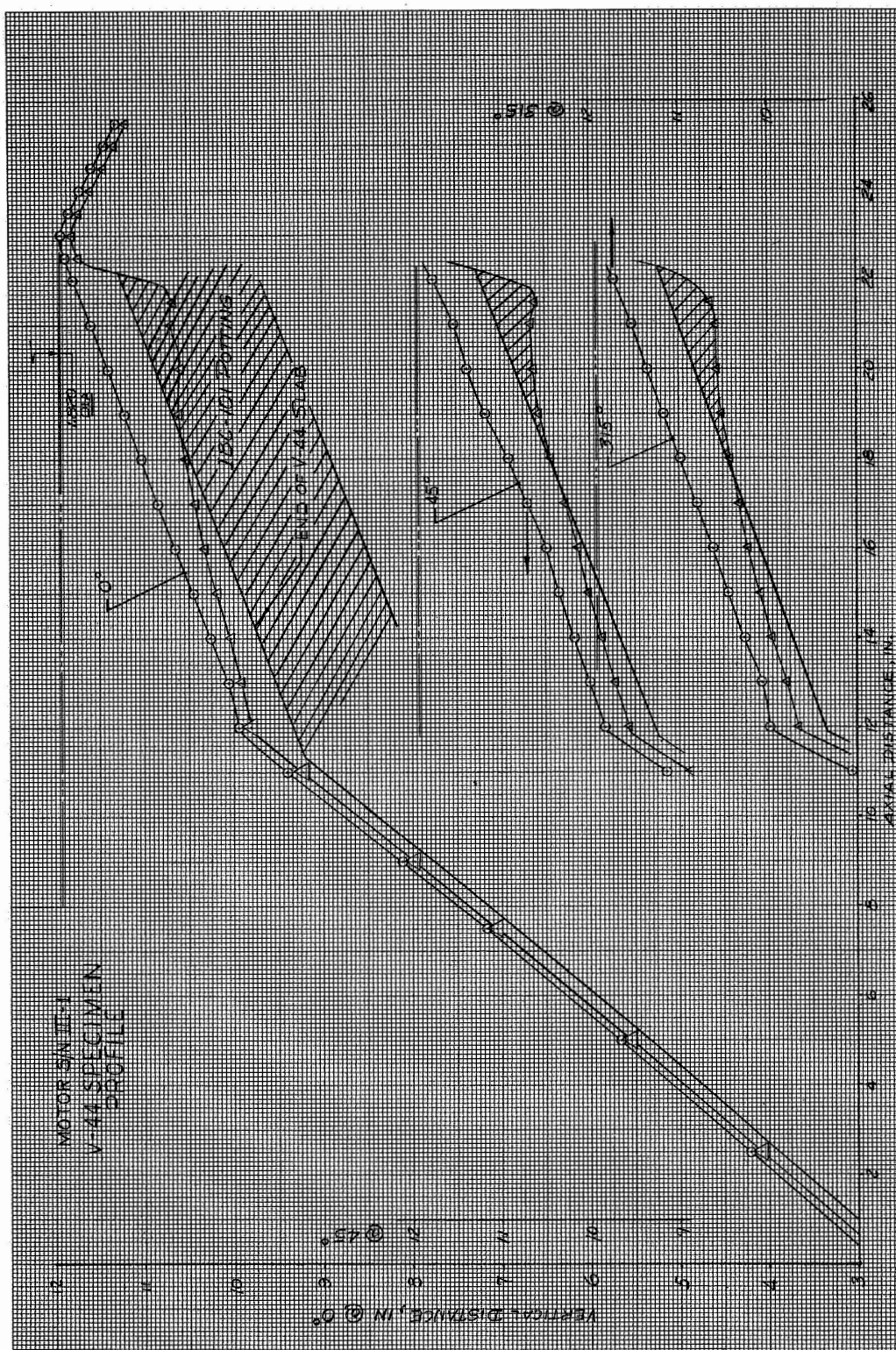
Comparison of TLR-vs-Initial Mach Number Data for IBT-100, TI-H704B, and V-44 Controls in Motors I-1, I-3A, and III-5

**APPENDIX I**  
**BALLISTIC PERFORMANCE CURVES FOR**  
**TASK III LMISD TEST MOTORS S/N III-1 THROUGH S/N III-5**



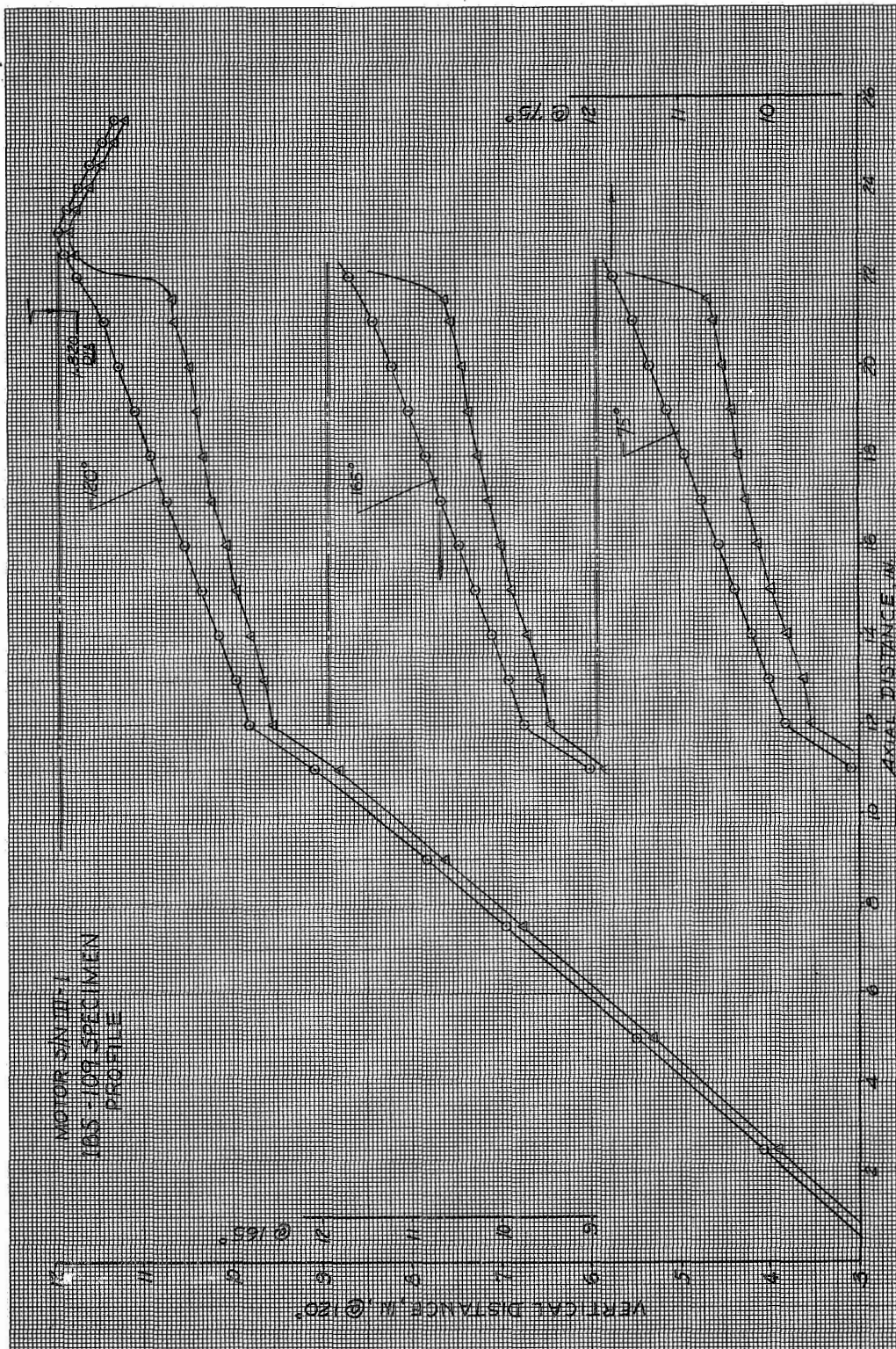
Ballistic Performance Curves for Task III IMISD Test Motors  
S/N III-1 through S/N III-5

**APPENDIX II**  
**INSULATION MATERIAL SPECIMEN PRE- AND POSTTEST PROFILES,**  
**MOTOR S/N III-1 THROUGH S/N III-5**



Motor S/N III-1, V-44 Specimen Profile

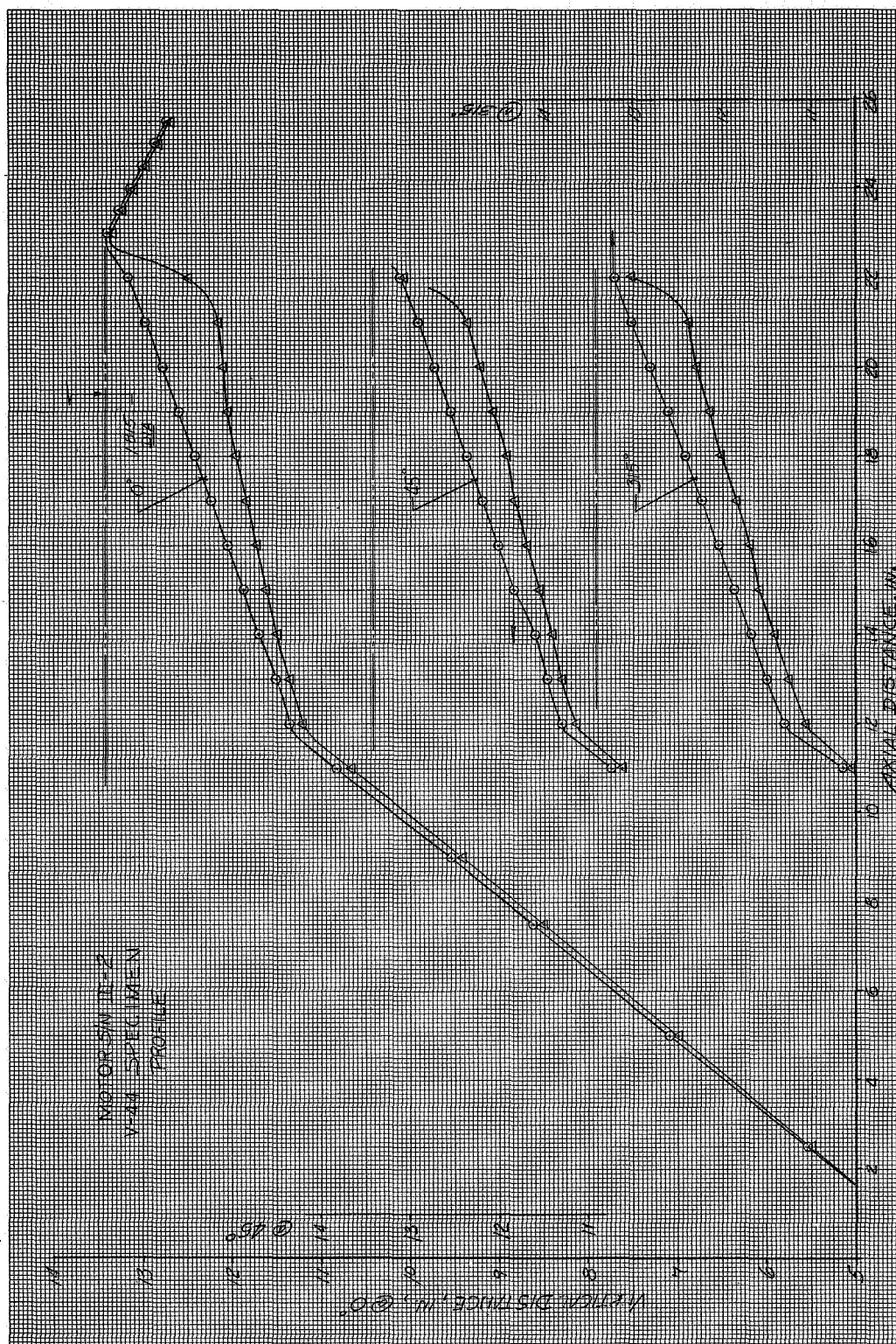
Figure 1



Motor S/N III-1, IBS-109 Specimen Profile

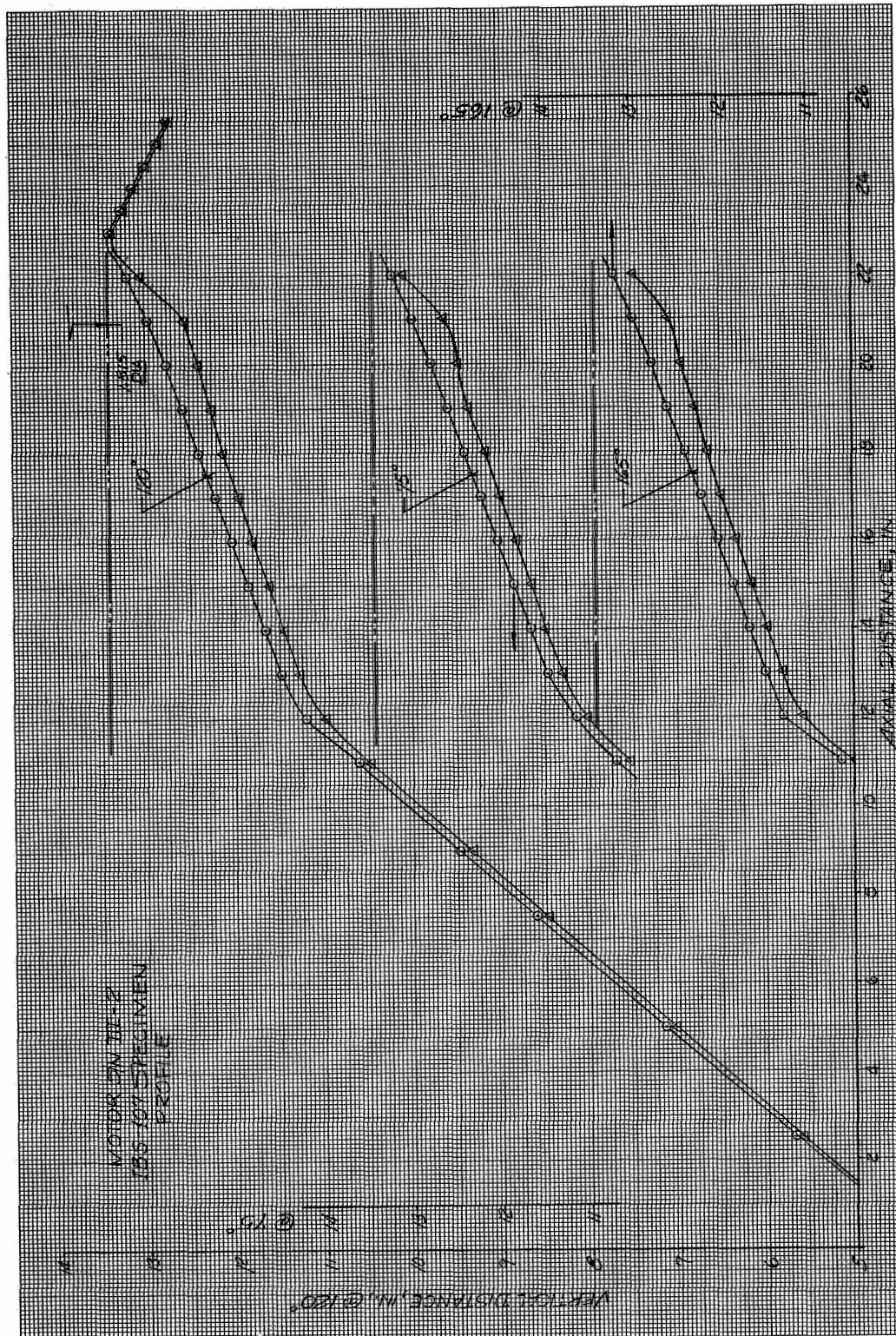
Figure 2

Figure 3



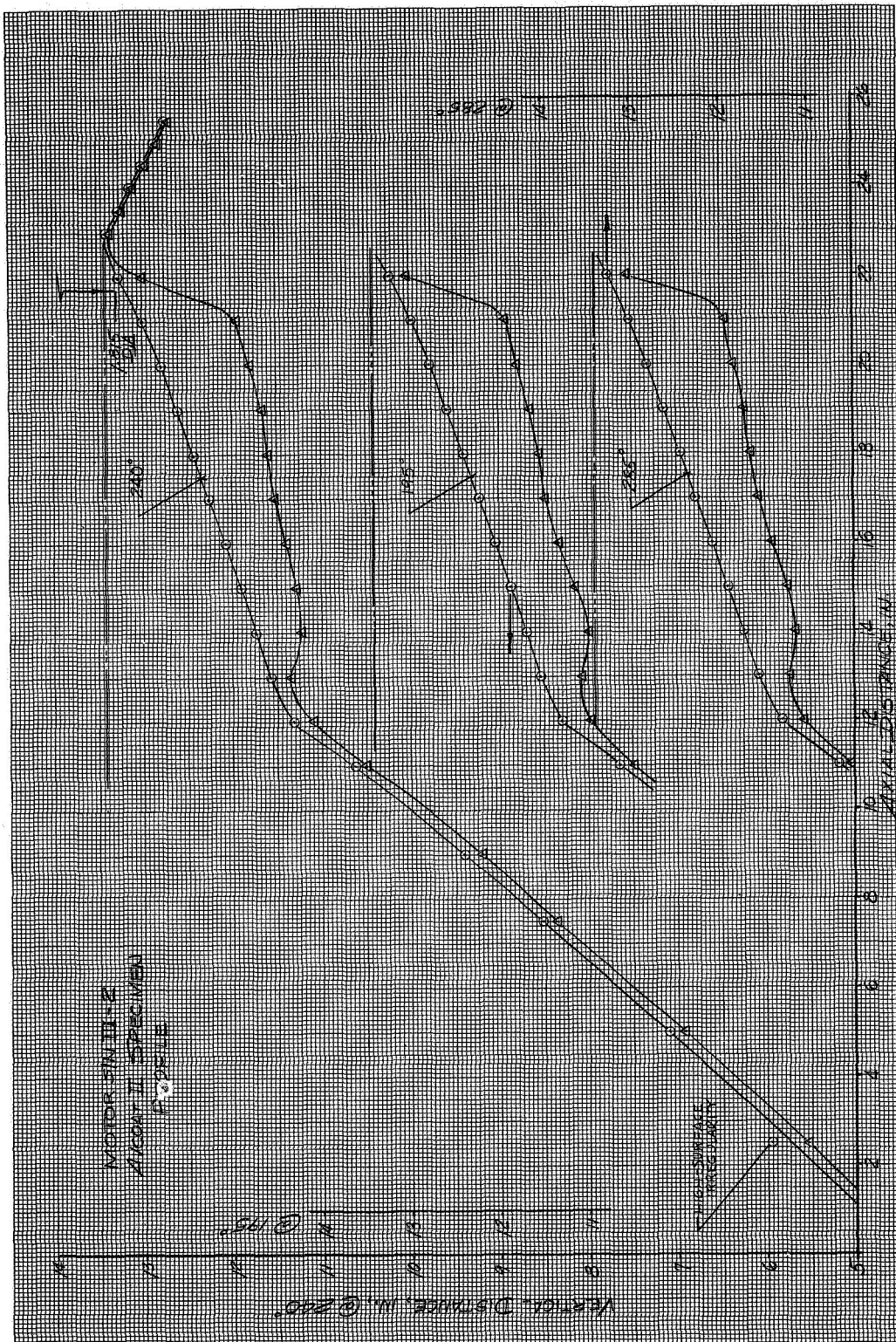
Motor S/N III-2, V-44 Specimen Profile

Figure 4



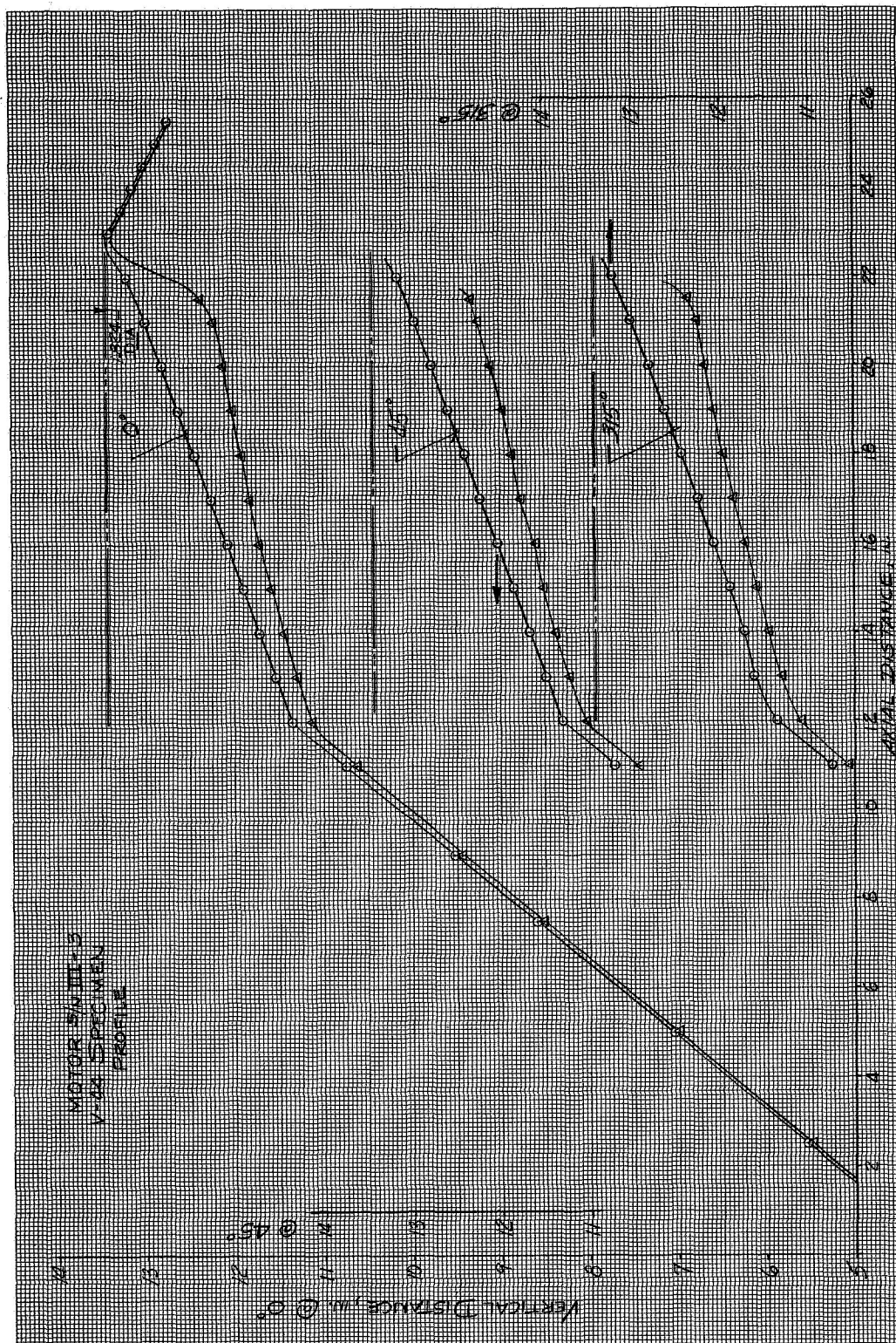
Motor S/N III-2, IBS-107 Specimen Profile

Figure 5



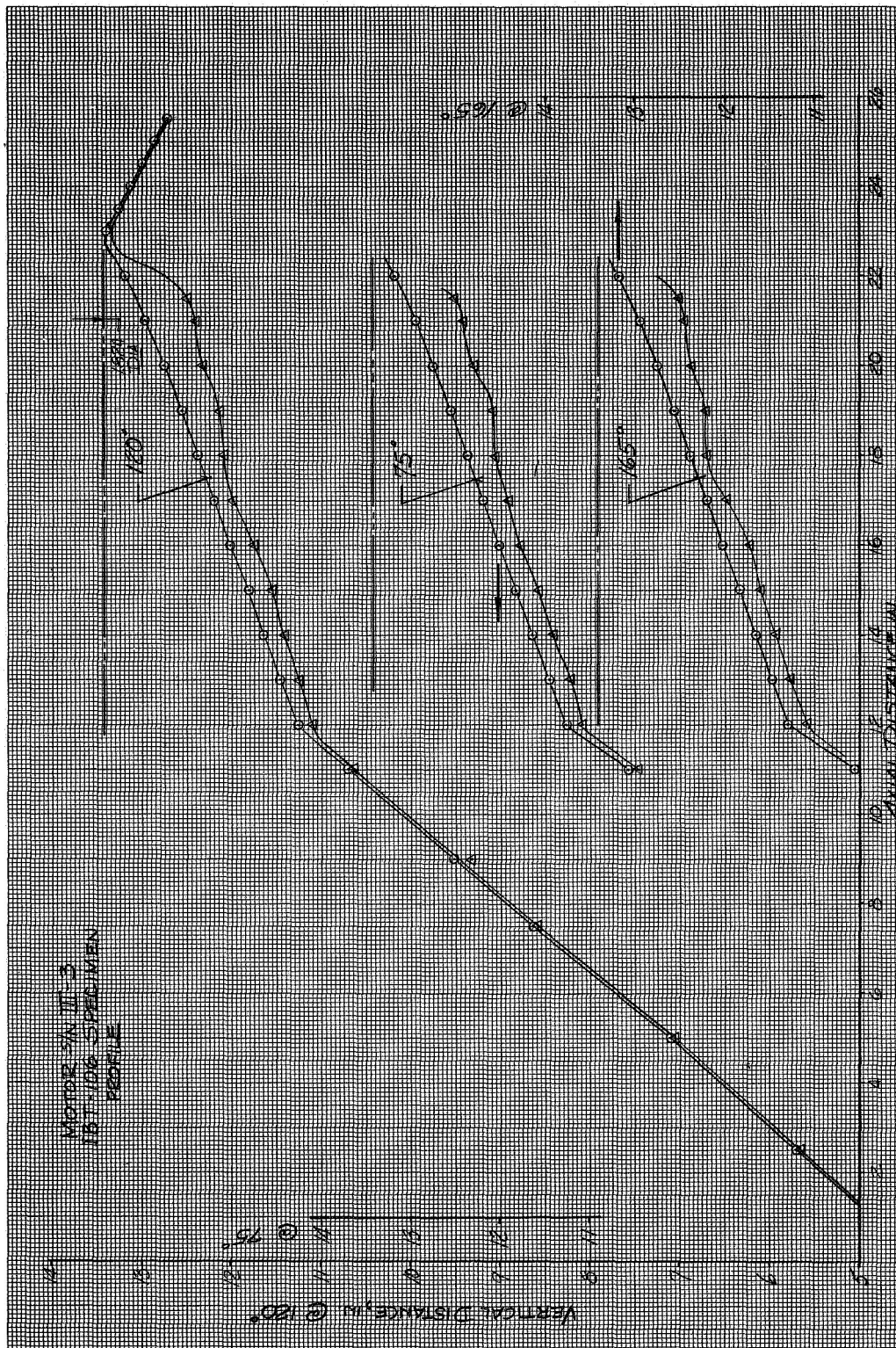
Motor S/N III-2, Avcoat II Specimen Profile

Figure 6



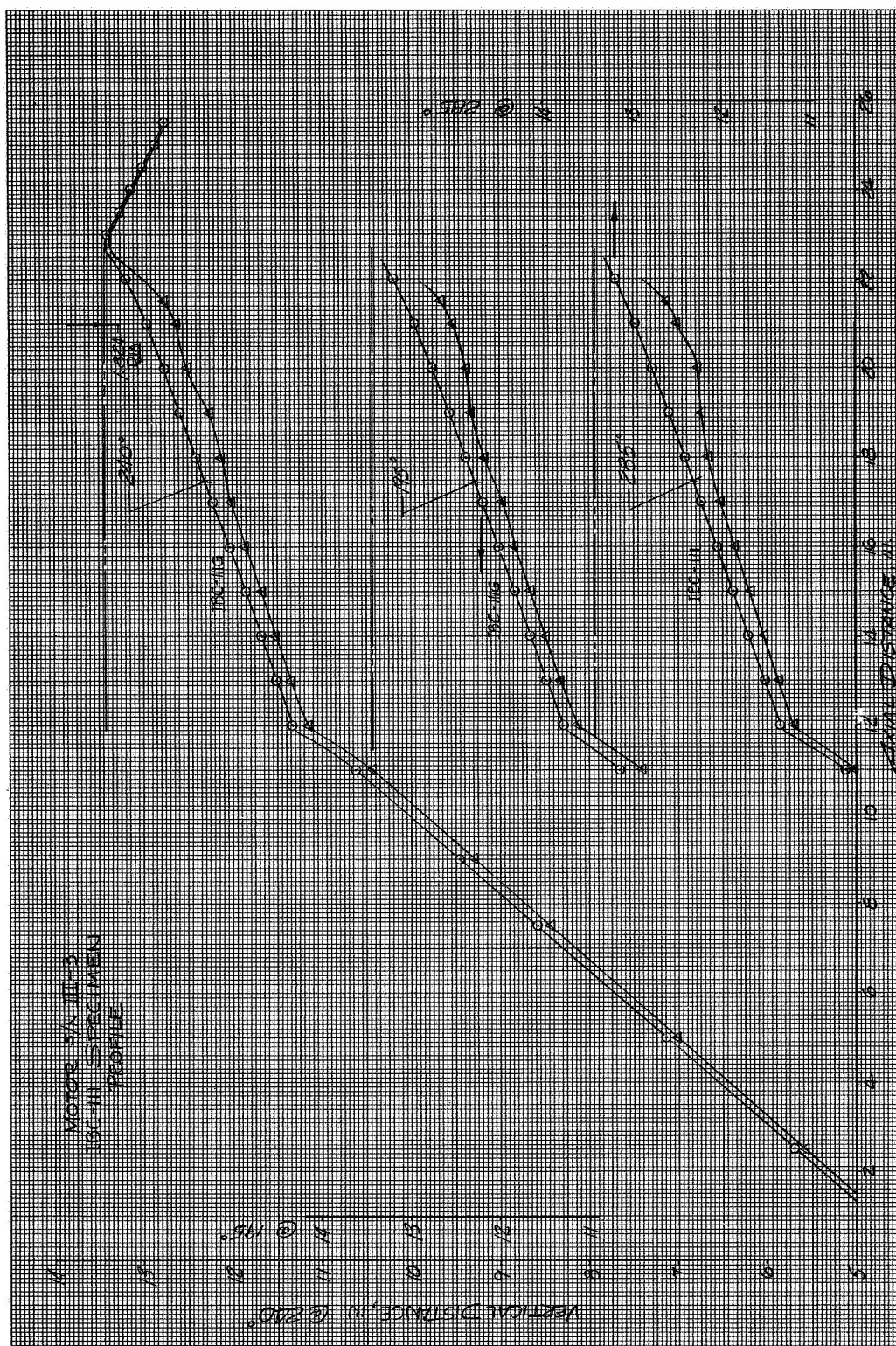
Motor S/N III-3, V-44 Specimen Profile

Figure 7



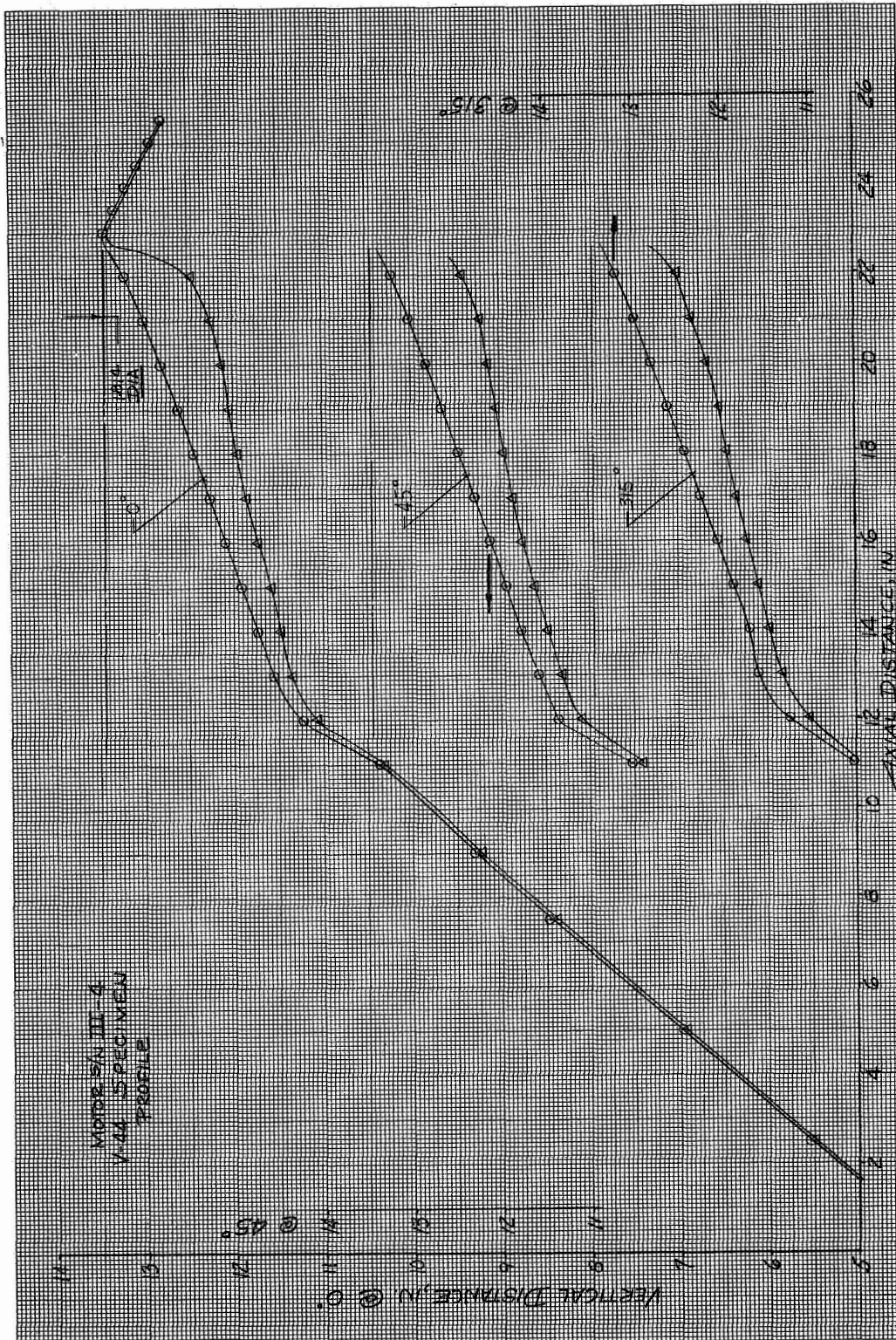
Motor S/N III-3, IBT-106 Specimen Profile

Figure 8



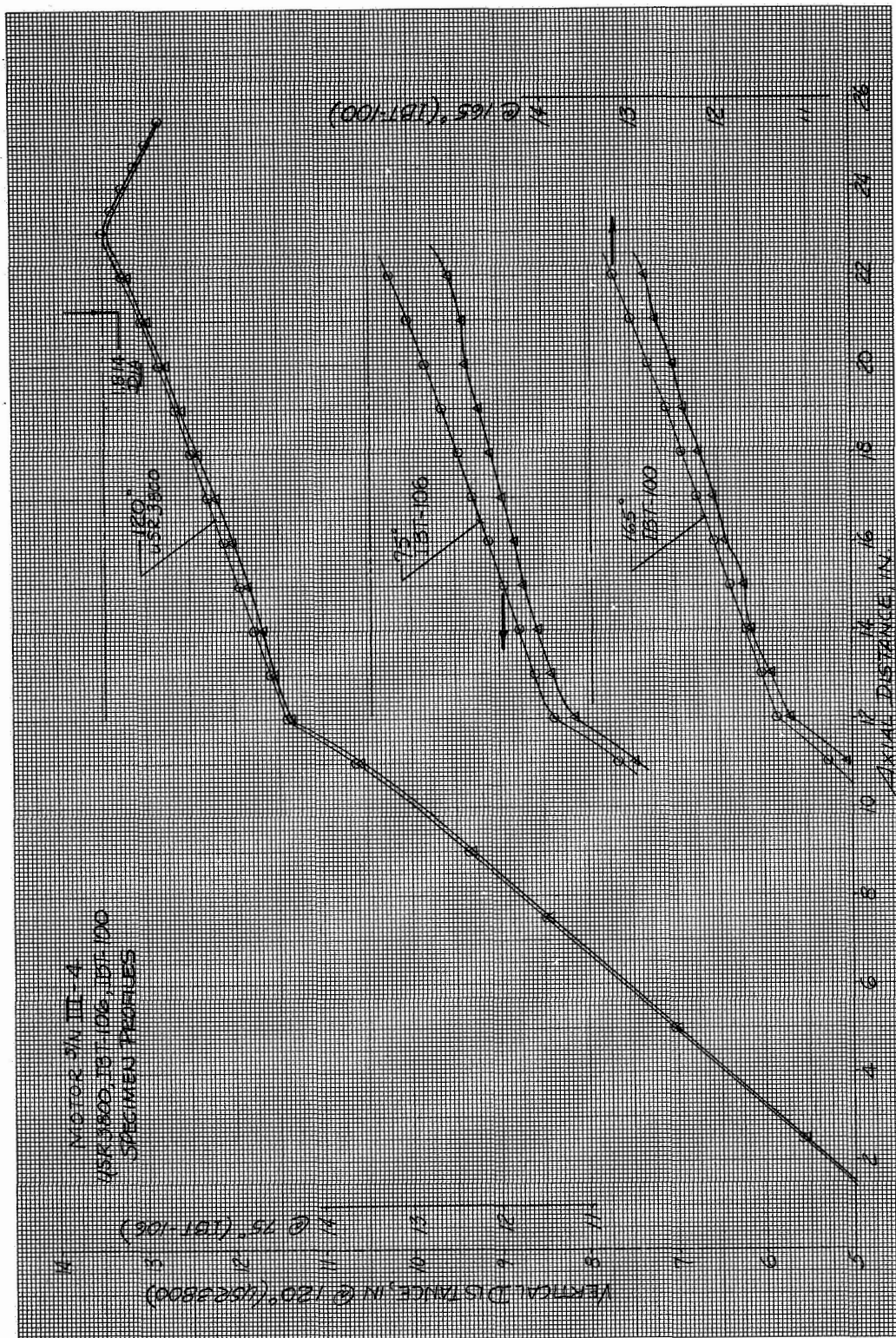
Motor S/N III-3, IBC-111 Specimen Profile

Figure 9



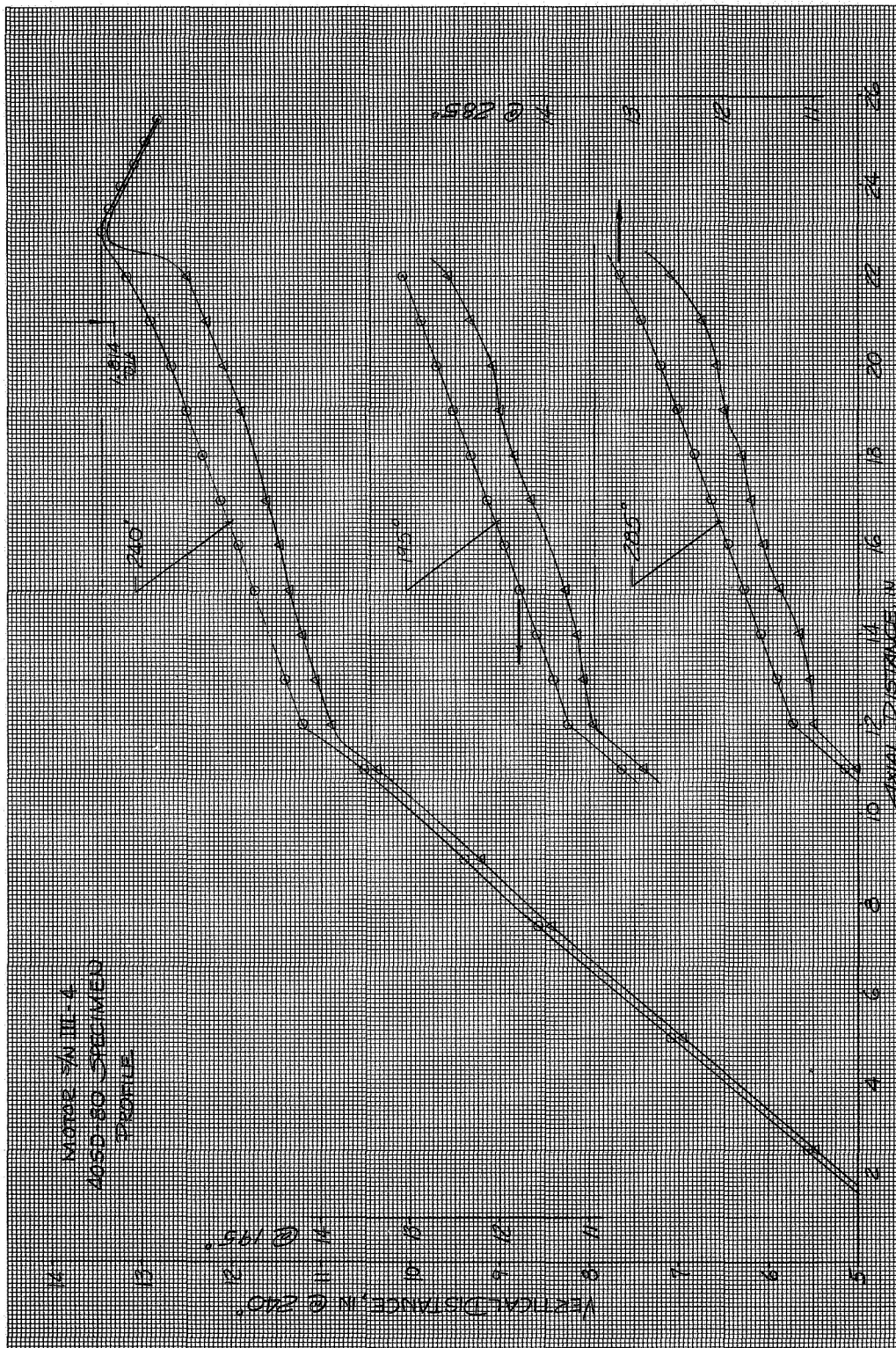
Motor S/N III-4, V-44 Specimen Profile

Figure 10



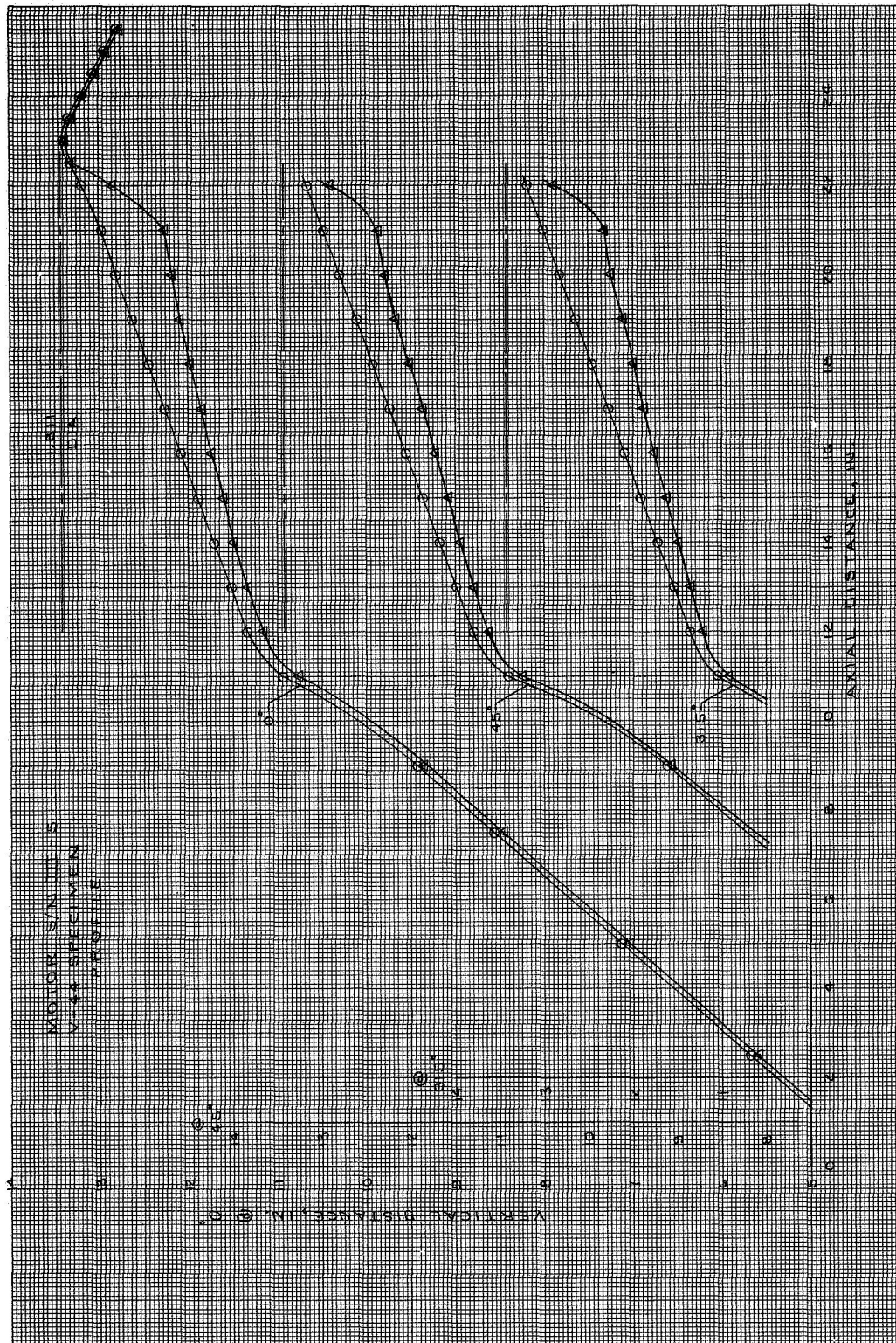
Motor S/N III-4, USR-3800, IBT-106, IBT-100 Specimen Profiles

Figure 11



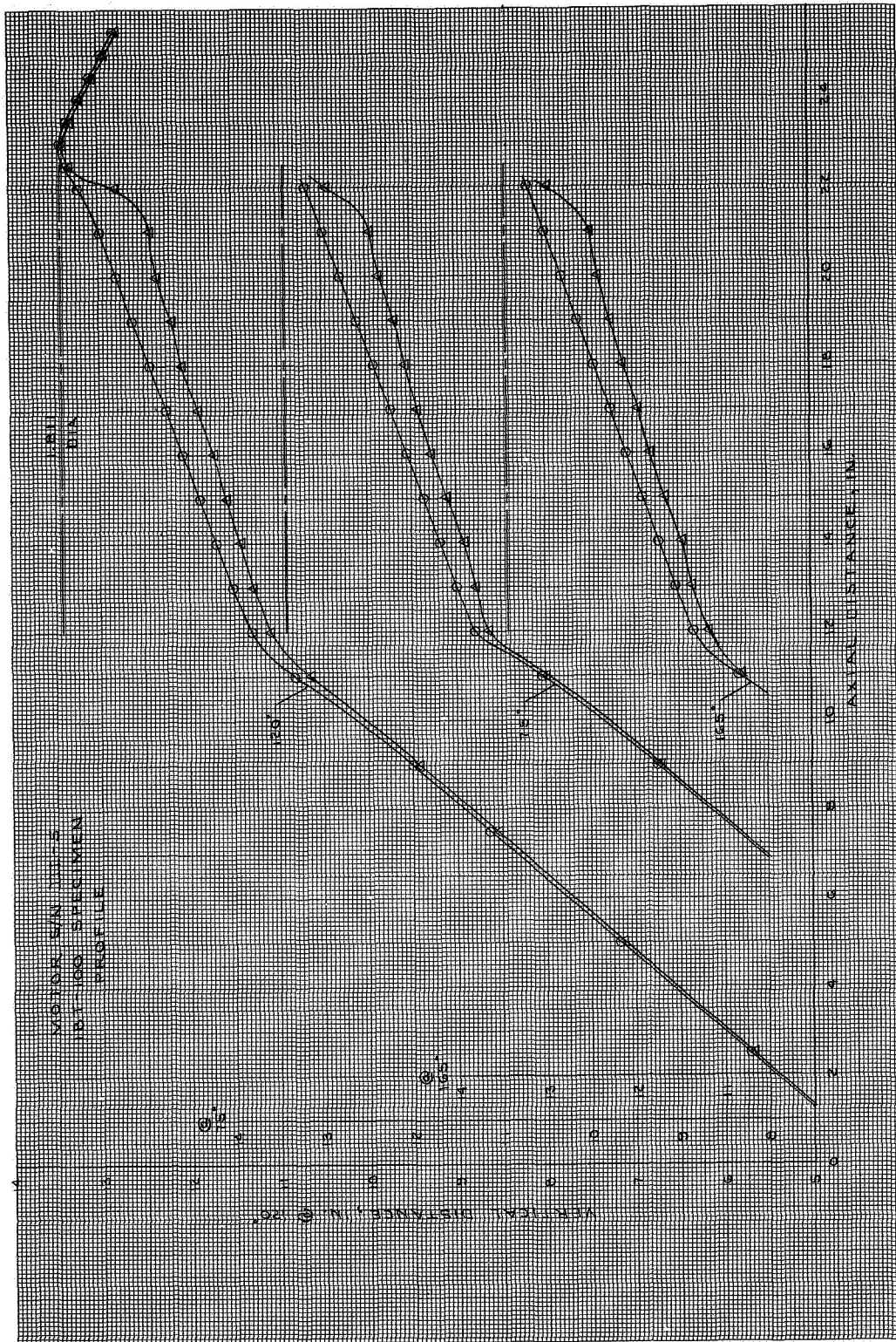
Motor S/N III-4, 40SD-80 Specimen Profile

Figure 12



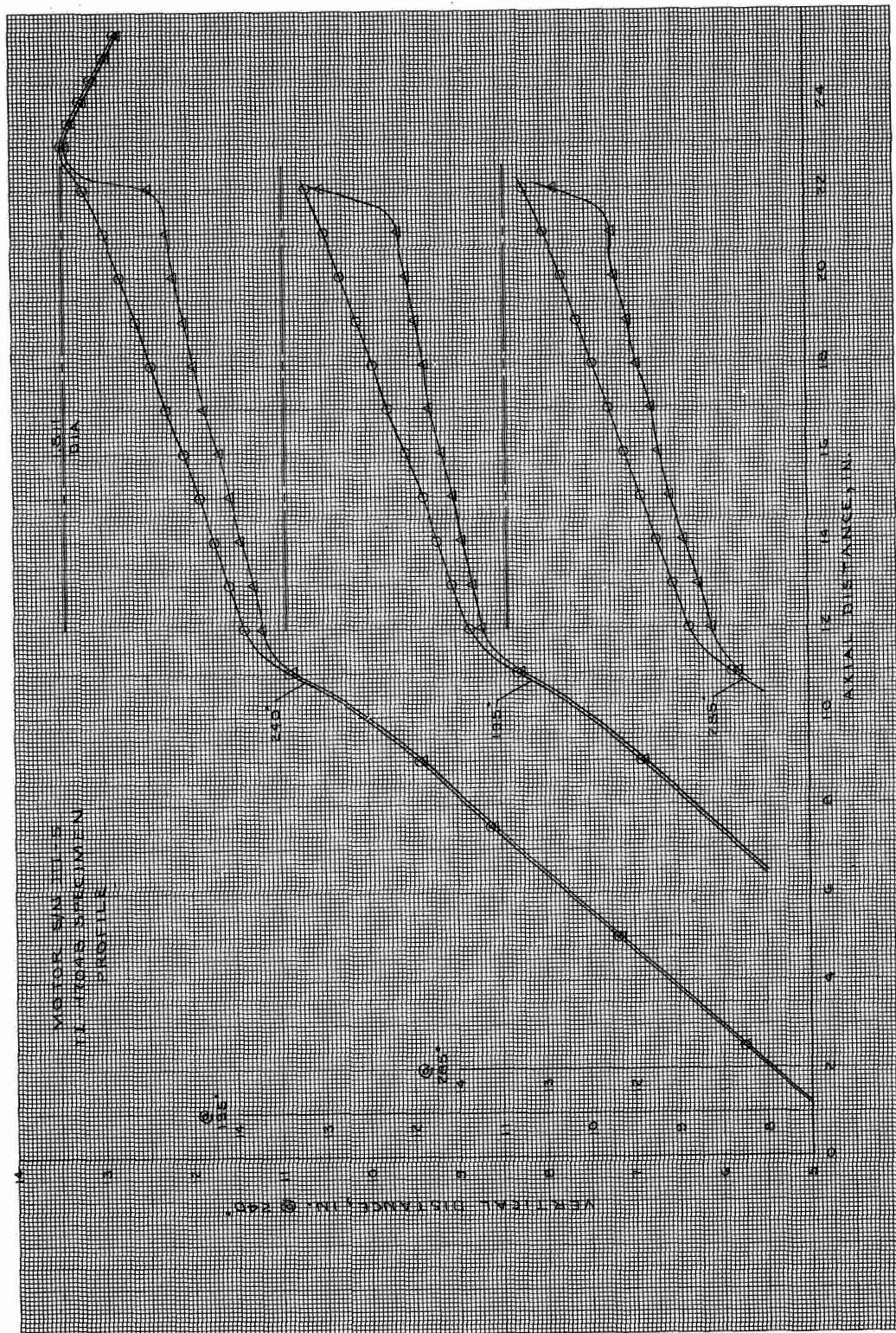
Motor S/N III-5, V-44 Specimen Profile

Figure 13



Motor S/N III-5, INT-100 Specimen Profile

Figure 14



Motor S/N III-5, TI-H704B Specimen Profile

Figure 15

## APPENDIX III

### THERMAL BEHAVIOR OF INTERNAL INSULATION

TABLE OF CONTENTS

	<u>Page</u>
I. Heat Fluxes or Environment	1
A. Exhaust Gas Composition and Transport Properties	1
B. Flow Field Analysis	2
C. Heat Transfer Criteria	2
II. Thermal Behavior	5
III. Experimental Data Requirements	8
IV. Thermal Response Calculations	13

FIGURE LIST

	<u>Figure</u>
Combustion Gas Compositions of ANB-3254 Propellant	1
Heat Transfer Coefficients and Surface Mach Number in Insulation Motor Test Section	2
Weight Loss in Virgin V-44 as a Function of Temperature	3
Weight Loss in Virgin IBT-100 as a Function of Temperature	4
Weight Loss of Virgin IBS-107 as a Function of Temperature	5
Weight Loss of Virgin IBS-109 as a Function of Temperature	6
Weight Loss of Virgin IBT-106 as a Function of Temperature	7
Weight Loss of Virgin IBC-101 as a Function of Temperature	8
Weight Loss of Virgin USR-3800 as a Function of Temperature	9
Weight Loss of Virgin TI-H704B as a Function of Temperature	10
Decomposition Rate Constants of Internal Insulation Materials	11
Ratio of Initial Erosion Rate to the Measured Value as a Function of Nozzle Radius	12
Initial Erosion Rate as a Function of Initial Heat Transfer Coefficient; Material: V-44	13
Initial Erosion Rate as a Function of Initial Heat Transfer Coefficient; Material: IBT-100	14
Initial Erosion Rate as a Function of Initial Heat Transfer Coefficient; Material: IBS-107	15
Assumed Variation of the Mass Removal Parameter as a Function of Surface Temperature	16
Predicted Char Density Distribution as a Function of Insulation Thickness; Material: V-44	17
Predicted Char Density Distribution as a Function of Insulation Thickness; Material: IBT-100	18
Predicted Char Density Distribution as a Function of Insulation Thickness; Material: IBS-107	19
Comparison of Measured Erosion with Predicted Results	20
Comparison of Predicted V-44 Erosion with Data from Seven Firings	21
Predicted Temperature Gradients within V-44 with Time as a Parameter	22
Comparison of Predicted Thermal Response with Thermocouple Data from Firing S/N III-1; Material: V-44	23

FIGURE LIST (cont)

	<u>Figure</u>
Predicted Temperature Gradients within IBT-100 with Time as a Parameter	24
Comparison of Predicted Thermal Response with Thermocouple Data from Firing S/N III-5; Material: IBT-100	25
Predicted Temperature Gradients within IBS-107 with Time as a Parameter	26
Comparison of Predicted Thermal Response with Thermocouple Data from Firing S/N III-2; Material: IBS-107	27
Erosion and Char Growth of V-44 as a Function of Time	28

I. HEAT FLUXES OR ENVIRONMENT

To provide a realistic basis for any thermal response investigation it is necessary to have available certain data on the properties of the heat transfer media. This includes the exhaust gas composition in any region of interest, thermal properties (specific heats, thermal conductivity), transport properties (diffusion coefficients, viscosity), and flow field analysis.

## A. EXHAUST GAS COMPOSITION AND TRANSPORT PROPERTIES

For evaluating transport properties, use is made of the chemical specie mole fraction data generated by analytical methods. Figure 1 depicts the gas composition for the booster propellant ANB-3254. These data, together with the local pressure and temperature of the mixture in the chamber, are used to obtain theoretical values of specific heat, absolute viscosity, thermal conductivity, Prandtl number and diffusion coefficients. The particular program and method of obtaining these properties represent a rigorous development of the kinetic theory of monoatomic molecules. The development of this theory (Reference 1) considers the potential energy of interaction between the colliding molecules to be defined for simple non-polar molecules by the Leonard-Jones potential. This method is first applied to each individual specie to obtain the viscosity and thermal conductivity for the pure gases. Subsequently, these data are modified by the use of combining laws which are again derived from kinetic theory applied to multi-component gas mixtures<sup>(1)</sup>. The results for the transport coefficients obtained by this method apply strictly to gases without internal degrees of freedom. Since the internal structure of a molecule will influence the transport of energy, the primary effect will be in the value of thermal conductivity. Thus, any additional correction is subsequently applied to the thermal conductivity to take into account the internal structure of the molecules. The second factor is often referred to as the "Eucken" correction.

Transport properties evaluated in the above manner for the propellant composition of Figure 1, are tabulated below.

Pressure, psia	500
Temperature, °F	5626
Specific heat, Btu/lb°F	0.493
Viscosity, lb/ft sec	$0.614 \times 10^{-5}$
Thermal conductivity, Btu/hr°F ft	0.227
Prandtl number	0.479

The above data represent values for the gas phase only. Inclusion of metal oxides are considered only in that they affect the chemical composition of the gas mixture.

## I. Heat Fluxes or Environment (cont)

## B. FLOW FIELD ANALYSIS

Since the convective heat transfer is dependent on the local mass fluxes (product of local density and velocity component parallel to the wall), this flow field is required to facilitate thermal calculations. The following discussion pertains to the method which is considered adequate for calculating the local surface mass fluxes in the chamber.

Since the test motor is designed to incorporate an end-burning grain, flow concentrations are eliminated and the initial flow streamlines are uniform and axisymmetric. Thus, the use of one-dimensional isentropic flow relationships is considered applicable in the regions of interest. This method in addition to its obvious ease of calculation is noted to provide reasonable estimates over more rigorous methods such as potential flow theory in areas where the wall curvature is not excessive. Regions which satisfy this criteria are nozzles with a long gradual approach (blast tube) and/or an entrance with a small convergent angle.

Since the entrance of the test nozzle falls in the category, the assumption is made that the velocity and other properties vary along and not across streamlines. Using the mass continuity relationship and the fact that the maximum mass flow is dependent only on the upstream pressure, the local mass flux becomes a function of area ratio only,

$$\begin{aligned} \text{thus,} \quad (\rho V)_{\text{local}} &= \frac{A_t}{A_{\text{local}}} (\rho V)_{\text{max}} \\ \text{and,} \quad (\rho V)_{\text{max}} &= C_w P_c \quad \text{(Equation 1)} \\ (\rho V)_{\text{local}} &= C_w P_c A_t / A_{\text{local}} \end{aligned}$$

## C. HEAT TRANSFER CRITERIA

Having discussed the preliminary data requirements, i.e., the exhaust gas composition transport properties and the local flow field, there remains the problem of establishing the net heat flux from the two-phase, high temperature exhaust gas to the exposed surfaces of the chamber. The basic mechanism which govern this energy transfer can be placed in three categories:

- convection from the gases
- radiation for metal oxides (particles)
- energy due to particle impingement

## I.C. Heat Transfer Criteria (cont)

The methods currently used to evaluate each mode of heat transfer are discussed in the following paragraphs.

1. Convection

The rate of heat transfer between any high-velocity fluid and its bounding surfaces is governed by an equation of the form,

$$\dot{q}_c = h_c (T_{BL} - T_w) \quad (\text{Equation 2})$$

Thus, to predict convection heat fluxes, the driving temperature,  $T_{BL}$ , the appropriate coefficient,  $h_c$ , represent the unknowns that must be evaluated. The instantaneous wall temperature,  $T_w$ , usually is known or it can be computed as part of a transient thermal analysis.

A standard approach has been adopted to evaluate the driving temperature. From the well established boundary layer concept, where the flow velocity is retarded as the wall is approached, an energy balance indicates the maximum temperature the surface could attain to be slightly less than the total temperature of the surrounding fluid.

Since high pressure nozzle flows are usually in the turbulent regime, the driving temperature can be expressed in terms of an isentropic exponent and the local Mach number by,

$$\frac{T_{BL}}{T_o} \text{ or } \frac{i_{BL}}{i_o} = \frac{2 + (\gamma - 1) Pr^{1/3} M^2}{2 + (\gamma - 1) M^2} \quad (\text{Equation 3})$$

From this expression, it is noted that in the chamber where the Mach numbers are low, the temperature that should be used for convection analysis becomes the theoretical flame temperature.

$$T_{BL} \sim T_o \quad (\text{Equation 4})$$

The method that will be used for heat transfer coefficients is essentially the boundary layer growth method derived by Elliott, Bartz, and Silver (Reference 2). This procedure is directed toward axisymmetric nozzle flow; it can be applied to chambers if the internal envelope forms a continuous upstream extension of the nozzle. Briefly, this method considers the effect of pressure gradient on the simultaneous solution of the momentum and energy equations. The boundary layer shape parameters are approximated using a one-seventh power profile of velocity and stagnation temperature, while skin friction and Stanton numbers are evaluated as a function of the boundary layer thickness by use of Van Karman's form of the Reynolds Analogy.

## I.C. Heat Transfer Criteria (cont)

2. Radiation

In analyzing the erosion and/or temperature predictions, the thermal radiation between the exhaust products and the exposed wall can be neglected. This conclusion has been substantiated numerous times by comparing analytical temperature prediction, which ignores radiation, with temperatures measured in a variety of rocket motors. The apparent anomaly introduced by this assumption is obvious if a simple blackbody radiation interchange calculation is performed for a particle cloud with high emissivity at  $6000^{\circ}\text{R}$  and a wall of  $4000^{\circ}\text{R}$ . The resulting value of heat flux is on the order of  $500 \text{ Btu/sec-ft}^2$  which is approximately the same magnitude as the hot wall convective heat fluxes. From this prediction, it is suggested that a "blocking" of the potential heat flux actually occurs in the particle cloud.

Development of the analytical model and techniques for calculation of particle radiation effects has been completed. The significant assumptions incorporated in this model are as follows: The solution considers the radiant heat transfer between the plate and participating medium, and within the medium (an anisotropically scattering, absorbing, and emitting medium), convective heat transfer within the medium and between the turbulent boundary layer and the plate, and the energy balance which relates the temperature gradient parallel to the plate with the heat flux normal to the plate. The resulting computer program, which represents an analytical estimate of the net absorption, emission, and reflection properties of the individual particles within the cloud, indicated a sharp temperature drop exists near the cooler wall. It is this cooled particle layer that causes the radiation blocking effect and lowers the radiation heat flux to a value less than  $1/20$  of the isothermal blackbody calculation. Since the added complexity of estimating the effective emittance for each analysis station is not warranted because of the small contribution it is considered valid to ignore the radiation contribution in analyzing the heat flux to the exposed surfaces during a firing.

3. Particle Impingement

In solid propellant chambers, the particle impingement problem has not been treated analytically. The usual approach is to ignore the problem until its importance is recognized or until qualitative indications of the problem are obtained from flow field analysis and cold flow experiments.

The analytical effort that has contributed only slightly to the understanding of the impingement problem is the determination of particle trajectories from a knowledge of the gas flow field. The usual procedure is to first approximate the gas-flow field by any of the previously discussed methods (potential flow, cold flow). Then, using the second law

## I.C. Heat Transfer Criteria (cont)

of motion and an appropriate drag law for various sized particles, the velocity and direction of each individual particle can be traced through the chamber to predict local areas of impingement. This technique revealed that entrance regions could be designed to minimize the effects of particle impacts. For example, if the wall curvature is gradual the particle impaction can then be ignored. Also, grain design has an important influence on impaction. It was found, for example, that cylindrical ports or end-burning grains were desirable. The role of particle impingement is therefore believed to be much less important than either the radiation or convection contribution.

In summary, for this design application the net heat flux to the insulation surface is governed solely by Equation 2. The local heat transfer coefficient,  $h_c$ , evaluated using a boundary layer growth solution and one-dimensional flow field is given as a function of nozzle axial length in Figure 2. Also, presented in this figure is the Mach number distribution which together with an isentropic exponent ( $\gamma = 1.2$ ) characterizes the flow field. Each of these curves represent values for the original, non-eroded contour are noted to vary within its test section between values of 40 to 1300 Btu/hr/ft<sup>2</sup>°F for the heat transfer coefficient and 0.005 to 0.40 for the Mach number. This wide range of values likewise provides for a wide range of test data on material thermal performance.

In addition, it is noted that by scaling surface regression from actual motor firings, as is done in this program, the contribution of radiation and particle impacts is inherent in the data and, accordingly, will be included in any scaled insulation design. Thus, particle effects, etc., are not completely ignored in this model.

The particle mass flux, however, is included in the total mass flow of propellant (See Equation 1).

II. THERMAL BEHAVIOR

Typical insulation materials for large booster application are composites that consist of elastomeric polymers and inorganic fillers. In the analytical treatment of such a composite, each component is considered to have a fraction that decomposes when it is heated and a residual (char) that remains after decomposition. In discussing the role of the various components, it is convenient to divide the material into three distinct zones, which are the virgin material, the decomposition zone, and the fully charred zone. In the virgin layer, the thermal transport phenomena are relatively simple. Since temperatures are relatively low, there are negligible changes in material properties and the thermal response is defined by simple conduction and absorption of sensible energy.

## II. Thermal Behavior (cont)

Within the decomposition zone, the material response becomes considerably more complex. The elastomeric material decomposes by a kinetically controlled process that is observed to be time- and temperature-dependent. As the temperature increases, the decomposition also increases and subsequently results in substantial weight loss (up to 90% for some materials).

The rate at which the density of the solid phase changes (also the gas evolution rate) is obtained from the rate equations that describe the decomposition rates of the solid phase components. These relations may be written in the following form:

$$\frac{\delta \rho}{\delta \theta} = -B_i \rho_{o_i} \left( \frac{\rho_i - \rho_n}{\rho_i} \right)^{\psi_i} \left( e^{-E/RT} \right) \quad (\text{Equation 5})$$

As decomposition governed by Equation 5 begins, two energy transfer modes are present. In addition to the usual conduction, energy is similarly transported by the decomposition gases that transpire toward the heated surface. It is assumed that these pyrolysis gases are in local thermal equilibrium with the char. Thus, the magnitude of the energy associated with the internal ablation process is a heat of decomposition and a sensible enthalpy increase of the gases. In general, it is believed that the occurrence of individual reactions may be slightly exothermic; however, if the sensible enthalpy is considered to be the net effect, the decomposition zone is endothermic.

In the third, or char zone, characteristics similar to those in the decomposition zone can be expected. As a result of very high temperatures, continued decomposition of organic components and some decomposition of inorganic components, such as the loss of occluded water in asbestos fillers used in some material formulation, will occur. The final product after complete decomposition will consist of a low density char made up of carbonaceous residue and the remaining filler material. The modes of energy transfer and absorption will be similar to those that occur in the decomposition zone.

Thus far, the discussion pertains to the response the internal structure of a typical insulation material produces when it is exposed to solid propellant exhaust products. As exposure continues, surface material is lost by a process commonly identified as erosion. The relative performance therefore becomes a measure of how well a particular material can resist decomposition and subsequent removal. Aerojet has adopted the term "surface regression" to describe the various modes of surface loss. These could include surface

## II. Thermal Behavior (cont)

chemical reactions (oxidation of carbon residue) with the propellant exhaust products, erosion from pressure and shear forces acting on the low density char layer, structural failure of the char as the result of thermal stresses, spallation resulting from pressure buildup within the decomposition zone, and combinations of chemical and mechanical modes acting on the exposed surface (i.e., particle impacts).

To accurately analyze and evaluate each material removal mode would be a formidable task. This is so because a detailed knowledge of the material's kinetic behavior is required to formulate a model that would clarify the ablation process sufficiently. In lieu of what could be termed a rigorous model for surface regression, a provisional model is proposed. This model will include all energy transport processes that occur in the virgin, decomposition and char zones suggested in the above discussion of the physical model, a basis for the prediction of char rates, erosion rate and transient temperature distributions, and a treatment of the surface regression by combining all modes of removal into an "effective removal rate", which will be obtained from actual motor firings. A detailed discussion of the proposed model follows.

The insulation type and amount required for a booster motor must obviously be scaled from subscale firings or obtained from applicable large motor erosion data. In either case, the insulation capability is better understood if there are analysis techniques available that provide realistic estimates of thermal penetration, decomposition and the mass transfer of reactants and products away from the exposed surfaces. In this manner, the insulation designer can scale internal insulation requirements to a wide variety of motor operating conditions.

The particular type of computer program which has been successfully utilized primarily for evaluating nozzle ablation can likewise be used for elastomeric type materials. This is due to the fact that, in general, the thermal degradation is analogous to the resin reinforced ablative materials. Only the rates of decomposition and regression differ. The type of computer program best suited for this analysis is basically the "Vidya" program described in Reference 3. This particular program is available to industry contractors and as previously mentioned has been widely used for analyzing ablative nozzles for solid propellant boosters. A modified version, is presently being used by Aerojet, to predict the rate of material removal (erosion), internal degradation rate (charring), and the transient temperature distributions in chamber insulations. The analytical treatment of these quantities requires first that the local environment be evaluated at the exposed surfaces (as discussed previously). Subsequently, these data are used as the boundary conditions to solve the one-dimensional transient heat conduction equation. The solution of this well known relationship defines the temperature distribution within a nonreacting body. For ablative materials

## II. Thermal Behavior (cont)

that decompose in depth, additional equations must be considered to account for the decomposition reactions and the transpiration of the gas-phase decomposition products. The energy equations and the corresponding mass balance relations are therefore solved simultaneously by the above program. A complete derivation of the appropriate equations have been reported by several sources and will not be repeated here, see for example References 3 or 4.

The particular form of the energy equation, which contains the ratio of the mass transfer coefficient to the convective heat transfer coefficient (equivalent to Lewis Number to the  $2/3$  power), allows by proper choice of Lewis Number a relationship between heat and mass transfer. If it is assumed that the surface material is removed solely by a reaction characterized by a diffusion-limited process, and the Lewis Number is taken as unity, then the mass transfer and convective heat transfer coefficients exactly equal. The resulting erosion rate then becomes proportional to the magnitude of the local heat transfer coefficient. By plotting the experimental surface mass regression rate as a function of local convective heat transfer coefficient, the resulting slope then becomes the scaling parameter ( $\dot{m}_{ch}/h'_c$ ). With this parameter, it is possible to predict erosion in any motor in which the local value of heat transfer coefficient is accurately known.

In brief, the similarity between the thermal response of ablative plastics used as nozzle components and filled elastomeric type materials suggests that the charring-ablation program is a realistic approach to defining the mechanism of degradation that occurs when internal insulations are exposed to propellant exhaust products. The data input requirements include experimentally determined mass transfer rates which are proportional to the local heat transfer, plus, internal decomposition rates which are characterized by Equation 5, where the particular kinetic constants are obtained from thermogravimetric analysis (TGA) measurements.

The utility of the charring-ablation program to define the mechanism of degradation of elastomeric materials will be discussed in the following sections.

## III. EXPERIMENTAL DATA REQUIREMENTS

In order to predict the thermal response of a given material in a particular chamber environment by the analytical methods discussed above it is necessary to have available, thermal conductivity, specific heat, density, decomposition rates, and mass transfer correlation. The first three are typical thermal properties which are required to solve the transient conduction equation. All values are directly measurable and for a large number of elastomeric material they are presented over a moderate temperature range in Phase I. The remaining two properties are the variables which define the total heat degradation characteristics of the material as discussed earlier.

## III. Experimental Data Requirements (cont)

The rate of decomposition as a function of temperature can be expressed in the form of an Arrhenius relation as given by Equation 5. Determination of the constants B, n and E' are accomplished by curve fitting the experimental TGA data for a particular material at a constant heating rate. Typical TGA curves are presented in (Phase I). These data represent instantaneous weight plotted as a function of sample temperature for a heating rate of 20°C/min. It is noted that several techniques exist for evaluating the constants, see for example Reference 5. The procedures used here consists of an IBM-1130 computer program (Reference 4) which passes an equation of the form,

$$\frac{d\alpha}{d\theta} = \frac{A}{\beta} \alpha^n \exp \left( -\frac{E'}{T} \right)$$

where  $\alpha$  = weight fraction  $\left( \frac{w - w_f}{w_o - w_f} \right)$  (Equation 6)

$\beta$  = temperature rate in  $T = \beta\theta + T_o$

through three points on the experimental TGA curve thus providing three equations for evaluating the three unknown kinetic parameters A, n and E'. Applying these results to the form of Equation 5 it is necessary to define,

$$B = \frac{A}{60\beta} \left( 1 - \frac{w_f}{w_o} \right)^{1-n}$$

$$\psi = n \quad \text{(Equation 7)}$$

$$E = E' R$$

Typical results for several materials are presented in Figures 3 to 10. Each figure contains the actual TGA data and the best curve fit of the form of Equation 6. For the candidate materials considered, most could be reasonably approximated by a single reaction, the exceptions being USR-3800 and TI-H704B. These materials exhibited two distinct reactions and as a result two sets of curves are required to define their overall decomposition rates. This is accomplished by applying the curve fit program twice with the final weight of the first reaction defined as the initial value for the second equation. A summary of the rate constants for nine candidate materials are presented in Figure 11. It is noted that in order to use these data in the charring-ablation program the correction factors given in Equation 7 must be applied.

### III. Experimental Data Requirements (cont)

During the LMISD Program eight motor firings were made for the purpose of obtaining material loss rates over a wide range of flow conditions. At high area ratios in the aft closure, the flow velocities and attendant shear forces acting on the surface are low and material loss (surface erosion) may be small. Conversely, near the throat the char layer is easily removed and high regression rates will occur. Thus, subsequent to a firing, the nozzle is sectioned, the various test specimens are scraped to remove all loose material, and measurements of total erosion obtained by the difference in pre- and post-firing contours. The depth now represents the thickness of material which was removed during the firing (erosion) plus a portion of decomposed (char zone) material which is formed not only during the firing, but also during the subsequent cooling period. Dividing this depth by the action time which gives an average thickness loss rate (TLR) does not represent the true char formation rate. This is especially true in the above noted high area ratio regions where it can be shown that the char rate is not linear but varies as the square root of time. This criterion could introduce large errors in terms of scaling char rates between two motors if the firing duration is less than that of the motor from which the data was obtained. This situation will be discussed further in the following paragraph.

In addition to the influence of the char zone growth on the measured TLR, a second criterion which must be included in the interpretation of the measured data is the variation in heating rate which occurs as the result of local erosion. Since the throat area is constant, the local area ratio (Mach number) varies as the material regresses and near the throat region, this variation could be in excess of 50%. Likewise, as noted in Figure 2, the local heat transfer coefficient will change by a similar value since it varies in a systematic manner with Mach number. As a result, the proposed correlation parameter,  $B'$ , must be evaluated using a consistent set of data, i.e., the local heat transfer coefficient at a given time and the instantaneous erosion rate. Since the heat transfer coefficients are known for the original contour (Figure 2), then the logical erosion rate should be the initial or early time value and not the TLR. To obtain this rate, the following data reduction technique was used. For the correlation parameter discussed previously, it is assumed that the value remains constant for all heating rates, thus,

$$B' = \dot{m}_c / h'_c = \frac{\dot{a}_c \bar{C}_p}{h_c(t)}$$

(Equation 8)

$$\text{and } \dot{a} = \frac{h_c(t) B'}{\rho c \bar{C}_p}$$

## III. Experimental Data Requirements (cont)

Since the regression rate represents the rate of change of the local radius and the heat transfer coefficient can be expressed as function of the radius by:

$$h(t) = h_o \left( \frac{r_o}{r} \right)^{1.8} \quad (\text{Equation 9})$$

where,  $h_o$ , is the value at a radius,  $r_o$ , then Equation 8 becomes,

$$\frac{dr}{dt} = h_o \left( \frac{r_o}{r} \right)^{1.8} \frac{B'}{\rho_c \bar{C}_p}$$

Integrating between the limits of time from zero to,  $\theta$ , gives

$$\frac{r(\theta)}{r_o} = \left( 1 + \frac{2.8 \dot{a}_o \theta}{r_o} \right)^{1/2.8} \quad (\text{Equation 10})$$

which represents the value of the local radius at time,  $\theta$ .

From the above definition of the thickness loss rate, if the initial radius were subtracted from Equation 10 and the result divided by the firing duration,  $\theta_f$ , an expression for the initial erosion rate as a function of the average value is obtained,

$$\text{TLR} = \left[ r_o \left( 1 + \frac{(2.8) \dot{a}_o \theta_f}{r_o} \right)^{1/2.8} - r_o \right] / \theta_f \quad (\text{Equation 11})$$

noting that the measured erosion,  $\Delta r$ , is equal to  $\text{TLR} \times (\theta)$ , then

$$\frac{\dot{a}_o}{r_o} = \left[ \left( \frac{\Delta r}{r_o} + 1 \right)^{2.8} - 1 \right] \frac{1}{2.8 \theta_f} \quad (\text{Equation 12})$$

The functional relationship indicated by Equation 12 is plotted in Figure 12.

## III. Experimental Data Requirements (cont)

The data reduction technique for evaluating the mass transfer correlation parameter, thus consisted of four steps:

1. From the total erosion at the various measurement stations the values of  $\Delta r$ ,  $r_0$  and Mach number are obtained.
2. For a given ratio of  $(\Delta r/r_0)$  a corresponding value of  $(\dot{a}_0/r_0)$  is obtained from Figure 12.
3. At a given radius  $r_0$ , (or Mach number) the local heat transfer coefficient is obtained from Figure 2. This value is scaled by pressure to the 0.8 power to correspond to the average pressure occurring during the respective firing.
4. The resulting value of  $\dot{a}_0$  from Step 2 is then plotted as a function of the heat transfer coefficient obtained in Step 3.

Typical results obtained in this manner for V-44, IBT-100 and IBS-107 are presented in Figures 13, 14, and 15, respectively. In the case of V-44, a total of 5 separate firings are plotted. Firing numbers S/N I-2 and S/N I-3A are noted to fall below the proposed correlation curve. This is presumably due to the fact that certain materials tested during these firings exhibited somewhat higher regression rates and thus reduced the heat transfer to the selected V-44 sample. Similar conditions occurred during firing S/N III-4 for the IBT-100 material. As a result, these data were ignored in defining the correlation curve in that only the higher erosion rates were considered valid. From Figures 13 to 15 and the char density given in Figure 11, the resulting correlation parameters for the three respective materials were found to be:

<u>Material</u>	<u>Char Density - <math>\rho_c</math></u>	<u>Correlation Parameter - <math>B'</math></u>
V-44	28.9 lb/ft <sup>3</sup>	0.217
IBT-100	35.2	0.210
IBS-107	14.5	0.074

With these data, all the required input parameters have been established. There remains only the actual prediction of the thermal response.

IV. THERMAL RESPONSE CALCULATIONS

The thermal response of the three materials were predicted at four stations (five for the V-44) which represent the extremes in environment. The location of each station is noted in Figure 2. Due to the wide range of heat fluxes, the correlation parameter was input to the program as a function of temperature as depicted in Figure 16. This particular form was chosen on the basis of the measured surface loss data. It was found that at low flux (also surface temperatures less than 3000°F) the material loss could be predicted by considering only the char growth. As the heat flux increased a threshold was reached where the measured erosion exceeded the predicted char depth. Thus, surface removal becomes important and the correlation parameter,  $B'$ , provides a better prediction. Since the transition between the two regimes is not considered a step function and in order to provide a smooth interpolation curve for the computer the data of Figure 16 was used. With this model, the resulting thermal response calculations are presented in Figures 17 through 28. Figures 17, 18 and 19 represent the density profiles (after complete cook-out) which were predicted for V-44, IBT-100 and IBS-107, respectively. These data depict the depth of the virgin layer, which is given by the location of maximum density, the thickness of the char zone, region where the density varies, and the thickness of material eroded, i.e., termination of density profile.

As noted previously, the surface treatment prior to taking postfire measurements removes a portion of the char layer. The exact percentage is unknown, however, for the purpose of comparing the predicted data with measurement a density reduction of 20% was assumed. A direct comparison of measured erosion for each analysis station is presented in tabular form in Figure 20. Also noted are the data from several firings which indicate a significant range of measured values occur at each respective measurement station. A better correlation of the data is noted in Figure 21. Here the predicted post-firing contour for V-44 is presented with the range of measured values superimposed. It is now noted that at all stations, the predicted values lie well within the range of measurements and the analytical model provides fairly realistic results throughout the range of test data.

Figures 22 and 23 represent temperature data predicted for V-44 insulation. The predicted thermal gradients of Figure 22 (Station 4) indicate surface temperatures of the char attain values of 4100°R (3640°F) with ambient values being reached within 0.125 in. of the surface. These data can be compared with the thermocouple measurement obtained from firing S/N III-1. Typical installation and approximate location of the thermocouple was shown previously in Figure 3 of the main report text. Since the inner contour was noted to vary slightly between firings, the exact location (depth with respect to the surface) was not accurately known. Thus, provided the thermocouple was located at a depth of approximately 0.44 as noted in Figure 22, the comparison of measured and predicted temperatures in Figure 23 is valid.

#### IV. Thermal Response Calculations (cont)

Presumably, a better comparison is noted in Figure 25. These data represent a comparison between the predicted temperature profiles for IBT-100 (Figure 24) and the TC data of firing III-5. In this test the thermocouple was within the zone which eroded during the firing. This is indicated by the loss of signal at 9.7 sec at a measured value of 2237°F.

Similar data are presented for IBS-107 in Figures 26 and 27. Again, if the TC location was 0.35 in. below the original surface then a reasonable comparison exists.

The analytical model predicts thermal growth as a function of time per the curves of Figure 28. Two distinctly different heat flux environments are presented. The first represents the low-heat flux regions where negligible surface removal occurs, only charring. As noted, the curves which represent the interface between virgin and charred zone (about 500°F), indicates a growth rate which is not linear but varies as the square root of time. In the second region, the erosion rate being high, the char growth approximates a linear rate. However, it is noted that due to the aforementioned variation in heating rate due to erosion, the erosion rate is not quite linear but decreases slightly during the firing. As this data indicates, care must be exercised in interpreting experimental erosion data on the basis of average thickness loss rates. A better method is to match the measured char depth by analytical calculations using the procedures outlined above.

NOMENCLATURESymbol

$A_t$	-	Throat area, in. <sup>2</sup>
$\dot{a}$	-	Erosion rate, in./sec
$A$	-	Pre-exponential coefficient in Equation 6
$B$	-	Frequency factor, 1/sec
$B'$	-	Correlation parameter for erosion
$\bar{C}_p$	-	Specific heat of combustion products, Btu/lb°F
$C_w$	-	Mass flow coefficient, 1/sec
$E$	-	Activation energy, cal/mole
$E'$	-	$E/R$ , °K
$h'_c$	-	$h_c/\bar{C}_p$ , lb/hr ft <sup>2</sup>
$h_c$	-	Convective heat transfer coefficient, Btu/hr ft <sup>2</sup> °F
$i_{BL}$	-	Enthalpy, Btu/lb
$\dot{M}_{ch}$	-	Mass rate of char, lb/sec
$M$	-	Mach number
$n$	-	Order of reaction
$P_c$	-	Chamber pressure, lb/in. <sup>2</sup>
$P_r$	-	Prandtl number
$\dot{q}_c$	-	Convective heat flux, Btu/hr ft <sup>2</sup>
$R$	-	Gas constant, cal/mole °K
$r$	-	Radius, in.
$\Delta r$	-	Measured material loss, in.

NOMENCLATURE (cont)

Symbol

$T_o$	-	Stagnation temperature, °F or °R
$T$	-	Absolute temperature, °K
$W$	-	Sample weight, mg
$TLR$	-	Thickness loss rate, in./sec
$T_{BL}$	-	Adiabatic wall temperature, °F or °R
$T_w$	-	Surface temperature, °F or °R
$V$	-	Local velocity, ft/sec

Greek Symbols

$\gamma$	-	isentropic exponent
$\rho$	-	density, lb/ft <sup>3</sup>
$\beta$	-	TGA heating rate, °C/min
$\psi$	-	Order of reaction
$\theta$	-	Time, min or sec
$\alpha$	-	See Equation 6

Subscripts

$i$	-	$i$ th component
$o$	-	initial
$r$	-	remaining
$f$	-	final
$c$	-	char

LIST OF REFERENCES

1. Curtis, C. F., Hirschfelder, J. O., Bird, R. B., Theories of Gas Transport Properties," Proceedings of the Second Biennial Gas Dynamics Symposium, Northwestern University Press, January 1958, Pages 3-11.
2. Elliot, D. G., Bartz, D. R., and Silver, S., "Calculation of Turbulent Boundary-Layer Growth and Heat Transfer in Axi-Symmetric Nozzles," Technical Report 32-387, JPL, California Institute of Technology, February 1963.
3. McCuen, P. A., et al, "A Study of Solid Propellant Rocket Motor Exposed Materials Behavior," Report No. AFRPL-TR-65-33, Vidya Division of Itek Corporation, February 1965.
4. Bradley, W., et al, "Investigation and Evaluation of Motor Insulation for Multiple Restart Application," Technical Report AFRPL-TR-67-287, November 1967.
5. Nelson, J. B., "Determination of Kinetic Parameters of Six Ablation Polymers by Thermogravimetric Analysis," NASA TN-D-3919, April 1967.

	Gas Composition, moles/100 g Propellant			
	Chamber Pressure, 500 psia		Chamber Pressure, 1000 psia	
	Chamber	Exhaust	Chamber	Exhaust
HCl	0.4768	0.5716	0.4807	0.5787
N <sub>2</sub>	0.3083	0.3098	0.3085	0.3098
H <sub>2</sub> O	0.6046	0.5815	0.6145	0.5723
H <sub>2</sub>	0.9637	1.0196	0.9680	1.0331
O <sub>2</sub>	0.0008	-	0.0006	-
O	0.0034	-	0.0023	-
OH	0.0399	0.0019	0.0340	0.0004
Cl	0.0481	0.0084	0.0392	0.0025
NO	0.0030	0.0001	0.0026	-
Cl <sub>2</sub>	0.0001	-	0.0001	-
H	0.1423	0.0201	0.1159	0.0059
CO	0.8887	0.8711	0.8886	0.8626
CO <sub>2</sub>	0.0700	0.0876	0.0701	0.0961
SiO	0.0033	0.0033	0.0033	0.0023
SiO <sub>2</sub>	0.0001	-	0.0001	0.0010
Al	0.0004	-	0.0003	-
AlCl	0.0123	0.0001	0.0108	-
AlCl <sub>2</sub>	0.0221	0.0010	0.0250	-
AlCl <sub>3</sub>	0.0004	-	0.0006	-
AlO	0.0003	-	0.0002	-
AlO <sub>2</sub>	0.0001	-	0.0001	-
Al <sub>2</sub> O <sub>3</sub>	0.2636	0.2808	0.2629	0.2813
Fe	0.0006	-	0.0005	-
FeCl	0.0043	0.0046	0.0044	0.0042
FeCl <sub>2</sub>	-	0.0004	-	0.0007
Mol. Wt.	27.829	28.729	28.009	28.380
Temp, °F	5626	3714	5734	3320

Combustion Gas Compositions of ANB-3254 Propellant

Figure 1

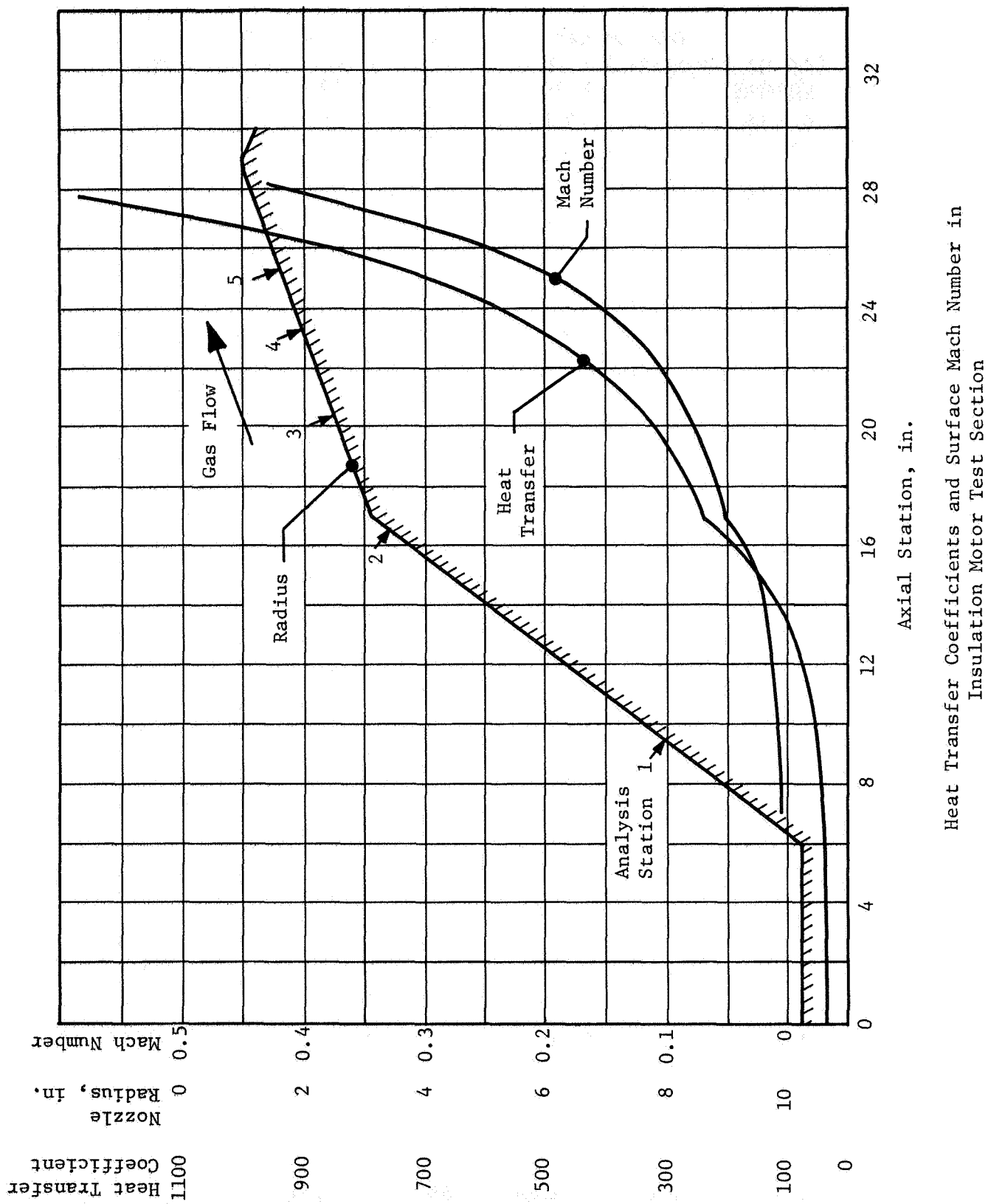


Figure 2

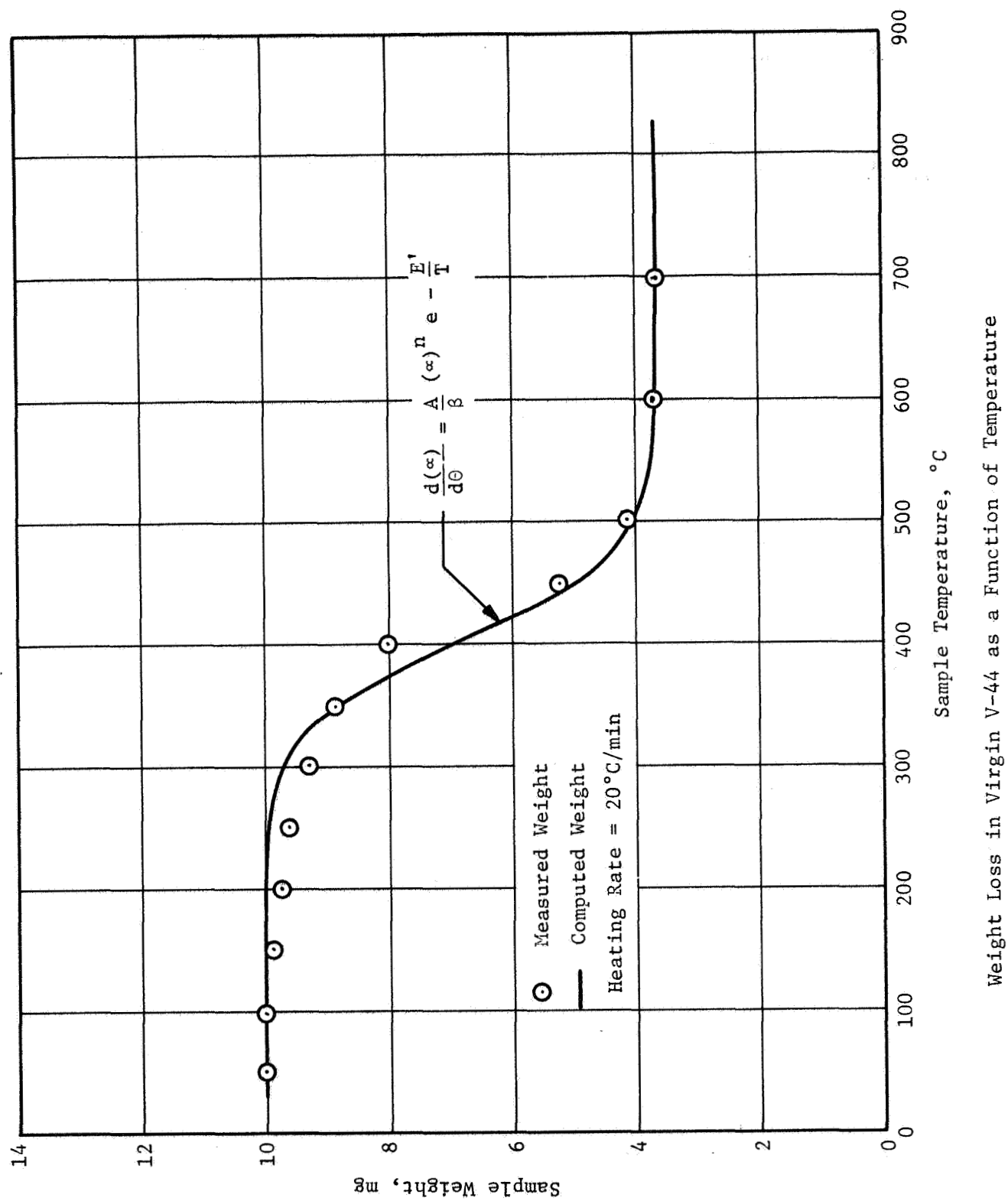
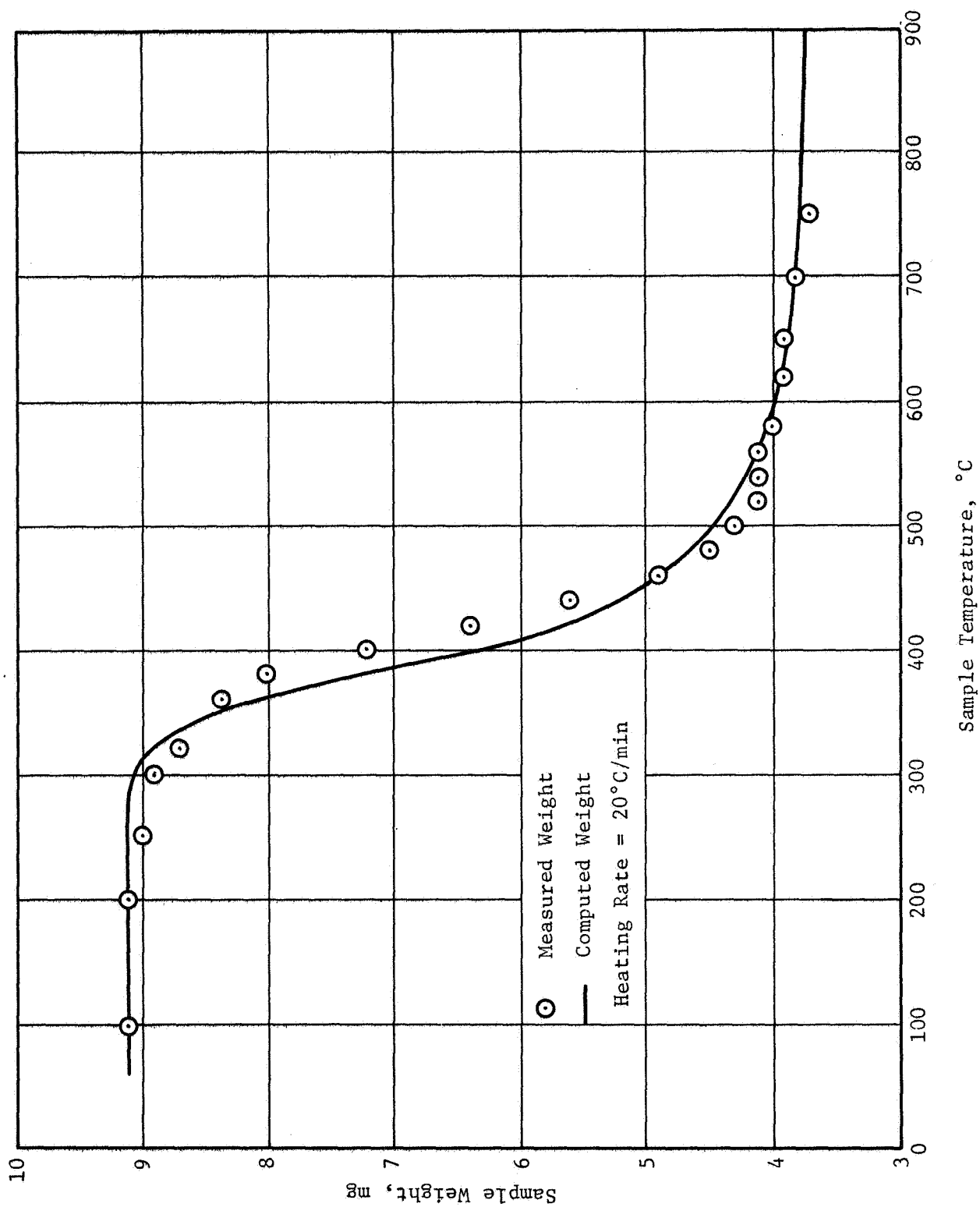


Figure 3



Weight Loss in Virgin IBT-100 as a Function of Temperature

Figure 4

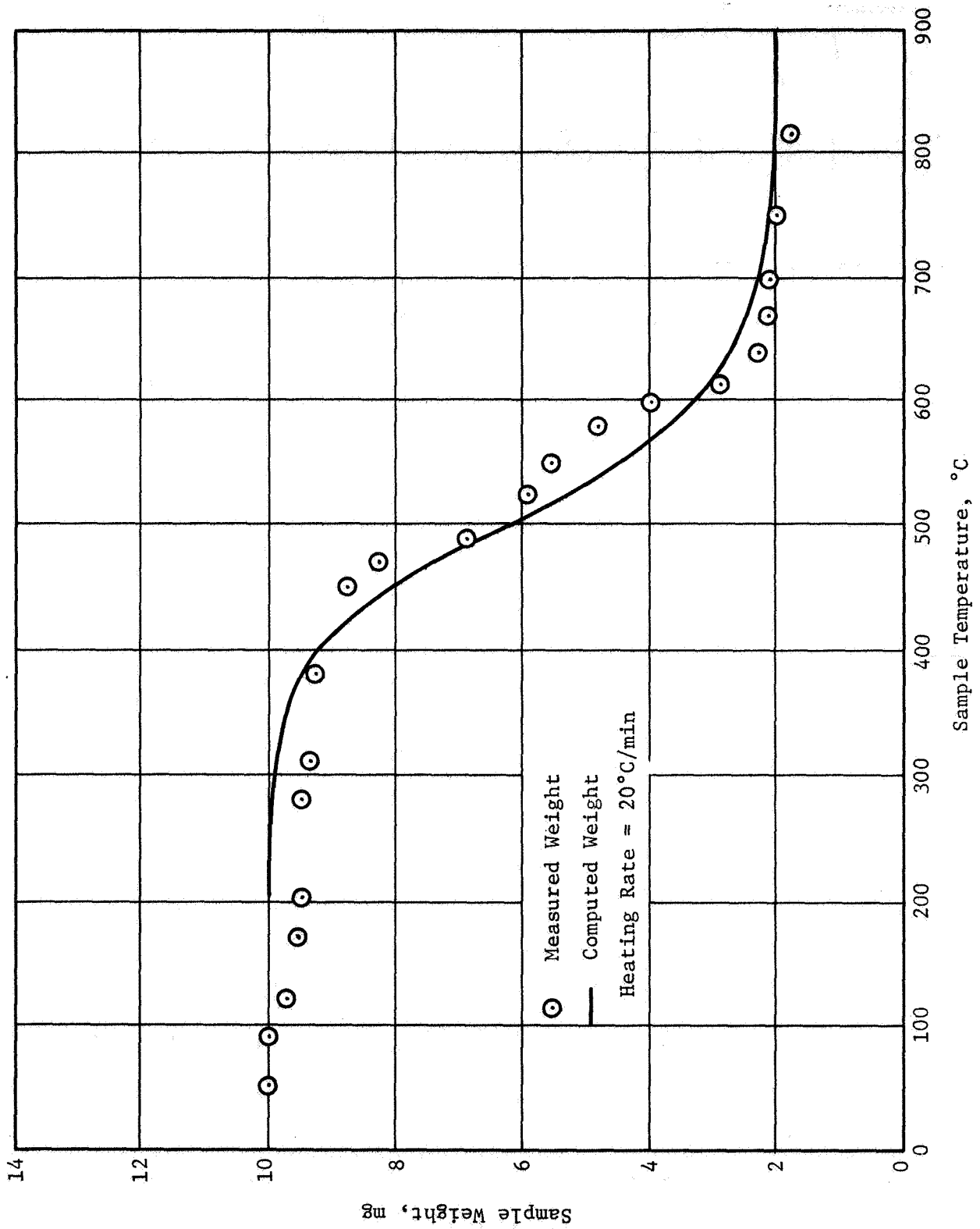
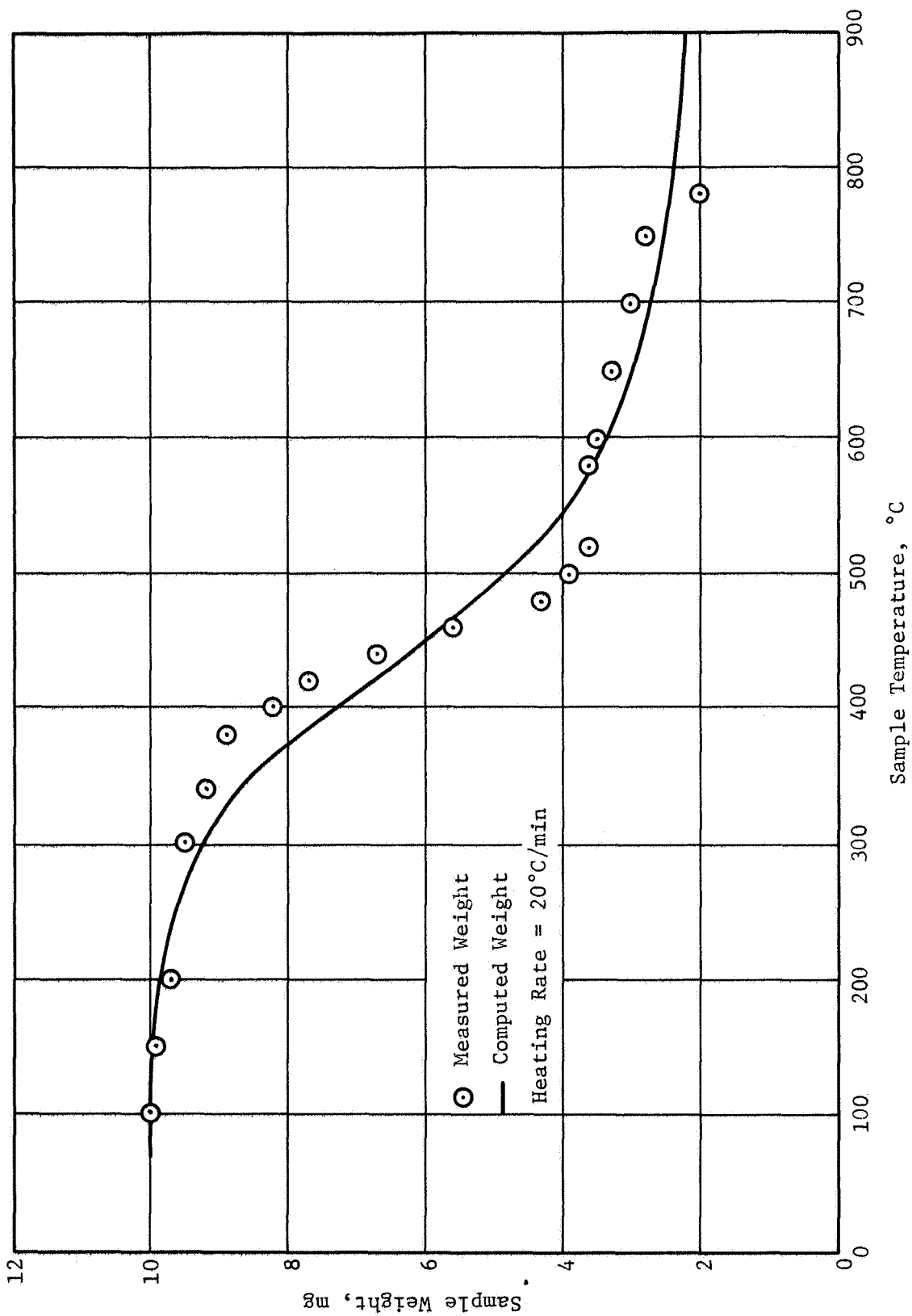


Figure 5

Weight Loss of Virgin IBS-107 as a Function of Temperature



Weight Loss of Virgin IBS-109 as a Function of Temperature

Figure 6

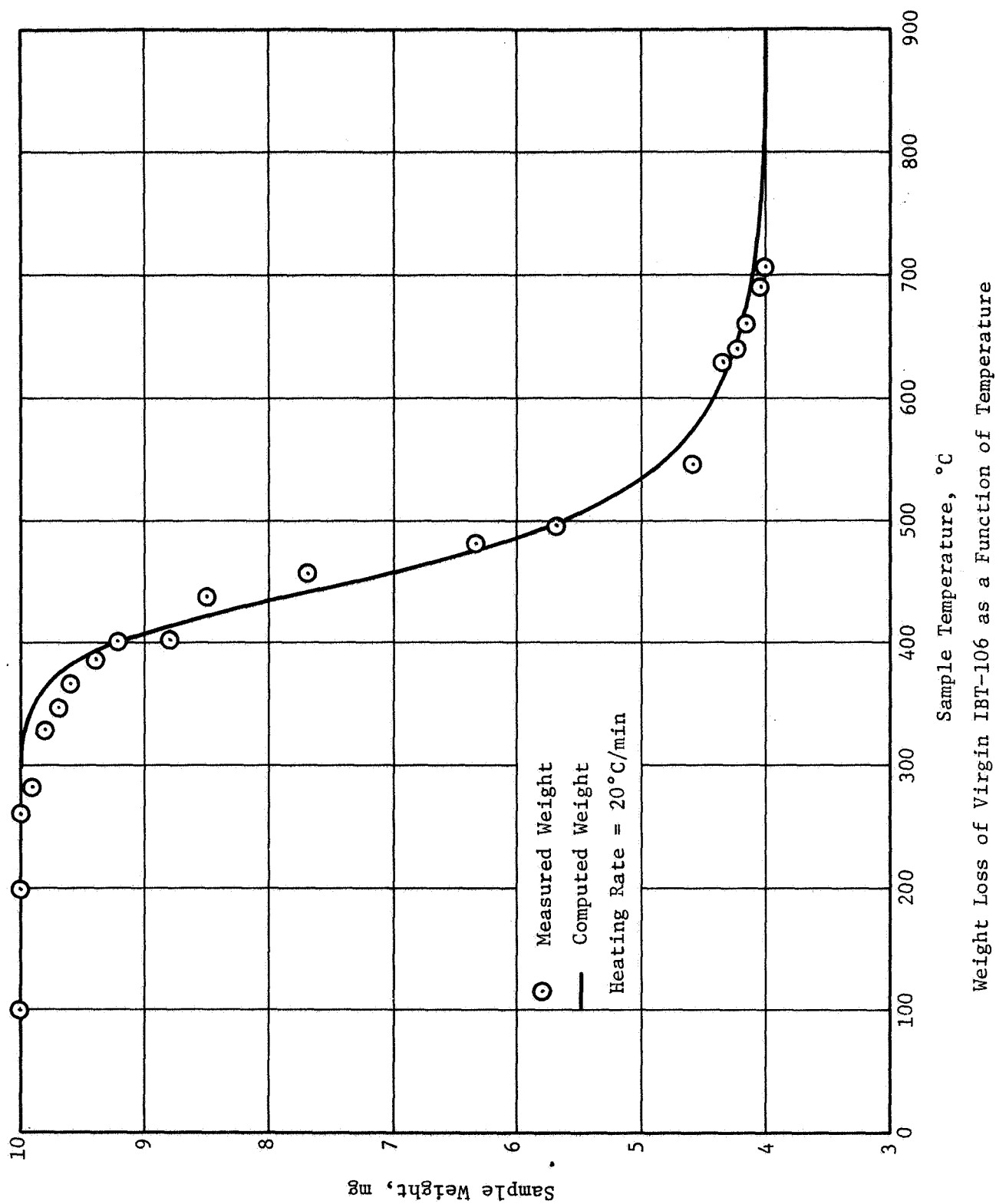


Figure 7

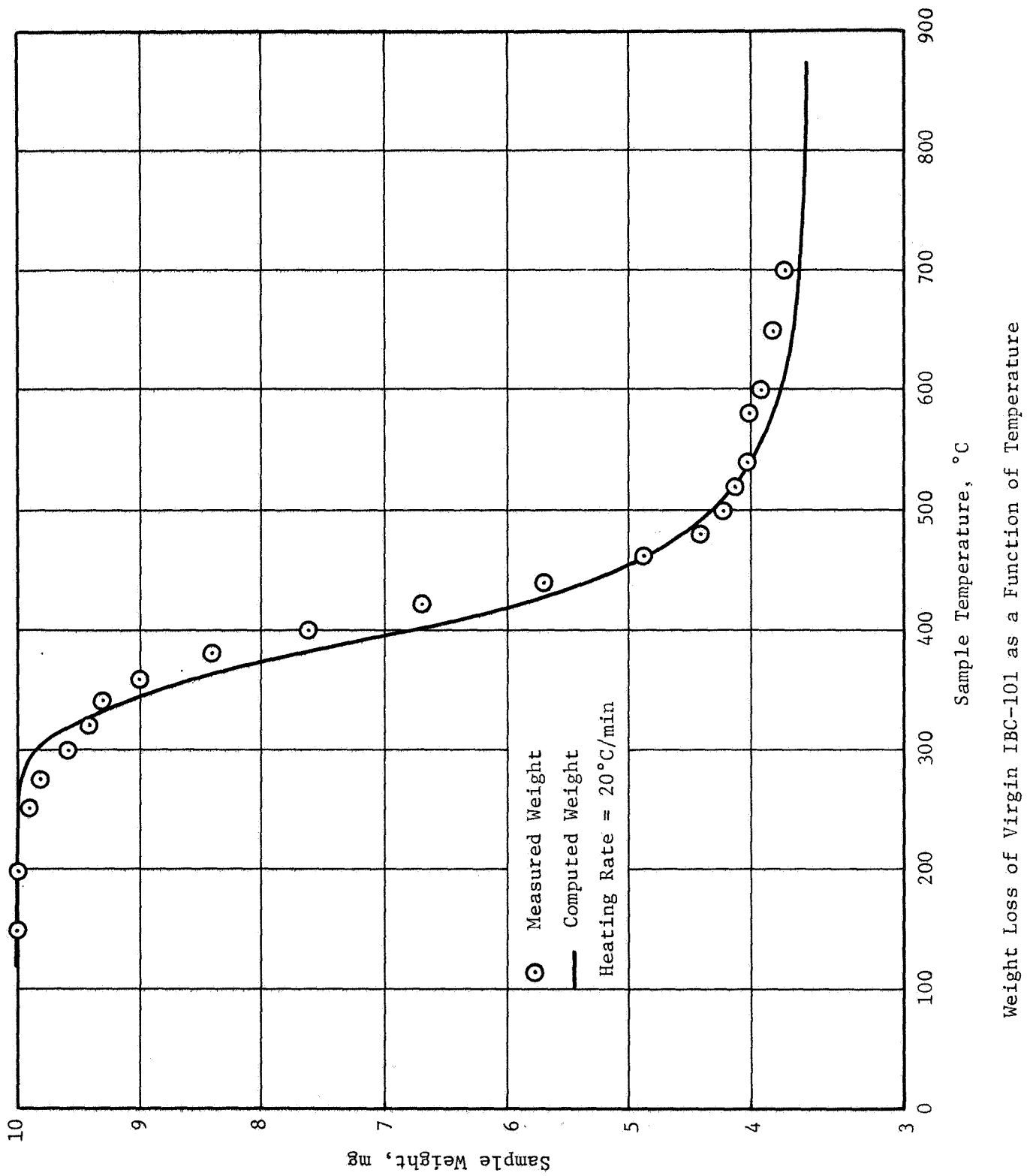


Figure 8

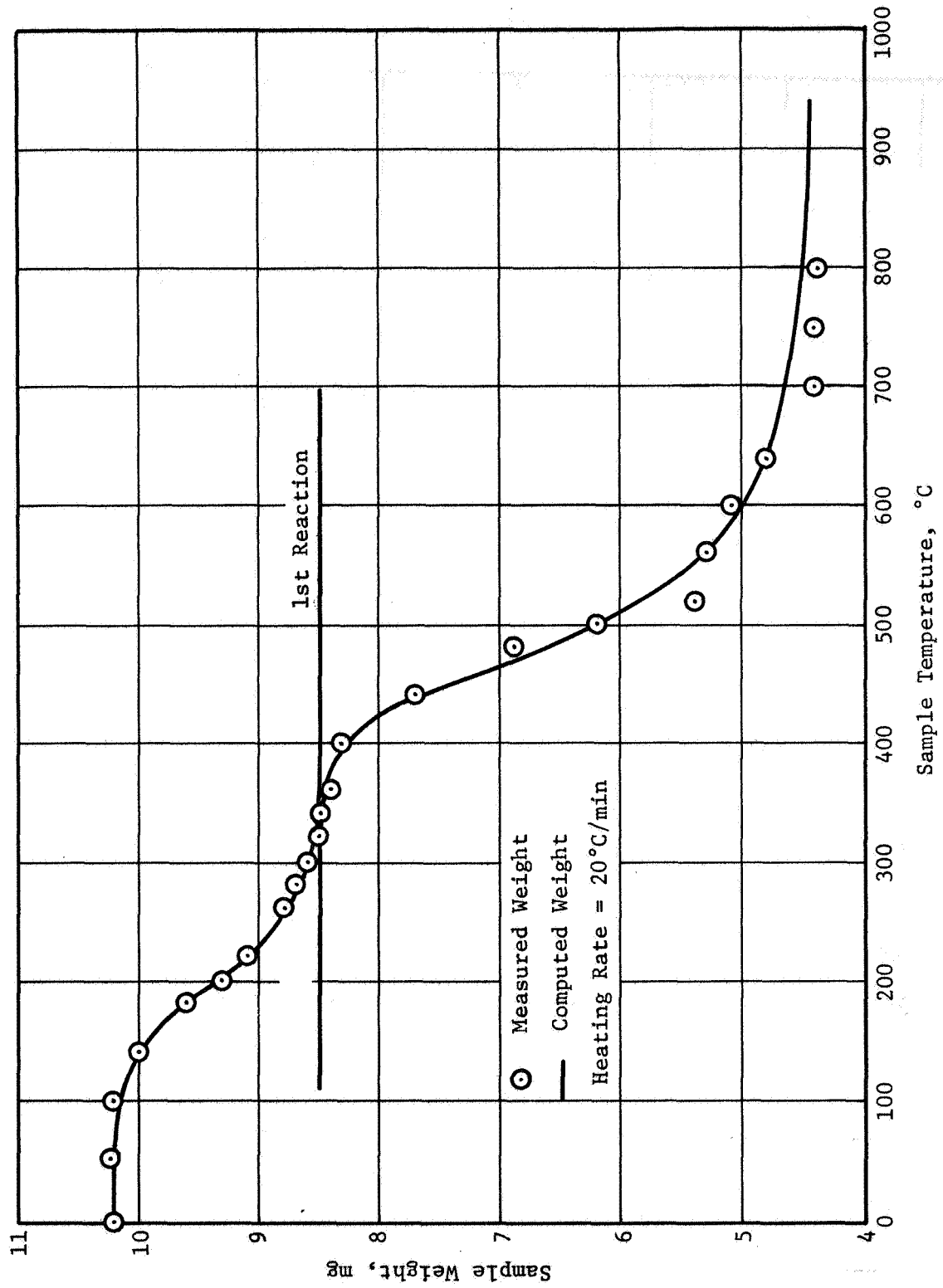
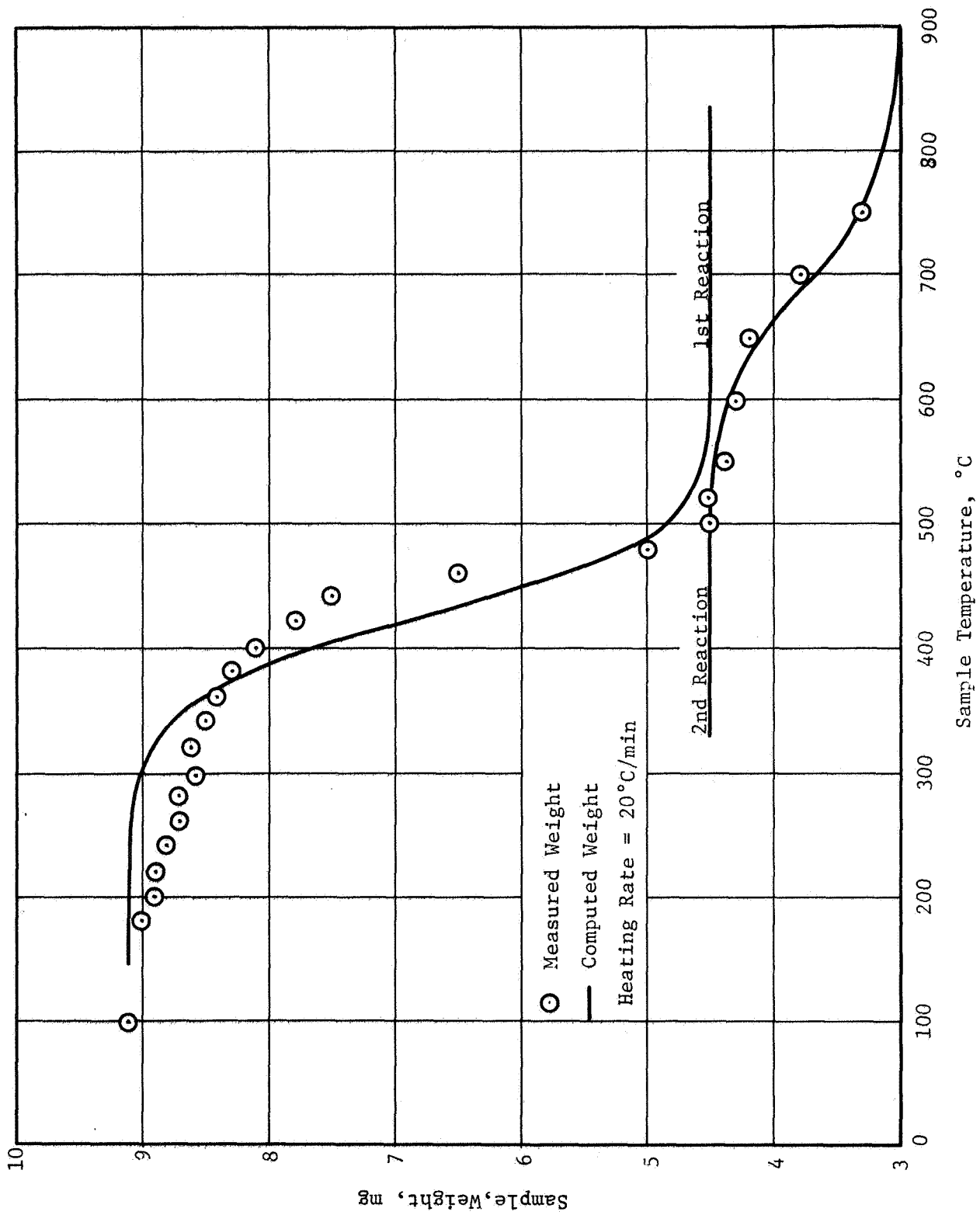


Figure 9

Weight Loss of Virgin USR-3800 as a Function of Temperature



Weight Loss of Virgin TI-H704B as a Function of Temperature

Figure 10

<u>Material</u>	<u>(A/β)</u>	<u>E'</u>	<u>η</u>	<u>Final Weight in Percent of Original Value</u>
V-44	9480.	17024.	1.524	36.5
USR 3800	646.1	9592.	1.704	12. *
	$2.658 \times 10^9$	34794.	3.708	43.1 **
IBT-100	$3.14 \times 10^{17}$	51084.	5.725	40.6
IBT-106	$1.972 \times 10^9$	33156.	3.188	40.0
TI-H704B	$1.835 \times 10^4$	18774	1.225	49.5 *
	$9.818 \times 10$	36684.	1.727	33.0 **
IBC-111	NO TGA (LIKE IBT-100)			
IBC-101	$5.528 \times 10^7$	26424.	3.07	35
IBS-109	3.98	8890.	1.964	20
IBS-107	$6.87 \times 10^2$	16051.	1.855	19

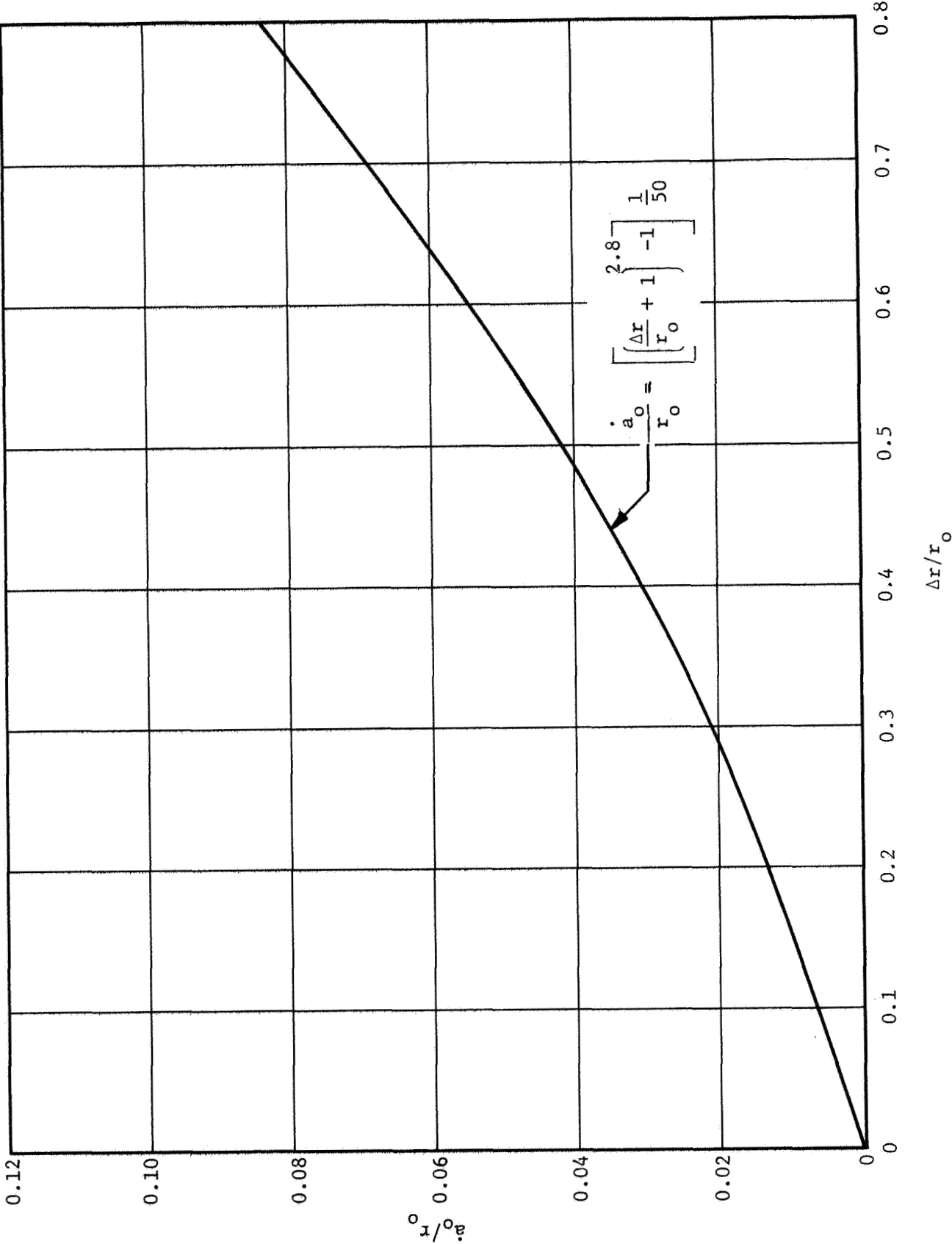
---

\* First Reaction

\*\*Second Reaction

Decomposition Rate Constants of Internal  
Insulation Materials

Figure 11



Ratio of Initial Erosion Rate to the Measured Value as a Function of Nozzle Radius

Figure 12

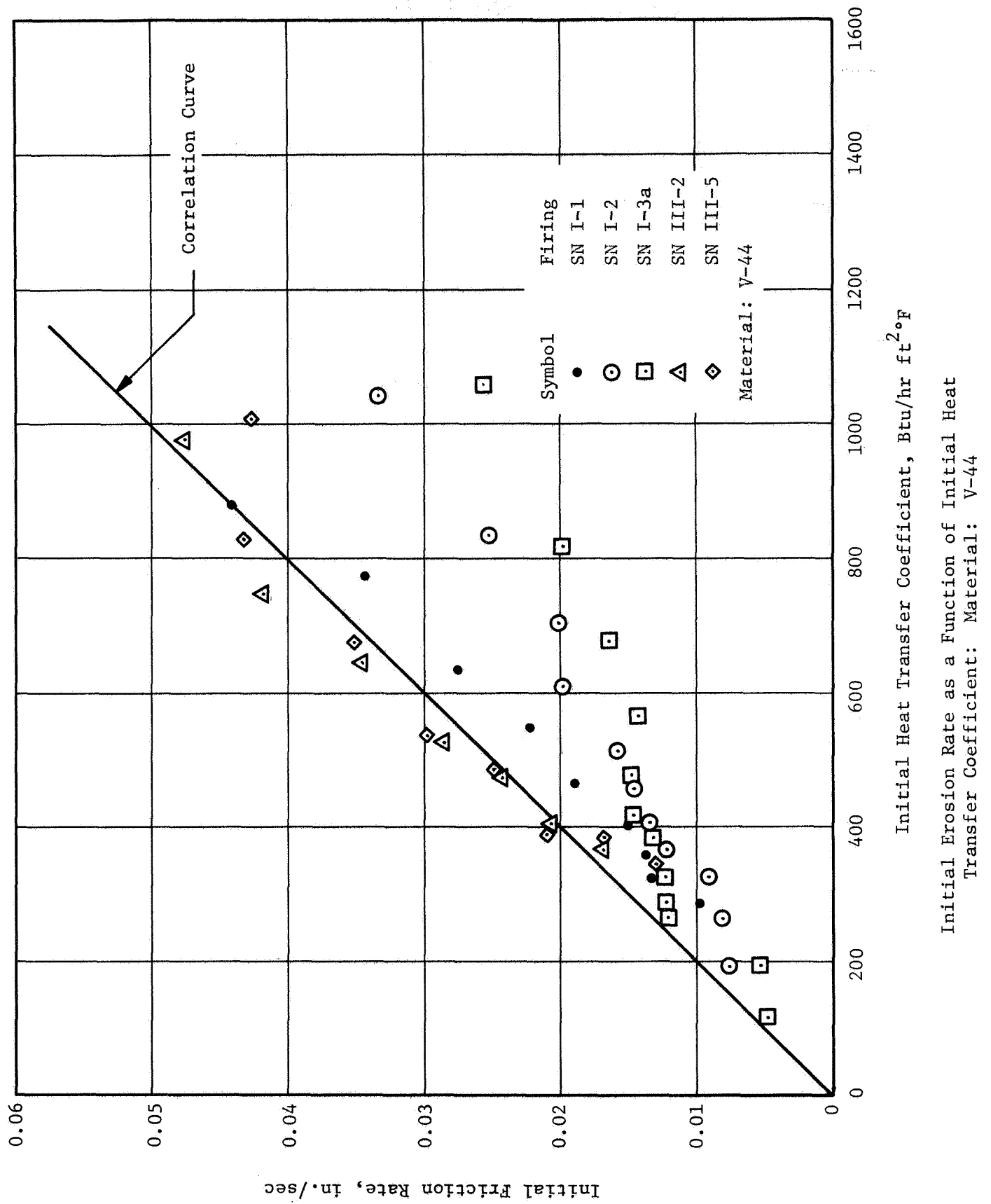


Figure 13

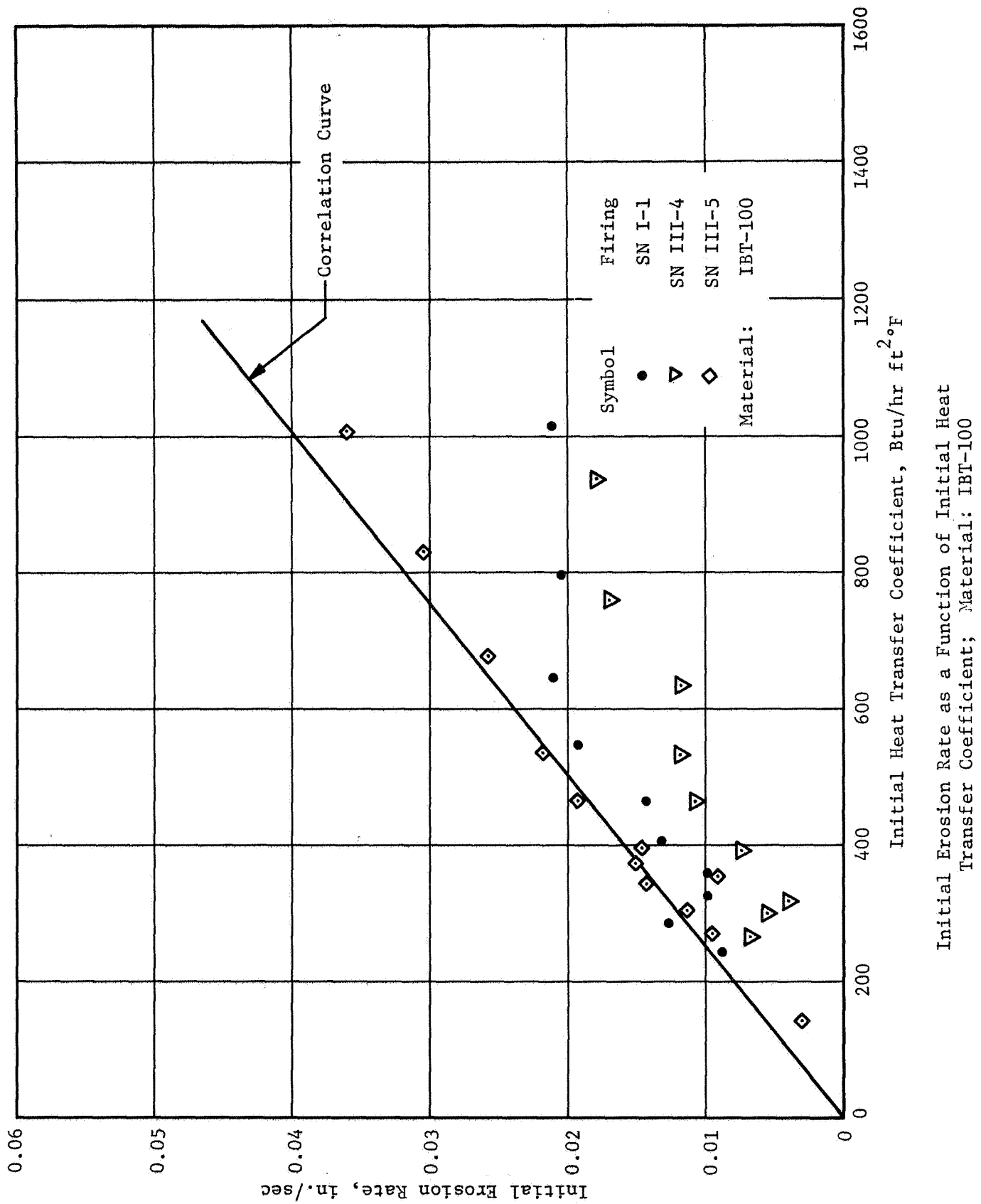


Figure 14

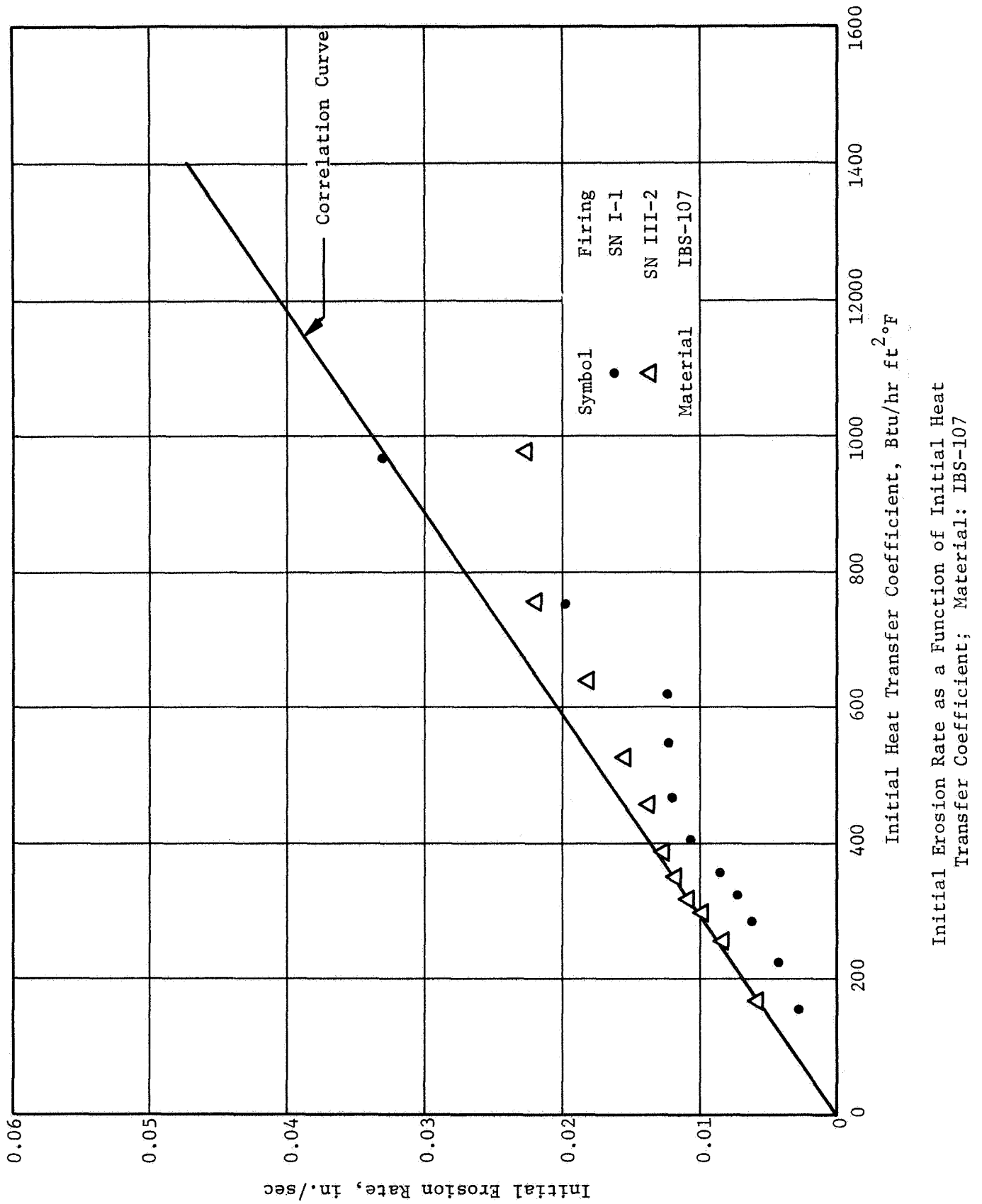


Figure 15

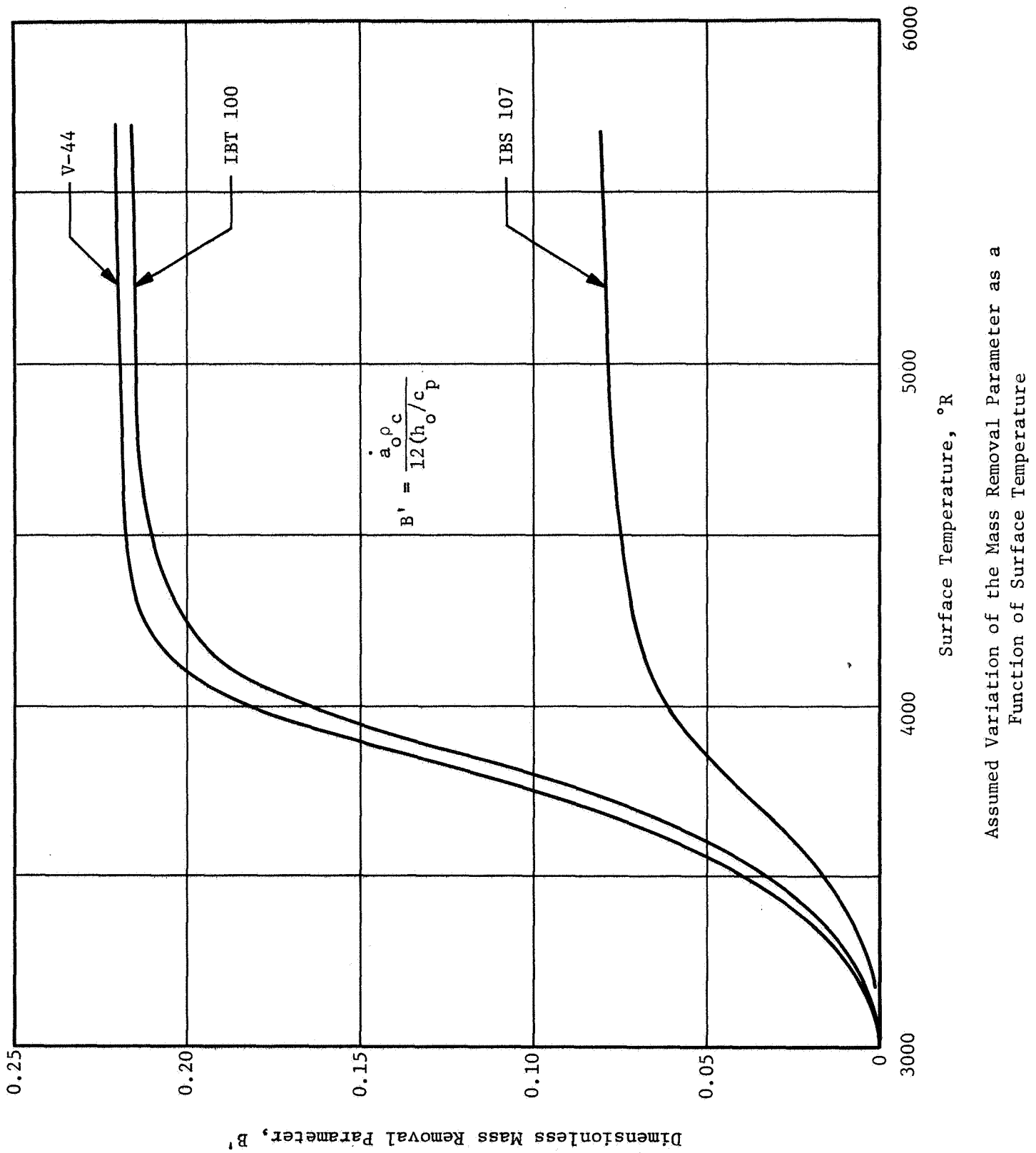
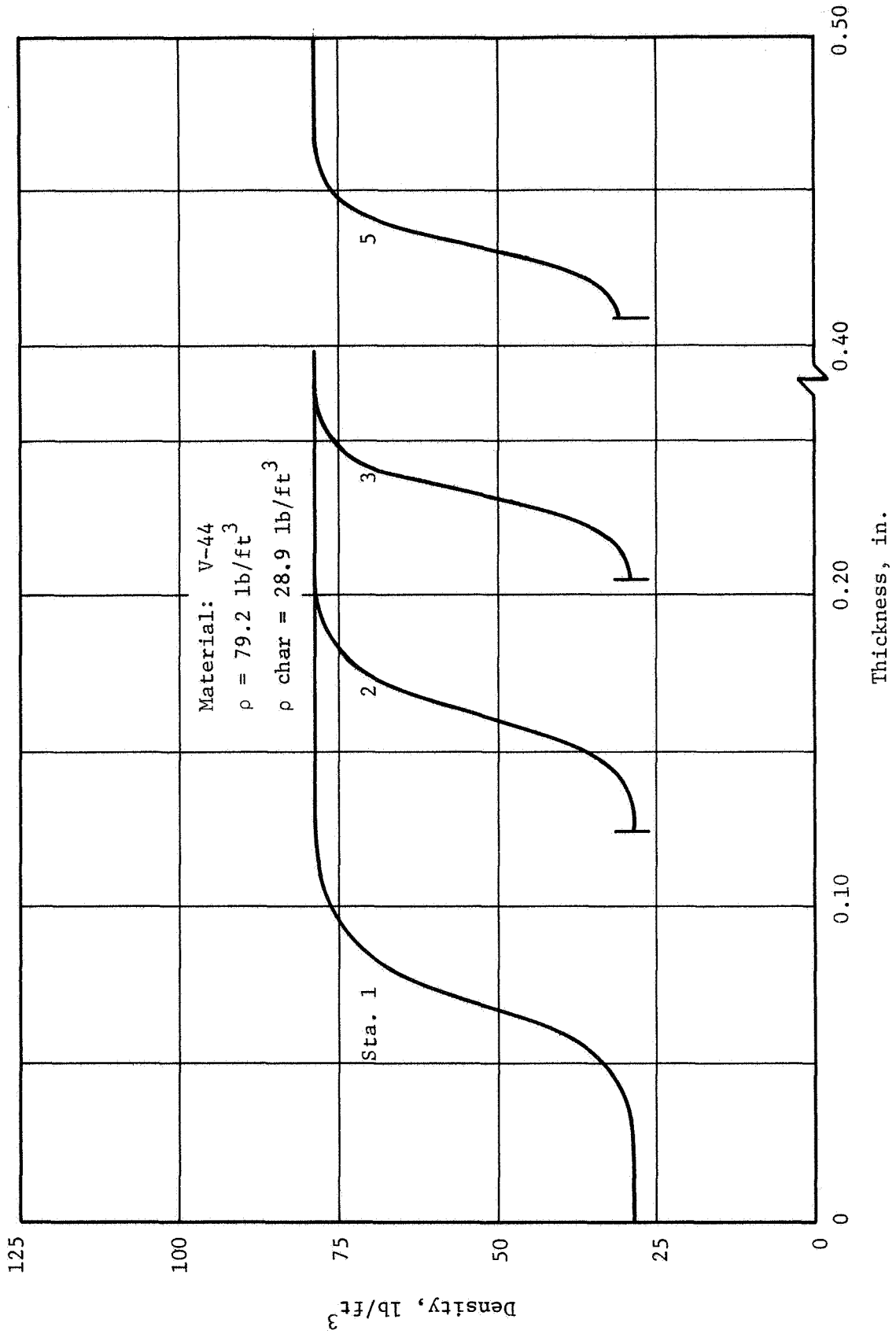
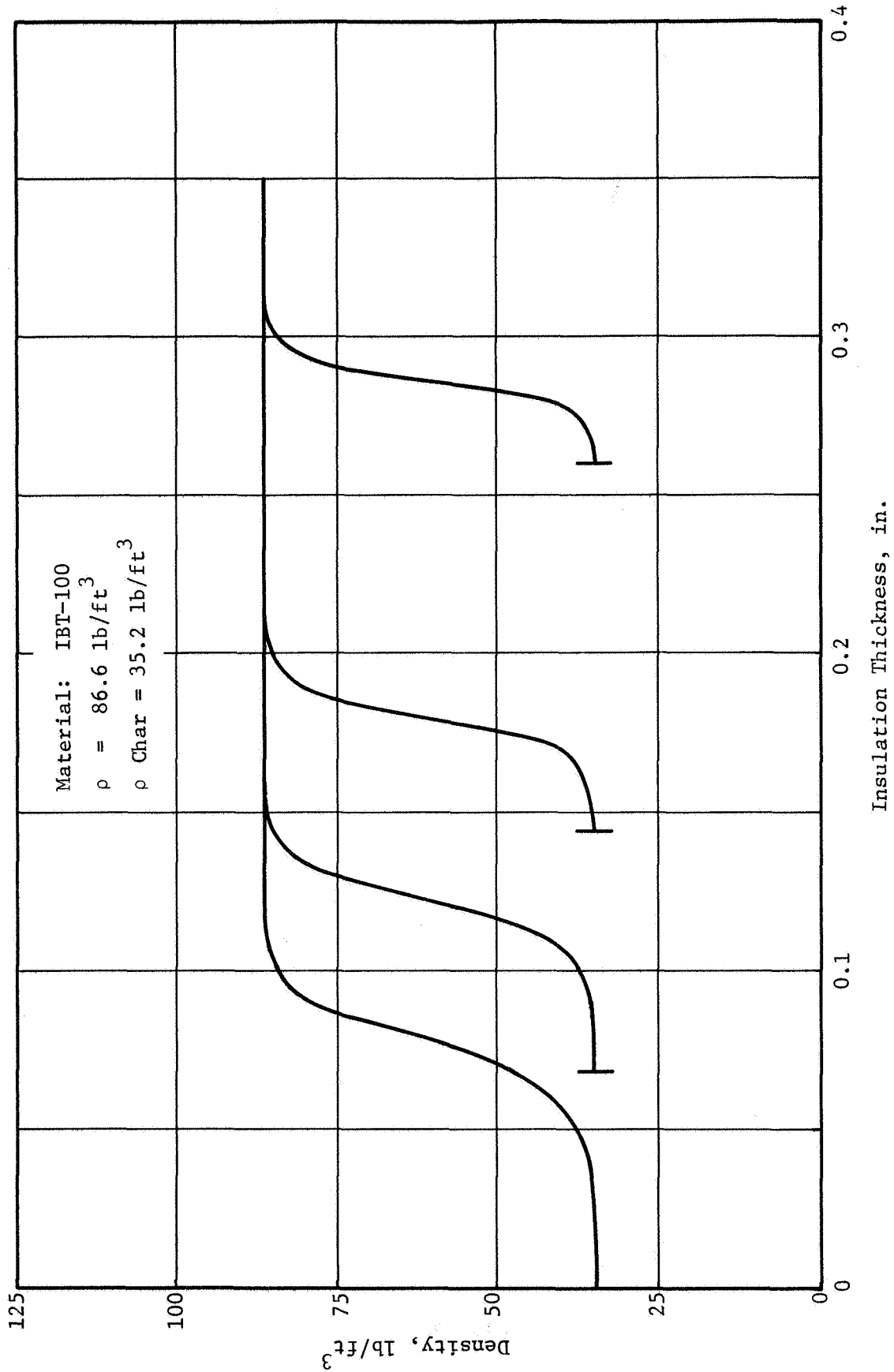


Figure 16



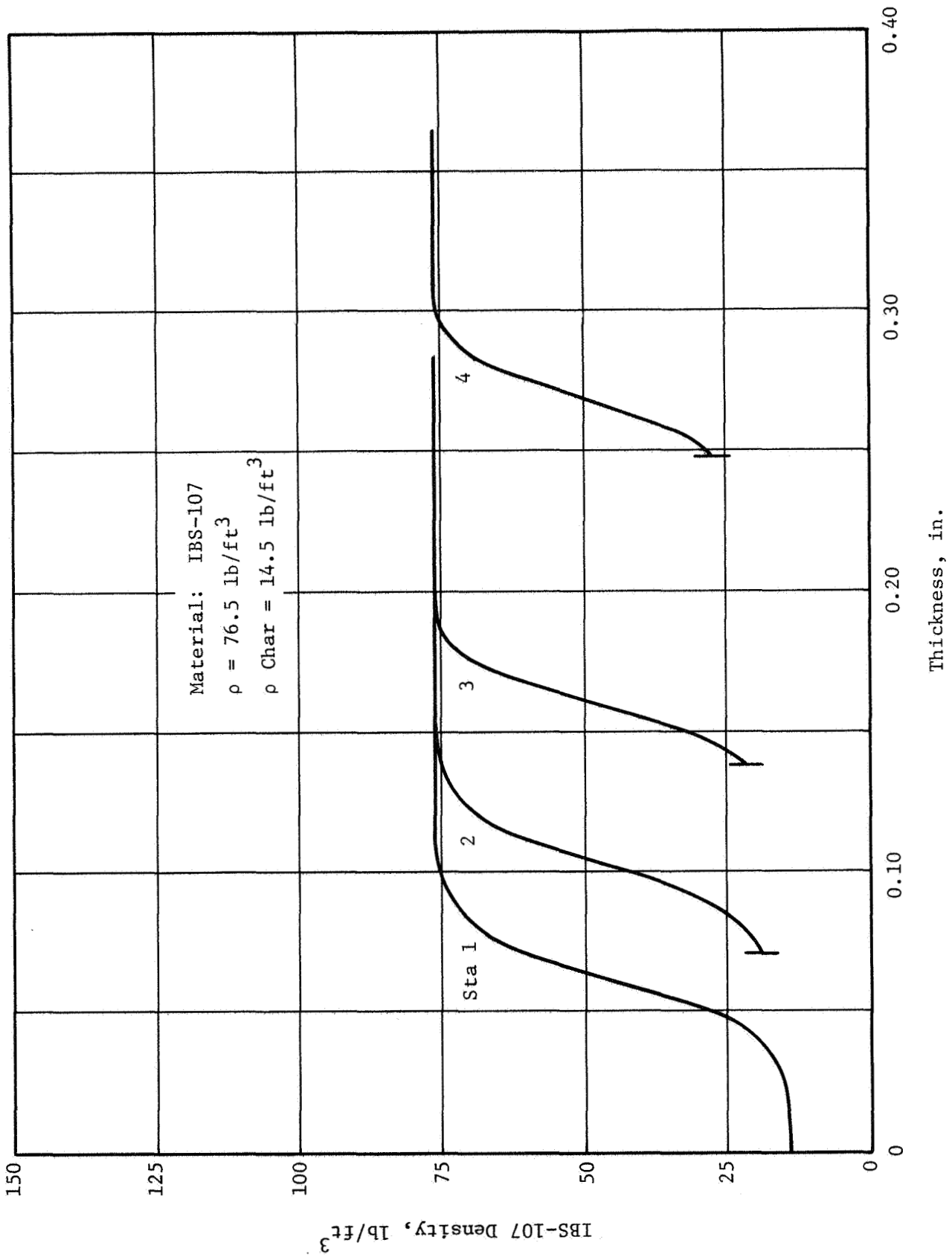
Predicted Char Density Distribution as a Function of  
 Insulation Thickness; Material: V-44

Figure 17



Predicted Char Density Distribution as a Function of Insulation Thickness; Material: IBT-100

Figure 18



Predicted Char Density Distribution as a Function of  
 Insulation Thickness; Material: IBS-107

Figure 19

V-44

	Analysis Station			
Firing	1 (0.006)*	2 (0.043)	3 (0.0815)	5 (0.202)
I-1	0.088 in./sec	0.12 in./sec	0.202 in./sec	0.476 in./sec
I-2	0.053	0.12	0.195	0.360
I-3a	0.090	0.136	0.216	0.280
III-2	0.087	0.140	0.226	0.473
III-3	0.066	0.172	0.327	0.63
III-4	0.060	0.115	0.301	0.63
III-5	0.086	0.128	0.265	0.535
Average	0.0757	0.133	0.247	0.483
Predicted**	0.076	0.168	0.237	0.436

IBS-107

Firing	1 (0.006)*	2 (0.03)*	3 (0.065)*	4 (0.135)*
I-1	0.091 in./sec	0.101 in./sec	0.114 in./sec	0.193 in./sec
III-2	0.091	0.107	0.170	0.269
Average	0.091	0.104	0.142	0.232
Predicted	0.071	0.112	0.168	0.277

IBS-100

Firing	1 (0.006)*	2 (0.03)*	3 (0.065)*	4 (0.135)*
I-1	0.088	0.097	0.132	0.275
I-3a	0.072	0.086	0.123	0.185
III-4	0.077	0.092	0.121	0.193
III-5	0.088	0.080	0.197	0.352
Average	0.0813	0.0888	0.143	0.251
Predicted	0.084	0.126	0.182	0.288

---

\* Initial Mach Number

\*\*Based on a 20% density loss

Comparison of Measured Erosion with Predicted Results

Figure 20

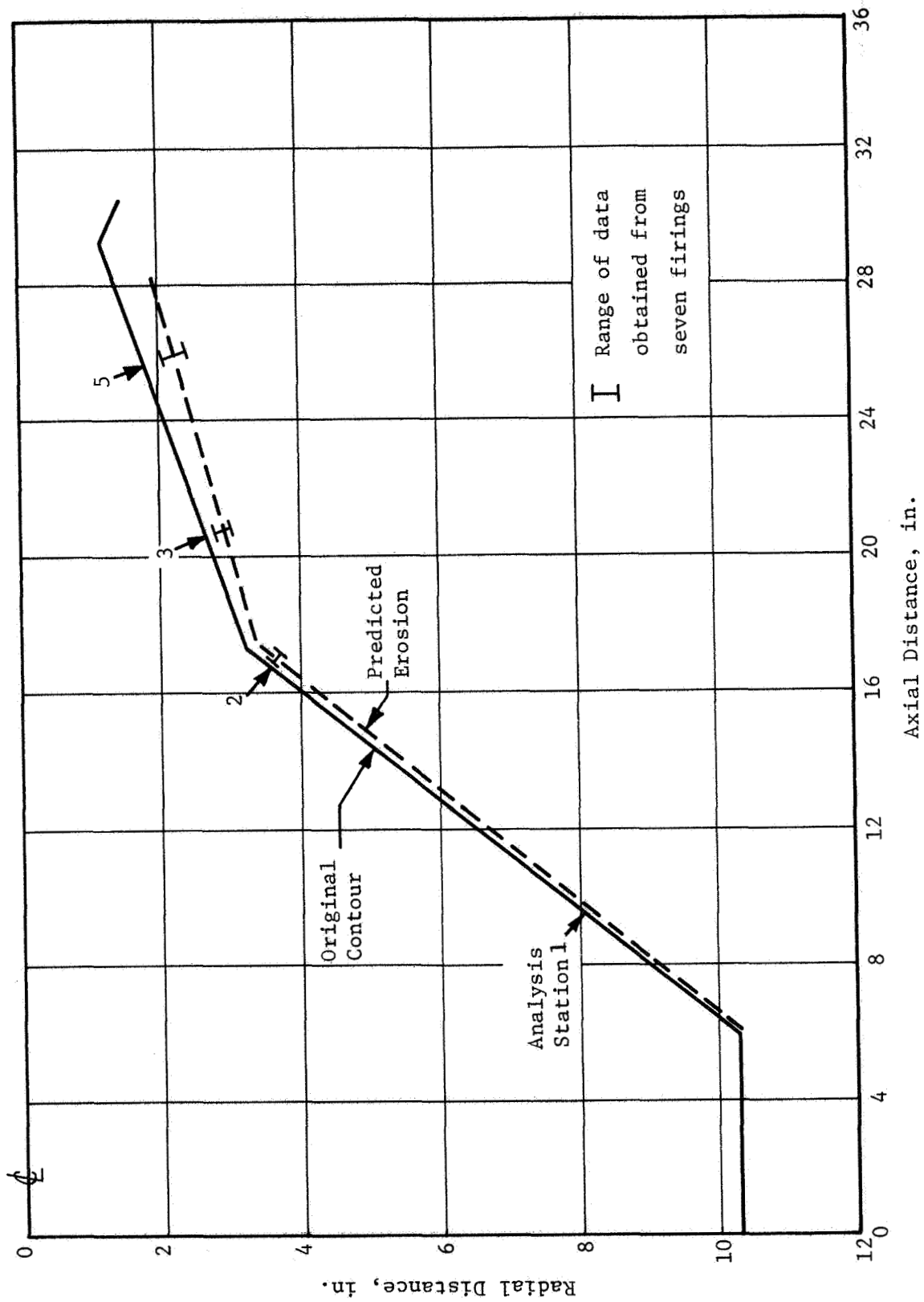


Figure 21

Comparison of Predicted V-44 Erosion with Data from Seven Firings

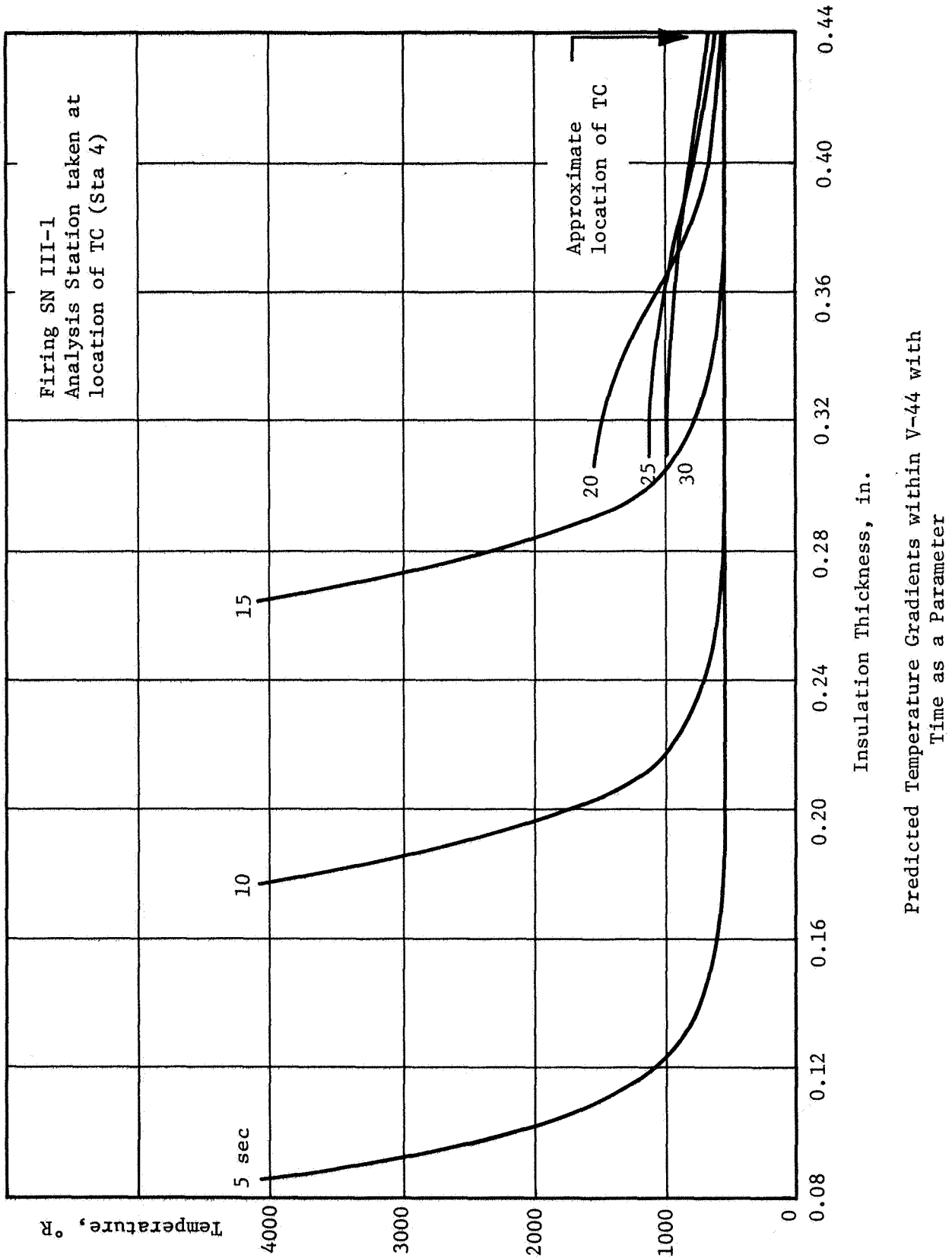
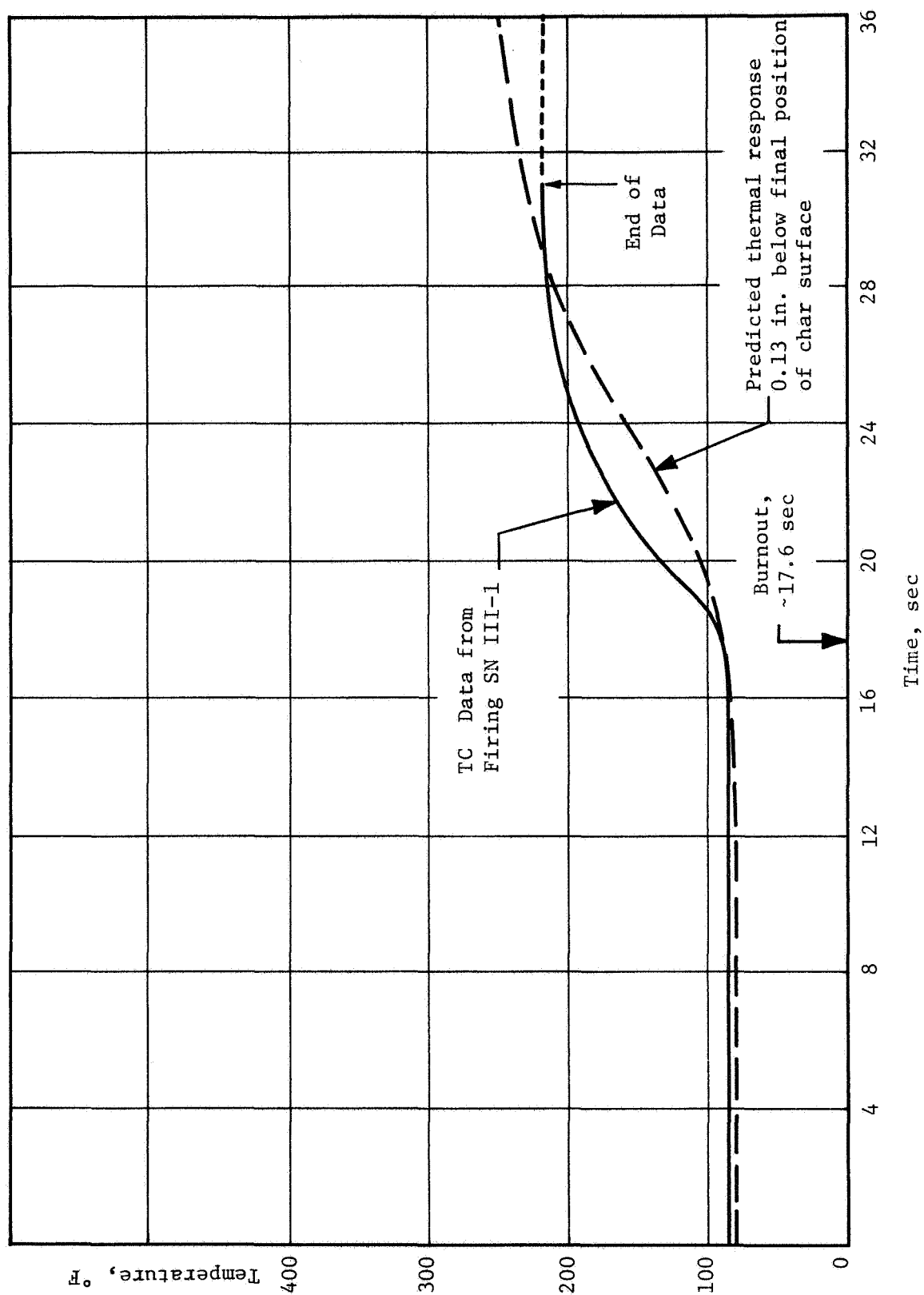


Figure 22



Comparison of Predicted Thermal Response with Thermocouple  
Data from Firing S/N III-1; Material: V-44

Figure 23

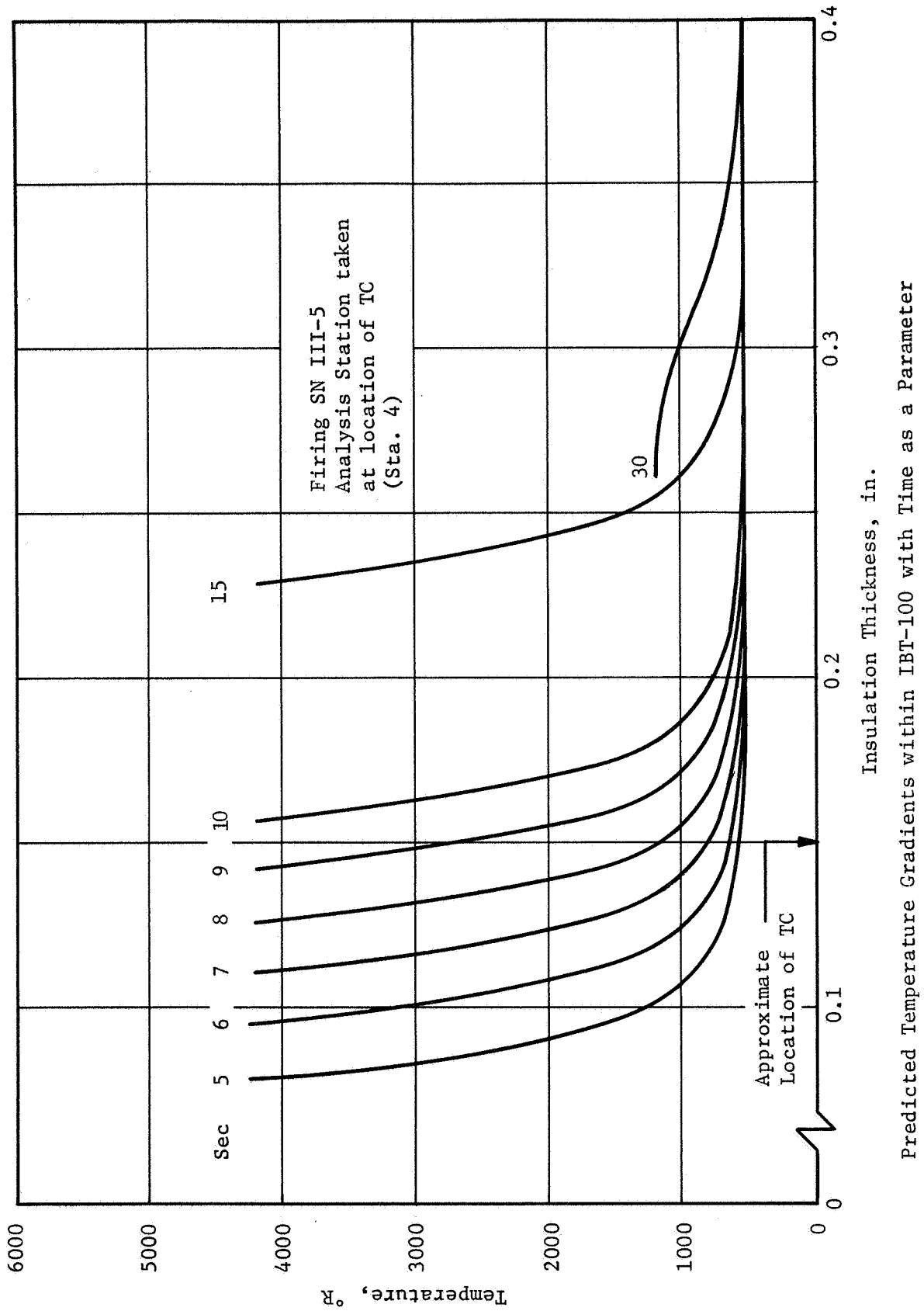
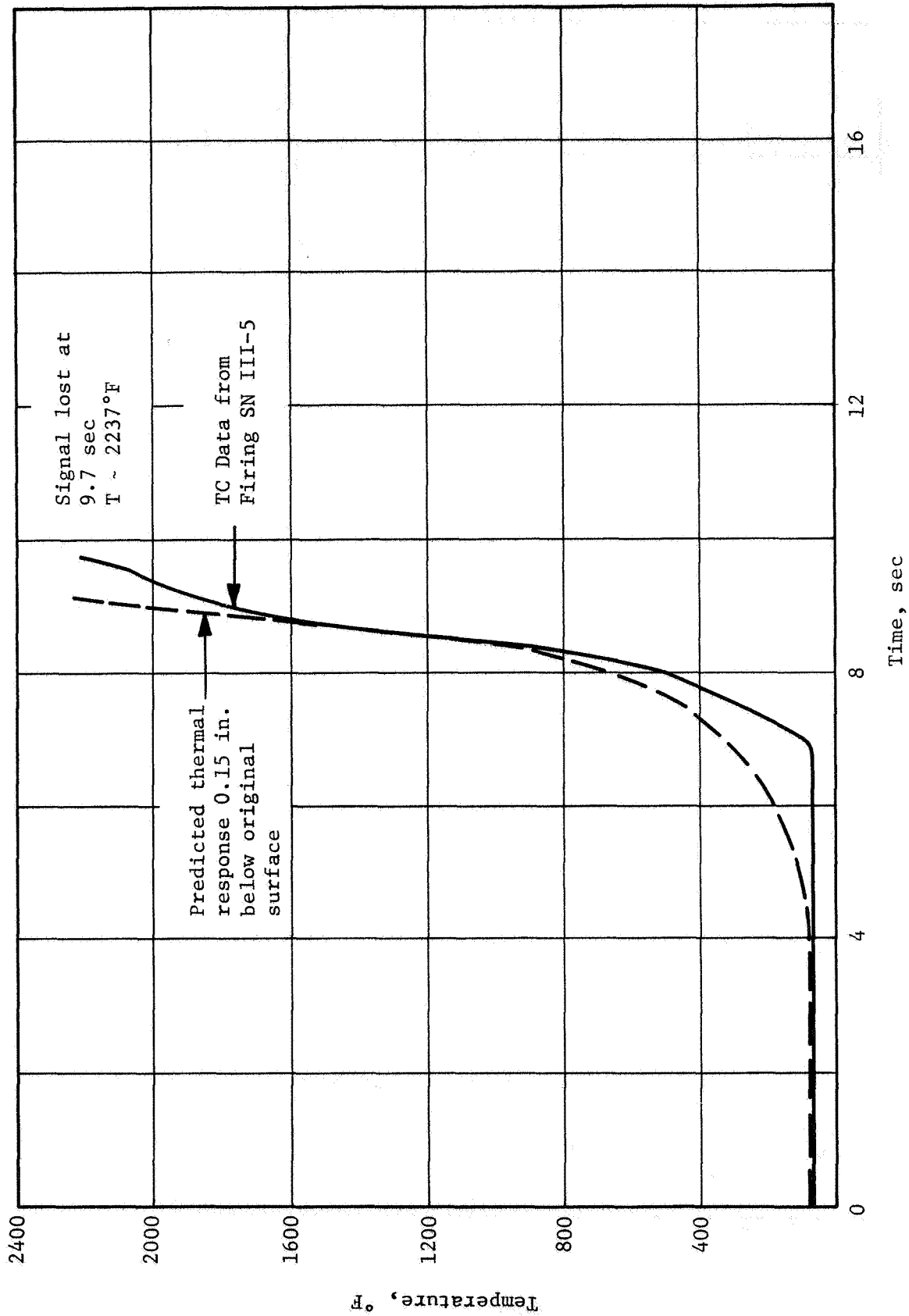


Figure 24



Comparison of Predicted Thermal Response with Thermocouple  
Data from Firing S/N III-5; Material: IBT-100

Figure 25

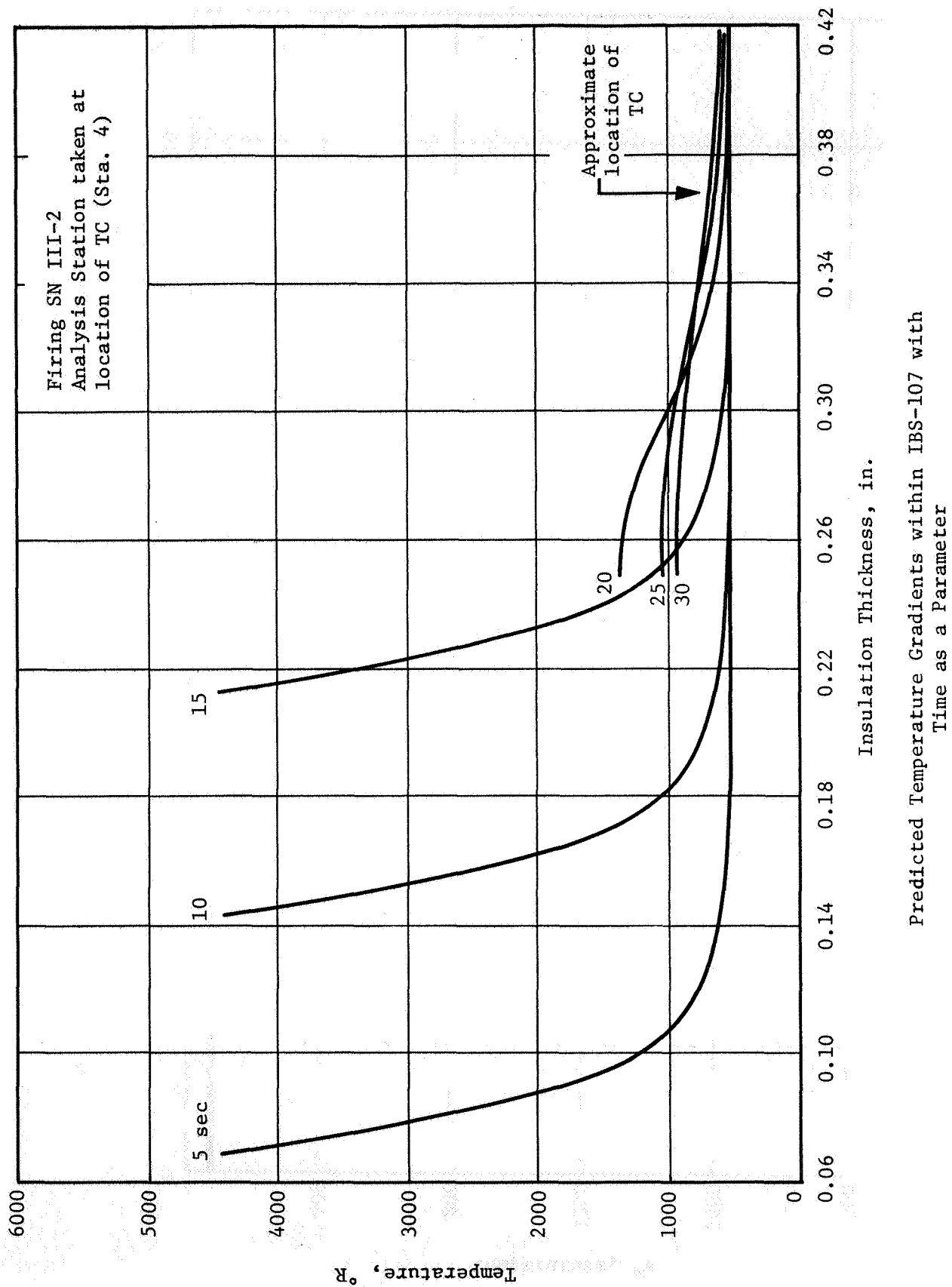
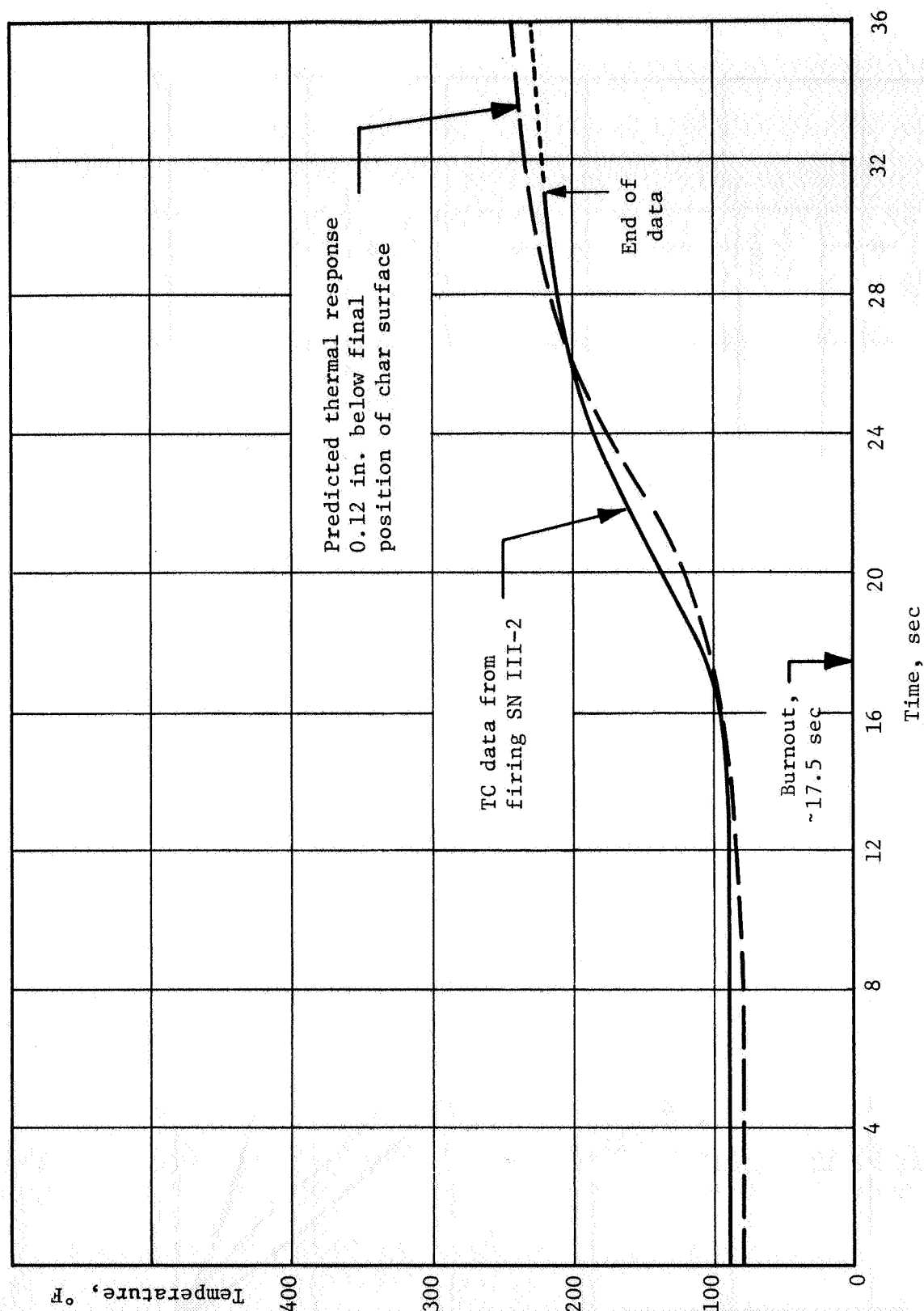
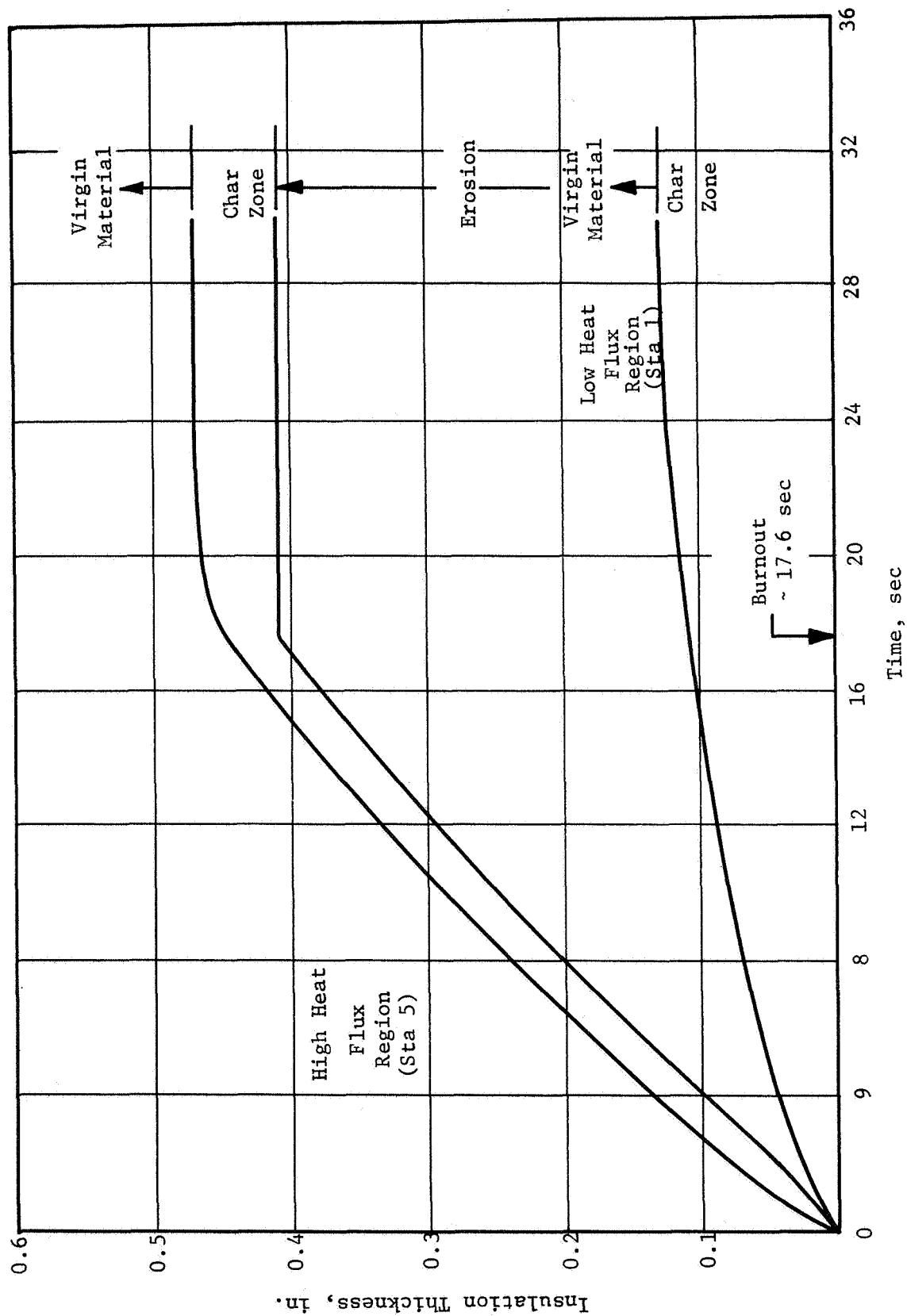


Figure 26



Comparison of Predicted Thermal Response with Thermocouple  
Data from Firing S/N IIII-2; Material: IBS-107

Figure 27



Erosion and Char Growth of V-44 as a Function of Time

Figure 28

FINAL REPORT DISTRIBUTION LIST

NASA Lewis Research Center		NASA George C. Marshall Space	
21000 Brookpark Road		Flight Center	
Cleveland, Ohio 44135		Redstone Arsenal	
Attn: Contracting Officer		Huntsville, Alabama, 35812	
Mail Stop 500-313	(1)	Attn: Technical Library	(1)
Solid Rocket Technology Branch		R-P&VE-PA/K, Chandler	(1)
Mail Stop 500-205	(8)		
Technical Library		Jet Propulsion Laboratory	
Mail Stop 60-3	(2)	Calif. Institute of Technology	
Tech. Report Control Office		4800 Oak Grove Drive	
Mail Stop 5-5	(1)	Pasadena, California 91103	
J. Kennard		Attn: Richard Bailey	(1)
Mail Stop 3-17	(1)	Technical Library	(1)
Tech. Utilization Office			
Mail Stop 3-19	(1)	Scientific & Technical Information	
Patent Counsel		Facility	
Mail Stop 500-311	(1)	NASA Representative	
		P.O. Box 33	
National Aeronautics and Space		College Park, Maryland 20740	
Administration		Attn: CRT	(6)
Washington, D.C. 20546			
Attn: RPM/William Cohen	(3)	<u>GOVERNMENT INSTALLATIONS</u>	
RPS/Robert W. Ziem	(1)		
ATSS-AL/Technical Library	(2)	AF Space Systems Division	
		Air Force Unit Post Office	
NASA Ames Research Center		Los Angeles, California 90045	
Moffett Field, California 94035		Attn: Col. E. Fink	(1)
Attn: Technical Library	(1)		
		AF Research and Technology Division	
NASA Langley Research Center		Bolling AFB, D.C., 20332	
Langley Station		Attn: Dr. Leon Green, Jr.	(1)
Hampton, Virginia 23365			
Attn: Robert L. Swain	(1)	AF Rocket Propulsion Laboratory	
Technical Library	(1)	Edwards AFB, California 93523	
		Attn: RPM/Mr. C. Cook	(2)
NASA Goddard Space Flight Center			
Greenbelt, Maryland 20771		AF Materials Laboratory	
Attn: Technical Library	(1)	Wright-Patterson AFB, Ohio 45433	
		Attn: MANC/D. Schmidt	(1)
NASA Manned Spacecraft Center		MAAE	(1)
2101 Webster Seabrook Road			
Houston, Texas 77058			
Attn:	(1)		

AF Ballistic Missile Division P.O. Box 262 San Bernadino, California Attn: WDSOT	(1)	Chemical Propulsion Information Agency Applied Physics Laboratory 8621 Georgia Avenue Silver Spring, Maryland 20910	(1)
Structures Division Wright Patterson AFB, Ohio 45433 Attn: FDT/R. F. Hoener	(1)	Defense Documentation Center Cameron Station 5010 Duke Street Alexandria, Virginia 22314	(1)
Army Missile Command Redstone Scientific Information Center Redstone Arsenal, Alabama 35809 Attn: Chief, Document Section	(1)	Defense Materials Information Center Battelle Memorial Institute 505 King Avenue Columbus, Ohio 43201	(1)
Ballistic Research Laboratory Aberdeen Proving Ground, Maryland 21005 Attn: Technical Library	(1)	Materials Advisory Board National Academy of Science 2101 Constitution Ave., N.W. Washington, D.C., 20418 Attn: Capt. A. M. Blamphin	(1)
Picatinny Arsenal Dover, New Jersey, 07801 Attn: Technical Library	(1)	Institute for Defense Analysis 1666 Connecticut Ave., N.W. Washington, D.C. Attn: Technical Library	(1)
Navy Special Projects Office Washington, D.C., 20360 Attn: H. Bernstein	(1)	Advanced Research Projects Agency Pentagon, Room 3D154 Washington, D.C., 20301 Attn: Tech. Information Office	(1)
Naval Air Systems Command Washington, D.C. 20360 Attn: AIR-330/Dr. O. H. Johnson	(1)	<u>INDUSTRY CONTRACTORS</u>	
Naval Propellant Plant Indian Head, Maryland 20640 Attn: Technical Library	(1)	Aerojet-General Corporation P.O. Box 1168 Solid Rocket Division Sacramento, California 94086 Attn: Dr. B. Simmons	(1)
Naval Ordnance Laboratory White Oak Silver Spring, Maryland 20910 Attn: Technical Library	(1)	Tech. Information Ctr. Space Booster Dept.	(1) (8)
Naval Ordnance Test Station China Lake, California 93557 Attn: Technical Library C. J. Thelen	(1) (1)	Aerojet-General Corporation P.O. Box 296 Azusa, California 91702 Attn: Technical Library	(1)
Naval Research Laboratory Washington, D.C., 20390 Attn: Technical Library	(1)		

Aerospace Corporation  
2400 East El Segundo Boulevard  
El Segundo, California 90245  
Attn: Technical Library  
Solid Motor Dev. Office

(1)  
(1)

Aerospace Corporation  
P.O. Box 95085  
Los Angeles, California 90045  
Attn: Technical Library

(1)

Atlantic Research Corporation  
Shirley Highway at Edsall Road  
Alexandria, Virginia 22314  
Attn: Technical Library

(1)

Battelle Memorial Library  
505 King Avenue  
Columbus, Ohio 43201  
Attn: Edward Unger

(1)

Boeing Company  
P. O. Box 3999  
Seattle, Washington 98124  
Attn: Technical Library

(1)

Chrysler Corporation  
Space Division  
Michoud Operations  
New Orleans, Louisiana  
Attn: Technical Library

(1)

Douglas Missiles & Space Systems  
Huntington Beach, California  
Attn: T. J. Gordon

(1)

Hercules, Inc.  
Allegany Ballistics Laboratory  
P.O. Box 210  
Cumberland, Maryland 21502  
Attn: Technical Library

(1)

Hercules Company  
Bacchus Works  
P.O. Box 98  
Magna, Utah 84044  
Attn: Technical Library

(1)

Thiokol Chemical Corporation  
Wasatch Division  
Brigham City, Utah 94302  
Attn: Dan Hess  
Technical Library

(1)  
(1)

Lockheed Missiles & Space Company  
P.O. Box 504  
Sunnyvale, California  
Attn: Technical Library

(1)

Lockheed Propulsion Company  
P.O. Box 111  
Redlands, California 93273  
Attn: Bud White

(1)

Martin Marietta Corporation  
Baltimore Division  
Baltimore, Maryland 21203  
Attn: Technical Library

(1)

Mathematical Sciences Corporation  
278 Renook Way  
Arcadia, California 91107  
Attn: M. Fourney

(1)

Philco Corporation  
Aeronutronics Division  
Ford Road  
Newport Beach, California 92660  
Attn: Technical Library

(1)

Rocketdyne  
Solid Propulsion Operations  
P.O. Box 548  
McGregor, Texas  
Attn: Technical Library

(1)

Rocketdyne  
6633 Canoga Avenue  
Canoga Park, California 91304  
Attn: Technical Library

(1)

Rohm and Haas  
Redstone Arsenal Research Division  
Huntsville, Alabama 35807  
Attn: Technical Library

(1)

Rohr Corporation  
Space Products Division  
8200 Arlington Boulevard  
Riverside, California

(1)

TRW Inc.  
Structures Division  
23444 Euclid Avenue  
Cleveland, Ohio 44117  
Attn: L. Russell

(1)

Thiokol Chemical Corporation  
Elkton Division  
Elkton, Maryland 21921  
Attn: Technical Library

(1)

Thiokol Chemical Corporation  
Huntsville Division  
Huntsville, Alabama 35807  
Attn: Technical Library

(1)

Uniroyal, Inc.  
Mishawaka, Indiana 46544  
Attn: Mr. D. O. Trok

Insulation Technology, Inc.;  
U.S. Polymeric, Inc.  
P.O. Box A.D.  
3601 Orangerie Way  
Carmichael, California  
Attn: Mr. J. C. Boswell

AVCO Corp.  
Space Systems Div.  
201 Lowell St.  
Wilmington, Mass. 01887  
Attn: Mr. K. M. Jacobs

Union Carbide Corp.  
Silicone Div.  
2770 Leonis Blvd.  
Los Angeles (Vernon), Calif. 90058  
Attn: Elastomer Materials Dept.

Narmco Materials Div.  
600 Victoria St.  
Costa Mesa, Calif.  
Attn: Mr. W. Chester

The Goodyear Tire and Rubber Co.  
Aviation Product Div.  
1144 E. Market St.  
Akron, Ohio  
Attn: Mr. J. T. Reynolds

H. I. Thompson Fiberglass Co.  
Defense Product Div.  
1600 W. 135th St.  
Gardena, Calif.  
Attn: Mr. R. I. Cox

Raybestos Manhattan, Inc.  
168 S. Beaker St.  
S. San Francisco, Calif.  
Attn: Mr. N. J. Cox

TRW Systems  
One Space Park  
Redondo Beach, California 90278  
Attn: M. Lipow (1)

United Technology Center  
P.O. Box 358  
Sunnyvale, California 94088  
Attn: Technical Library (1)

The B. F. Goodrich Co.  
Aerospace and Defense Products Div.  
1499 Bayshore Highway  
Burlingame, California  
Attn: Mr. R. S. Moore, District Manager

The American Poly-Therm Co.  
3574 Western Ave.  
P.O. Box 38619  
Sacramento, California 95838

AVCO Corp.  
Lycoming Div.  
550 S. Main St.  
Stratford, Conn. 06497  
Attn: Sales Dept.

Arrowhead Products  
4411 Katella Ave.  
Los Alamitos, Calif. 90720  
Attn: Mr. J. L. E'berly, Chief Engineer

Kirkhill Rubber Co.  
Aerospace Div.  
Brea, Calif.  
Attn: R. M. Rhoads

West American Rubber Co.  
2703 New Jersey Ave.  
San Jose, Calif. 95124  
Attn: Mr. D. E. Ulery

Ferro Corp., Cordo Div.  
3512-20 Helms Ave.  
Culver City, Calif. 90230  
Attn: Mr. M. Scott, Technical Sales

Fiberite West Coast Corp.  
690 No. Lemon St.  
P.O. Box 738  
Orange, Calif.  
Attn: Mr. H. Christensen

Dow Corning Corp.  
1299 Bayshore Blvd.  
Burlingame, Calif.  
Attn: Mr. L. C. Diebler

General Electric Co.  
401 Lesser St.  
Oakland, Calif. 94601  
Attn: Mr. F. E. Stanko

Atlantic Research Corp.  
Henry G. Shirley Memorial Highway at  
Edsall Rd.  
Alexandria, Virginia 22314  
Attn: Mr. E. L. Olcott,  
Director Materials Dept.

Garlock, Inc.  
220 E. Grand Ave.  
San Francisco, Calif. 94080  
Attn: Mr. J. W. Wright, Manager

Products Research and Chemical Corp.  
2919 Empire Ave.  
Burbank, Calif 91504  
Attn: Mr. D. Corkill, Manager,  
Engineering Service Dept.

Ohio Rubber Co.  
Ben Hur Ave.  
Willoughby, Ohio 44094  
Attn: Mr. G. S. Hackel,  
Product Sales Manager

Minnesota Mining and Manufacturing Co.  
1210 University Ave.  
St. Paul, Minnesota 55104  
Attn: Mr. J. W. Davis, Plastics Div.

The DeVilbiss Co.  
1335 No. Tenth St.  
San Jose, Calif 95112  
Attn: Mr. W. T. Jacobs